A model for the turbulent diffusion of turbulent kinetic energy in natural convection

Zur Erlangung des akademischen Grades eines

DOKTOR-INGENIEURS

von der Fakultät für Maschinenbau
der Universität Fridericiana Karlsruhe (TH)

genehmigte

DISSERTATION

von

M.Sc. Laltu Chandra
aus Kumardhubi/Indien

Tag der mündlichen Prüfung:	07. Juli 2005
Vorsitzender:	Prof. Dr. –Ing. H. –J. Bauer
Hauptreferent:	Prof. Dr. –Ing. T. Schulenberg
Korreferent:	Prof. Dr. –Ing. H. Oertel

Acknowledgement

This work has been performed in the Institute for Nuclear and Energy Technologies in the Karlsruhe Research Center (Forschungszentrum Karlsruhe GmbH), Karlsruhe, Germany.

I take this opportunity as a privilege to convey my regards to Prof. Dr. –Ing. T. Schulenberg for the useful suggestions and being the Main Referee. I am also thankful to Prof. Dr. –Ing. H. Oertel for considering this work as the Co-referee and Prof. Dr. –Ing. H. –J. Bauer as the Chairman.

I am grateful to Dr. –Ing. G. Grötzbach for his friendly guidance, criticisms, discussions and motivations which helped me during this period. I also convey my regards to Prof. Dr. C. Günther, Dr. M. Wörner (IRS, FZKA), Dr. I. Otić, Dr. X. Cheng and other colleagues for their personal suggestions and fruitful discussions.

Last but not the least; I thank my family and friends for their constant moral support, patience and understanding.

Erklärung

Ich versichere, die Dissertation bis auf die dort angegebenen Hilfen selbständig angefertigt, alle benutzen Hilfsmittel vollständig und genau angegeben und alles kenntlich gemacht zu haben, was aus Arbeiten anderer und eigenen Veröffenlichungen unverändert oder mit Änderungen entnommen wurde.

A model for the turbulent diffusion of turbulent kinetic energy in natural convection

Abstract

The widely used standard Reynolds Averaged Navier-Stokes models, e.g. 1-equation or 2-equation models, use the transport equation for the turbulent kinetic energy. They are known to be problematic in describing thermally stratified flow. In the transport equation for the turbulent kinetic energy the turbulent diffusion term is modeled with the gradient-diffusion approximation which is inadequate in internally heated fluid layers and Rayleigh-Bénard convection. These flow types are explained by means of direct numerical simulation (DNS) data. The data also include a new simulation of internally heated fluid layers with Rayleigh number $Ra = 10^9$ and Prandtl number $Pr = 7.0$. This simulation is performed using the TURBIT code.

One of the possible deficiencies in the gradient-diffusion model for the turbulent diffusion of the turbulent kinetic energy is discussed using the direct numerical simulation data. Based on this study and the investigations in meteorology, extended forms of the gradient diffusion model for the turbulent diffusion are derived. For this deduction, the different closure terms in the turbulent diffusion, namely the velocity-fluctuation triple correlation and the velocity-pressure fluctuation correlation, are modeled separately. Coupling of these models results in a Reynolds Averaged Navier Stokes model for the turbulent diffusion. In this model a variable Daly and Harlow model for the buoyancy contribution, i.e. the turbulent convection of the heat flux, is used to derive an extended Reynolds Averaged Navier Stokes model 1 for the turbulent diffusion. Based on an analysis of the transport equation for the buoyancy contribution a Daly and Harlow extended model for this term is obtained. Incorporating this extension in the model for the turbulent diffusion gives an extended Reynolds Averaged Navier Stokes model 2 for the turbulent diffusion.

The modified or new models for the closure terms in the turbulent diffusion are validated using the direct numerical simulation data of internally heated fluid layers and Rayleigh-Bénard

convection. The Daly and Harlow extended model for the buoyancy contribution is also tested on both flow types.

Also, the extended models 1 and 2 for the turbulent diffusion are analyzed and validated using the direct numerical simulation data of internally heated fluid layers. Their performance is also tested in Rayleigh-Bénard convection. The model 1 shows an acceptable improvement in comparison to the gradient-diffusion model for the turbulent diffusion in internally heated fluid layers. In Rayleigh-Bénard convection a small improvement is observed. The model 2 gives a slight improvement over model 1 in certain height points in these flow types. The resulting 3-equation model should lead to more accurate calculations for buoyant convection in fluid layers involving both stable and unstable stratification.

Table of contents

Nomenclature

c_μ, C_1 C_2, C_p, c_θ $C_\theta, C'_\theta, C_{u3p}$ $C_{\theta 1}, C'_{u3p}, C_{\theta 2}$	Coefficients
D	channel height
Da	Damköhler Number = $q_v D^2 / (\lambda \Delta T_{max})$
$D_{E,m}$	molecular diffusion of $\overline{E'}$
$D_{\varepsilon,m}$	molecular diffusion of $\overline{\varepsilon'}$
$D_{3,m}$	molecular diffusion of $\overline{u_3'^2}$
$D_{T,m}$	molecular diffusion of $\overline{T'^2}$
$D_{E,t}$	turbulent diffusion of $\overline{E'}$
$D_{\varepsilon,t}$	turbulent diffusion of $\overline{\varepsilon'}$
$D_{3,t}$	turbulent diffusion of $\overline{u_3'^2}$
$D_{T,t}$	turbulent diffusion of $\overline{T'^2}$
$\overline{E'}$	turbulent kinetic energy = $\overline{u_i' u_i'}$ / 2
E_{total}	total kinetic energy
g	gravitational acceleration
Gr	Grashof number = (Ra_E / Pr) or $(Ra_I / (Pr\, Da))$
h_{max}	maximum grid width
k_i	wave number along x_i
l	length scale
N_i	number of grid points along x_i

Nu	Nusselt number
N_{time}	number of time steps performed in DNS within Δt_{av}
N_{tav}	number of time steps in Δt_{av}
p	pressure
P_E	production of $\overline{E'}$
$P_{\varepsilon,1}, P_{\varepsilon,2}$	production of $\overline{\varepsilon'}$
Pr	Prandtl number = $\hat{\nu} / \hat{\kappa}$
Pr_t	turbulent Prandtl number for heat transport
q_v	volumetric heat source
q, q_l, q_u	heat flux density
Ra_E	external Rayleigh number $= \hat{g}\hat{\gamma}\Delta\hat{T}_0\hat{D}^3/(\hat{\nu}\hat{\kappa})$
Ra_I	internal Rayleigh number $= \hat{g}\hat{\gamma}\hat{q}_v\hat{D}^5/(\hat{\nu}\hat{\kappa}\hat{\lambda})$
Re	Reynolds number = $\frac{\hat{u}_o\hat{D}}{\hat{\nu}} = \sqrt{Gr}$
Re_t	turbulent Reynolds number $= \frac{\overline{\hat{E}'}^2}{\hat{\nu}\overline{\hat{\varepsilon}'}}$
t	time
Δt_{av}	time interval
t_{max}	maximum time
T	temperature
u_i	velocity component in x_i direction
x_i	Cartesian co-ordinate ($i = 1,2$: horizontal, $i = 3$ vertical)
Δx_i	mesh width x_i
$X_{1,2}$	periodic lengths along $x_{1,2}$.

Scaling variables

$\hat{u}_o$	velocity scale, $(\hat{g}\hat{\gamma}\Delta\hat{T}_0\hat{D})^{1/2}$
$\hat{t}_0$	time scale, ($\hat{D}$ / $\hat{u}_0$)
$\hat{p}_0$	pressure scale, $\left(\hat{\rho}_0\hat{u}_0^2\right)$
$\Delta\hat{T}_0$	temperature scale

Greek Symbols

γ	coefficient of the volume expansion.
α, β	parameters
δ_{ij}	Kronecker delta
Δ	difference operator
$\overline{\varepsilon'}$	dissipation of $\overline{E'}$
$\overline{\varepsilon_3'}$	dissipation of $\overline{u_3'^2}$
$\overline{\varepsilon_T'}$	dissipation of $\overline{T'^2}$
ε_H	eddy conductivity
κ	thermal diffusivity
λ	thermal conductivity
ν	kinematic viscosity
ν_t	eddy viscosity
Π_3	pressure strain of $\overline{u_3'^2}$
ρ	density
χ_ε	destruction of $\overline{\varepsilon'}$

σ_k	turbulent Prandtl number of $\overline{E'}$
σ_ε	turbulent Prandtl number of $\overline{\varepsilon'}$
τ , τ_{new}	time scale
$\bar{\tau}_{ij}$	time averaged shear stresses

Superscripts

$( )$	non-dimensional quantities
$\hat{( )}$	dimensional quantities
$\overline{( )}$	time average
$( )'$	fluctuating component with respect to $\overline{( )}$
${}^{v}\overline{( )}$	volume average
${}^{j}\overline{( )}$	surface average
$\langle \rangle$	mean over $x_1 - x_2$ plane and time (t)
$( )''$	fluctuation with respect to $\langle \rangle$
${}^{v}\langle \rangle$	volume average over the complete channel

Subscripts

i	node indices along the direction x_i
l	lower
max	maximum
u	upper
[ ]	no Einstein-summation

Abbreviations

ASM	algebraic stress model
CBL	Convective Boundary Layer

CGHF	Counter Gradient Heat Flux
DES	detached eddy simulation
DNS	direct numerical simulation
DH	Daly and Harlow model for $\overline{u_3'^2 T'}$, eqn (4.9a)
DHE	Daly and Harlow Extended model for $\overline{u_3'^2 T'}$, eqn (4.11)
EVM	eddy viscosity model
IHL	internally heated fluid layers
LES	large eddy simulation
LHS	Left Hand Side
RANS	Reynolds Averaged Navier-Stokes
RBC	Rayleigh-Bénard convection
RHS	Right Hand Side
RMS	root mean square
SGS	sub-grid scale
TKE	turbulent kinetic energy
VDH	variable Daly and Harlow model for $\overline{u_3'^2 T'}$, eqn (4.9b)
VLES	very large eddy simulation

1 Introduction

Natural fluid flow and convective heat transfer are important in environmental, astrophysical and industrial flow types. These flow types are generally turbulent in nature.

Mostly the local and instantaneous detail of turbulence is not of practical importance. That is why methods of numerical investigation for turbulence are based on the so-called Reynolds equations. It means averaging of conservation equations for mass, momentum and energy is performed over suitable time intervals to filter out the turbulence effect. This approach is the RANS (Reynolds Averaged Navier-Stokes) method. In due course, the unknown Reynolds stresses and turbulent heat fluxes appear in the Reynolds equations. Mostly, the concept of eddy diffusivity and eddy conductivity has been employed to calculate these stresses and heat fluxes.

Instead of above, solving the local and the instantaneous Navier-Stokes equations is known as the direct numerical simulation (DNS). The structures which appear in turbulence are broadly classified into two categories, one is so-called the ‘Large eddies’ whose size is comparable with the width of the computational domain. Whereas, those eddies which are smaller than the Large eddies or the width of the computational cells are the ‘Small eddies’. The Ratio of the size of largest to the smallest eddy increases with the increasing Reynolds number (Re). In order to perform a DNS even the smallest scale needs to be resolved. Therefore, DNS is restricted only to low Re even with the fastest computer available. In the high Re flows it is only possible to resolve the large eddies and the small eddies are modeled by the sub-grid scale (SGS) models. This approach is known as the large eddy simulation (LES). LES is benefited with the facts that the large eddies which determine the characteristics of turbulence are directly simulated. The small eddies that need to be modeled, found to obey widely universal laws. Therefore, LES can be regarded as fairly universal but not fully. As a result, it has been used for some industrial flow problems instead of RANS.

1.1 Motivation and problem specification

The present work deals with buoyant convection which requires special attention in many technical applications. Several efforts have been made to study the buoyant convection in meteorological and industrial flows which involve different types of fluid, e.g. air, water or liquid metal (e.g. Lumley et al. (1978), Moeng and Wyngaard (1989), and Canuto and Daalsgaard (1998)). Another crucial phenomenon which occurs in the natural or industrial flows is called the thermal stratification. It appears due to the temperature/density difference between the different layers of fluid. In fluid layers with the warmer (lighter) fluid over the colder (denser) fluid gives rise to stable thermal stratification whereas the colder (denser) fluid over the warmer (lighter) fluid results in an unstable thermal stratification.

Buoyancy effect as a result of the thermal stratification plays an important role in the different types of fluid flow, e.g. Rayleigh-Bénard convection (RBC), internally heated fluid layers (IHL) and Convective Boundary Layer (CBL). The CBL in atmosphere arises if turbulence generated by buoyancy due to upward heat flux from the surface dominates relative to turbulence generated by mean shear due to horizontal wind. The sign of temperature gradient can be used to classify the thermal stratification as stable (positive temperature gradient), unstable (negative temperature gradient) and neutral (zero temperature gradient). The unstable stratification amplifies whereas the stable stratification attenuates the turbulence. This damping cannot be accounted by the isotropic assumption in the standard RANS model (e. g. $\overline{E'}-\overline{\varepsilon'}$ model see e.g. Davidson (1990), here the notation for turbulent kinetic energy $\overline{E'}$ and its dissipation $\overline{\varepsilon'}$ are used instead of k and ε). LES investigation of the unstably stratified fluid layers by Lee and Pletcher (2001) indicates that the sub-grid scale models are not perfect and that they need further improvement. Therefore, analytical, numerical (DNS) and experimental methods have been used to study the thermal stratification. However, the DNS is restricted to only low Re flows depending on the available computational resources. This limitation of DNS makes the turbulence modeling approaches (RANS/LES) inevitable for numerically investigating the different flow types.

Mostly the RANS method is applied for the numerical study of engineering flow problems. Some of these problems are also thermally stratified in which the Rayleigh

(Ra) number, which is the ratio of buoyant force and the product of viscous drag and rate of heat diffusion, can attain very high values (e.g. Dinh and Nourgaliev (1997)). The experimental investigations in such cases are usually supported and their results are usually transferred to the actual technical parameters by numerical simulations in which engineering codes are employed. The quality of the numerical results strongly depends on the reliability of the turbulence models. Dinh and Nourgaliev (1997) had used a standard low Reynolds number $\overline{E'} - \overline{\varepsilon'} - Pr_t$ model to recalculate an experiment of natural convection in fluids with an internal heat source. According to the authors, this model fails to describe the mean temperature or heat transfer in the regime of interest. They proposed several phenomenological corrections for this model. Finally, they concluded the need of further development to improve the predictive capability of this RANS model.

The standard RANS models (e.g. $\overline{E'} - \overline{\varepsilon'}$ model) use the transport equation for the turbulent kinetic energy ($\overline{E'}$). In this equation the turbulent diffusion appears as one of the closure terms. The turbulent diffusion consists of the turbulent-transport (velocity-fluctuation triple correlation $\overline{u_j' E'}$ term) and the pressure-transport (velocity-pressure fluctuation correlation $\overline{u_j' p'}$ term). They are modeled together in the gradient-diffusion model for the turbulent diffusion. Wörner et al. (1997) had shown that this gradient diffusion model for the turbulent diffusion of $\overline{E'}$ is not adequate in IHL.

Such inadequacy of the gradient diffusion model for the turbulent diffusion was also observed in a LES study of CBL by Moeng and Wyngaard (1989). They observed that the gradient diffusion model for the turbulent transport can not explain the counter gradient transport of $\overline{E'}$. The importance of the counter gradient transport of $\overline{E'}$ in the upper part of the atmospheric boundary layer was described by Lumley et al. (1978). According to the authors, the anisotropic effect of buoyancy (see e.g. Schemm and Lipps (1976)) could explain the counter gradient flux of $\overline{E'}$. Therefore, Moeng and Wyngaard (1989) recommended the inclusion of the buoyancy effect in the modelling of turbulent transport of $\overline{E'}$. This could also be one of the possible reasons that the standard low Reynolds number $\overline{E'} - \overline{\varepsilon'} - Pr_t$ model fails seriously to ex-

plain such thermally stratified flow types as experienced by Dinh and Nourgaliev (1997).

The above studies indicate that the effect of buoyancy needs to be included in the RANS as well as in the LES modeling approaches to improve their predictive capability for investigating thermally stratified flow types.

1.2 Literature status

During the last few decades many scientists had provided a basic know-how about the effect of buoyancy /stratification in general. Monin and Yaglom (1971) and Tennekes and Lumley (1972) are among some of the classical authors in the discipline of turbulence theory and RANS modelling approach. These authors had given a bird-eye view of the effect of stratification/buoyancy and explained its influence on $\overline{E'}$.

The widely used RANS model for the velocity-fluctuation triple correlation term in the turbulent diffusion of $\overline{E'}$ was derived by Hanjalić and Launder (1972); it is a tensorial model. Afterwards, Deardorff (1974) had employed this model for a LES investigation of the mean structures of planetary boundary layer. A simplified form of this model is the gradient-diffusion model for the turbulent diffusion of $\overline{E'}$ (see e.g. Launder and Spalding (1972)). In this model the contribution of buoyancy was not considered. In order to include the effect of buoyancy, Lumley et al. (1978) had investigated the turbulent transport term in the transport equations for turbulent kinetic energy, turbulent heat flux etc. In his model the presence of the buoyancy effect makes the different third order-moments in the different transport equations inter dependent.

One way to include the influence of buoyancy in stable stratification is the introduction of additional near-wall damping functions in the eddy viscosity and eddy conductivity as explained by Murakami et al. (1996). These functions were introduced to describe the damping effect of buoyancy in the stable stratification.

A better approach to deal with the effect of buoyancy is the algebraic stress modeling (ASM) or the algebraic turbulent heat flux modeling. Launder et al. (1975) had developed an ASM model for the Reynolds stresses. This model found to be suitable for

both the homogeneous and inhomogeneous shear flows. Later on, Davidson (1990) had developed a hybrid model for the Reynolds stresses. This model takes from an algebraic Reynolds stress model that part of the non-isotropic Reynolds stresses which is due to the buoyancy, and the remaining part from the standard $\overline{E'} - \overline{\varepsilon'}$ model. As an extension of this approach and based on Hanjalić et al. (1996), Liu and Wen (2002) had introduced additional wall-reflection functions in the model for Reynolds stresses and turbulent heat fluxes. In absence of the vertical solid surface these functions reduce to zero. According to this study, these modifications have achieved quantitatively good agreement with the experimental data of velocity and temperature distributions in buoyant diffusion flames. Using the Davidson (1990) ASM model for the Reynolds stress, Yan and Holmstedt (1999) had proposed a modified form of the standard $\overline{E'} - \overline{\varepsilon'}$ model in which the turbulent heat flux is approximated in accordance with the Daly and Harlow (1970) model. A comparison between predicted and experimental values in case of a two-dimensional plane thermal plume shows a better agreement in comparison to the standard $\overline{E'} - \overline{\varepsilon'}$ model. However, the authors considered that further development in this direction will enhance the predictive capability of this modified $\overline{E'} - \overline{\varepsilon'}$ model. Considering the algebraic heat flux model by Launder (1988) and Nagano and Kim (1988), Otić et al. (2005) have proposed a modified 4-equation model which is based on the transport equation for $\overline{E'}$, for the dissipation of $\overline{E'}$ $\left(\overline{\varepsilon'}\right)$, for the temperature variance $\left(\overline{T'^2}\right)$ and for the dissipation of $\overline{T'^2}$ $\left(\overline{\varepsilon'_T}\right)$. This model should be applicable for wide range of low Prandtl number (Pr) flows (see e.g. Grötzbach et al. (2004)). In these approaches the gradient-diffusion approximation for the turbulent diffusion of $\overline{E'}$ has been used.

A more sophisticated method to study the buoyant flow types is the second-moment closure modeling. Hanjalić (1999) had discussed the improvements of the second-order closure approach over the eddy-viscosity model for complex flow types. In an investigation of the turbulent natural convection, Dol et al. (1997) had made a comparative assessment of the statistical (RANS) models which are related to the transport equations for turbulent heat fluxes and to the turbulent temperature variance. They observed that the coefficients which appear in the Daly and Harlow (1970) model for the turbulent diffusion terms in these transport equations are not constant. Afterwards, Dol et al. (1999) had modified the Daly and Harlow (1970) model for the

turbulent diffusion of temperature variance and used the statistical second moment-closure approach to study the buoyant convection. Later on, Carteciano (1996) had successfully developed a 7-equation Turbulence Model for Buoyant Flows (TMBF). This is a combination of the standard $\overline{E'} - \overline{\varepsilon'}$ model for the turbulent Reynolds stresses and a full second-order model for the turbulent heat fluxes including the transport equations for $\overline{T'^2}$ and $\overline{\varepsilon'_T}$ for buoyancy influences. In recalculating a forced jet experiment with this model, it has been found that the mean temperature field is better predicted by the TMBF in comparison to the $\overline{E'} - \overline{\varepsilon'} - Pr_t$ (see e.g. Carteciano and Grötzbach (2003)). These sophisticated approaches show remarkable improvement over the standard RANS models for also investigating the turbulent natural convection which involves different types of fluids.

Usually LES and RANS are discussed in separate framework. However, the idea of blending LES and RANS was proposed by Spalart et al. (1997) which is known as the detached eddy simulation (DES). According to this concept, whole boundary layer which is populated with the 'attached eddies' is entrusted to a RANS model, and only in the separated region, the 'detached eddies' is entrusted to LES. In order to capture the coherent large-scale structures, while still remaining within the RANS framework a combination of LES and RANS strategies was analyzed by Hanjalić (2002)). He discussed the concept of very large eddy simulation (VLES) in which the large coherent eddy structures are resolved. The remaining incoherent parts are modeled by a RANS-type closure, serving as a sub-scale model. Even these approaches use the transport equation for $\overline{E'}$. Hanjalić (2002) emphasized on the inclusion of buoyancy effect in the RANS models for the turbulent diffusion of turbulent heat fluxes and temperature variance. He has not considered the effect of buoyancy in the turbulent diffusion of $\overline{E'}$ in order to obtain a simple model for this term.

Most of the above approaches (RANS/LES/combination of LES and RANS) use the gradient-diffusion model for the turbulent diffusion of $\overline{E'}$. Thus, any improvement in this model may further enhance the predictive capability of the standard or the advanced models for numerically investigating buoyant flow types. Based on experience, the gradient-diffusion model for the turbulent diffusion of $\overline{E'}$ assumes that the

velocity fluctuation triple correlation $\overline{u_j' E'}$ and velocity-pressure fluctuation correlation $\overline{u_j' p'}$ can be modeled together. On the other hand, Wörner and Grötzbach (1998) had described the different behavior and importance of $\overline{u_j' E'}$ and $\overline{u_j' p'}$ in IHL and RBC. At the same time, Dwyer et al. (1997) based on a LES of airflow above and within forest canopy had investigated the different terms in the transport equation for $\overline{E'}$. They found that the pressure-transport in the turbulent diffusion of $\overline{E'}$ plays a significant role. These studies show that $\overline{u_j' E'}$ and $\overline{u_j' p'}$ should not be modeled together in IHL and RBC. Moreover, $\overline{u_j' p'}$ needs special attention in the model for the turbulent diffusion of $\overline{E'}$.

At the same time some authors (e.g. Zeman and Lumley (1976)) consider the contribution of buoyancy in the turbulent diffusion of $\overline{E'}$ as a significant one. So far this effect has not been included along with the gradient-diffusion model for the turbulent diffusion of $\overline{E'}$.

Finally from the above studies, it can be concluded that:

- The different closure terms $\overline{u_j' E'}$ and $\overline{u_j' p'}$ in the turbulent diffusion of $\overline{E'}$ require separate modeling.

- The buoyancy effect needs to be included in the model for the turbulent diffusion of $\overline{E'}$.

1.3 Objectives

The aim of this work is to improve the gradient-diffusion model for the turbulent diffusion of $\overline{E'}$. In order to extend the gradient-diffusion model for the turbulent diffusion, the conclusion of Moeng and Wyngaard (1989) and analysis of the DNS data of RBC and IHL will be used as a starting point. For the deduction of a model, the velocity-fluctuation triple correlation $\overline{u_j' E'}$ and the velocity-pressure fluctuation correlation $\overline{u_j' p'}$ will be modeled separately. The RANS models for $\overline{u_j' E'}$ and $\overline{u_j' p'}$ will be cou-

pled to derive the required extended RANS models for the turbulent diffusion. In this study, RBC and IHL are used as a model problem.

In RBC, an infinite fluid layer between two horizontal isothermal walls which is heated uniformly from below and cooled from the top is considered. Whereas in IHL, the isothermal walls are at a lower temperature than the fluid confined in-between which is having a uniform volumetric energy source. The fluid layers in RBC are unstably stratified over the complete height of the channel. On the other hand, in IHL most of the region over the height of the channel is stably stratified with an unstably stratified upper thermal boundary layer. This thin layer drives the vertical heat and momentum exchange.

In IHL, presence of both the unstably and stably stratified fluid layers makes it problematic for modeling in comparison to RBC. At the same time, it is expected that the gradient-diffusion RANS model for the turbulent diffusion of $\overline{E'}$ may provide an acceptable result in the upper unstable region. This may not be acceptable near or in the stable region. Hence, in order to study the effect of buoyancy IHL is preferred which is also a prototype of the natural convection in astrophysics (see e.g. Canuto and Dalsgaard (1998)). Subsequently, the extended RANS model for the turbulent diffusion of $\overline{E'}$ will be tested in RBC. For this purpose the analyzing module of the TURBIT code (see e.g. Schumann (1973), Grötzbach (1977)) will be extended and employed to compare the existing and new models against DNS data.

Considering the above in this Ph.D. work, the following aspects are included in this thesis:

- Brief description of RANS modeling approach and some of the standard RANS models.

- Description of DNS and analysis of the DNS results of IHL and RBC. This also includes a recently performed DNS of IHL with $Ra = 10^9$ and Pr =7.

- Analysis of the terms in the transport equation for $\overline{E'}$ using the DNS data of IHL and RBC.

- Derivation of a RANS model for the velocity-fluctuation triple correlation $\overline{u_j' E'}$. For this purpose the transport equation for $\overline{u_j' E'}$ will be used. In this model the effect of buoyancy will be introduced.

- Short analysis of a modified RANS model for the velocity-pressure fluctuation correlation $\overline{u_j' p'}$.

- The RANS models for $\overline{u_j' E'}$ and $\overline{u_j' p'}$ will be joined to obtain an extended RANS model 1 for the turbulent diffusion of $\overline{E'}$. This model includes both the effect of buoyancy and $\overline{u_j' p'}$. In this model the buoyancy term $\overline{u_3'^2 T'}$ will be approximated with a variable Daly and Harlow (1970) model (VDH).

- In another approach for modeling the turbulent diffusion of $\overline{E'}$, the terms in the transport equation for $\overline{u_3'^2 T'}$ will be analyzed using the DNS data of both flow types. Based on this analysis an extended form of the Daly and Harlow (DH) model for $\overline{u_3'^2 T'}$ will be obtained. This will be referred to as Daly and Harlow Extended model for $\overline{u_3'^2 T'}$ (DHE).

- Derivation of the extended RANS model 2 for the turbulent diffusion of $\overline{E'}$ using the DHE model for $\overline{u_3'^2 T'}$ and the modified RANS model for $\overline{u_j' p'}$.

- Validation of the RANS models for $\overline{u_j' E'}$ and $\overline{u_j' p'}$ using the DNS data of IHL and RBC.

- Validation of the DHE model for $\overline{u_3'^2 T'}$ in both IHL and RBC.

- Validation of the model 1 and 2 for the turbulent diffusion of $\overline{E'}$ in both flow types.

- Additionally, a RANS model for the derivative of $\overline{u_j' p'}$ will be derived and validated using the DNS data of both flow types.

2 Description of RANS

This chapter deals with the basic RANS equations and some of the closure assumptions which are commonly used to solve the system of equations for thermally stratified flow types. In the present study two buoyant flow types, namely, IHL and RBC are considered.

2.1 Basic RANS equations

The basic equations for laminar and turbulent convection are the equations for the conservation of mass, momentum and energy. In the present case, the linear dependence of the stresses on the velocity deformation for the Newtonian fluid is considered. For simplicity, the Boussinesq approximation is adopted. This implies the assumption, that the physical properties in all terms of these equations are considered as constant except for the buoyancy. In this term a linear dependence of the density with temperature is assumed. Gray and Giorgini (1976) had shown that this approximation is valid in water and air up to a very high temperature difference. Sugiyama et al. (1991) had shown that this approximation is even applicable in liquid metals. Hence, without loss of generality, this approximation is employed in the present investigation which involves different types of fluid with $0.025 \le Pr \le 7.0$.

If the Cartesian co-ordinates are used with x_1 and x_2 as the horizontal and x_3 as the vertical direction, the conservation equations for mass, momentum and energy for the velocity component $u_i (i = 1,2,3)$, pressure p and temperature T in the non-dimensional form are given by (see e.g. Oertel (2004)),

$$\left.\begin{aligned}
&\frac{\partial u_i}{\partial x_i} = 0, \\
&\frac{\partial u_i}{\partial t} + \frac{\partial u_i u_j}{\partial x_j} = \frac{1}{\sqrt{Gr}} \frac{\partial}{\partial x_j}\left(\frac{\partial u_i}{\partial x_j} + \frac{\partial u_j}{\partial x_i}\right) - \frac{\partial p}{\partial x_i} + (\Delta T)\,\delta_{i3}, \text{ with } i = 1,2,3, \\
&\frac{\partial T}{\partial t} + \frac{\partial (T u_j)}{\partial x_j} = \frac{1}{Pr\sqrt{Gr}} \frac{\partial^2 T}{\partial x_j^{\,2}} + \frac{Da}{Pr\sqrt{Gr}}.
\end{aligned}\right\} \qquad (2.1)$$

The Einstein summation rule is applied to all the terms bearing the same subscript twice. The eqn (2.1) is normalized with the plate spacing $\hat{D}$, the temperature difference $\Delta\hat{T}_0$, the time scale $\hat{t}_0 = \hat{D}/\hat{u}_0$, the pressure scale $\hat{p}_0 = \hat{\rho}\hat{u}_0{}^2$, where $\hat{\rho}$ is the density and the velocity scale $\hat{u}_0 = (\hat{g}\hat{\gamma}\Delta\hat{T}_0\hat{D})^{1/2}$. Here Pr and Gr are the well known Prandtl and Grashof numbers, respectively. Another important dimensionless number is the Damköhler number $Da = \hat{q}_v\hat{D}^2/\left(\hat{\lambda}\Delta\hat{T}_0\right)$ characterizing the volumetric or sink of heat in the fluid.

In IHL $\Delta\hat{T}_0$ is the maximum temperature difference across the height of the channel. This is not fixed but is a dependent variable; it is linked by means of Da to $\hat{q}_v$. In RBC $\Delta\hat{T}_0 = \hat{T}_{lower} - \hat{T}_{uppper}$ where $\hat{T}_{lower}$ and $\hat{T}_{upper}$ indicate the temperature at the lower plate and upper plate, respectively, with the volumetric heat source $\hat{q}_v = 0$ and $Da = 0$. The velocity scale $\hat{u}_0$ is chosen to normalize the buoyancy term to unity.

Using suitable time intervals it is possible to capture slow as well as fast changes of the physical variables (e.g. $y = (u_i, p \text{ or } T)$). Application of the classical time average (Reynolds ansatz) decomposes these physical variables into their mean $\left(\overline{y}\right)$ and fluctuating parts (y'),

$$y = \overline{y} + y', \text{ with } \overline{\overline{y}} = \overline{y} \text{ and } \overline{y'} = 0.$$

Here, $\overline{(\,)}$ is the representation of the classical time average and $(\,)'$ is the fluctuation with respect to $\overline{(\,)}$. The time interval, over which the time mean value is taken, is chosen such that the lowest frequencies of the turbulent fluctuations are averaged out. So, the time mean values may still be dependent on larger time-scales which are associated with the change in the time mean field. Let us consider y and z are any two variables. Application of the time averaging operator to their product results in (see e.g. Monin and Yaglom (1971)),

$$\overline{yz} = \overline{\left(\overline{y} + y'\right)\left(\overline{z} + z'\right)} = \overline{\overline{y}\,\overline{z}} + \overline{y'\overline{z}} + \overline{\overline{y}z'} + \overline{y'z'}.$$

Considering the property of the time averaging operator one obtains finally,

$$\overline{yz} = \overline{y}\,\overline{z} + \overline{y'z'}\,. \tag{2.2}$$

The first term in the right hand side of this equation is the product of time averaged values and the last term is the time average of the product of fluctuations.

The RANS equations are obtained by applying the time averaging operator to the system of equations as given in eqn (2.1) and using the property of this operator as in eqn (2.2), which are as follows,

$$\left.\begin{aligned}
&\frac{\partial \overline{u}_i}{\partial x_i} = 0, \\
&\frac{\partial \overline{u_i}}{\partial t} + \overline{u}_j \frac{\partial \overline{u}_i}{\partial x_j} = -\frac{\partial \overline{u_i' u_j'}}{\partial x_j} + \frac{1}{\sqrt{Gr}} \frac{\partial}{\partial x_j}\left(\frac{\partial \overline{u_i}}{\partial x_j} + \frac{\partial \overline{u_j}}{\partial x_i}\right) - \frac{\partial \overline{p}}{\partial x_i} + \overline{\Delta T}\,\delta_{i3}, \ \text{with} \ i = 1,2.3, \\
&\frac{\partial \overline{T}}{\partial t} + \overline{u}_j \frac{\partial \overline{T}}{\partial x_j} = -\frac{\partial \overline{u_j' T'}}{\partial x_j} + \frac{1}{Pr\sqrt{Gr}} \frac{\partial^2 \overline{T}}{\partial x_j^{\,2}} + \frac{Da}{Pr\sqrt{Gr}}.
\end{aligned}\right\} \tag{2.3}$$

In the TURBIT code a combined plane and time average operator $\langle\ \rangle$ is employed in analyzing statistical data from the DNS or LES results. This linear operator is defined as mean over x_1-x_2 plane and time (t). The eqn (2.2) and (2.3) look formally identical with both $\overline{(\ )}$ and $\langle\ \rangle$. The main difference is that $\langle\ \rangle$ averaged quantities depend only on x_3 whereas $\overline{(\ )}$ averaged quantities depend on $x_i, i = 1,2,3$. However, the present theoretical discussion continues further using the classical $\overline{(\ )}$ operator.

2.2 Widely used closure assumptions

In eqn (2.3) the unknown Reynolds stresses $\overline{u_i' u_j'}$ and turbulent heat fluxes $\overline{u_i' T'}$ appear as a result of the Reynolds averaging. These are usually calculated using isotropic eddy viscosity and eddy conductivity models. Thus, in the first order models, the Reynolds stresses and heat fluxes are computed by assuming gradient diffusion:

$$\left.\begin{aligned}\overline{u_i' u_j'} &= \frac{2}{3}\overline{E'}\delta_{ij} - \nu_t\left(\frac{\partial \overline{u_i}}{\partial x_j} + \frac{\partial \overline{u_j}}{\partial x_i}\right),\\ \overline{u_i' T'} &= -\varepsilon_H \frac{\partial \overline{T}}{\partial x_i}\end{aligned}\right\} \qquad (2.4)$$

Where, $\nu_t = c_\mu \overline{E'^2} \big/ \overline{\varepsilon'}$ and $\varepsilon_H = c_\mu E'^2 \big/ \left(\overline{\varepsilon'} Pr_t\right)$ are the isotropic eddy viscosity and isotropic eddy conductivity, respectively, and Pr_t is called the turbulent Prandtl number for heat transport. This is one of the possibilities to calculate these unknowns. In the standard RANS models $c_\mu = 0.09$ and $Pr_t = 0.9$ is used. Calculation of ν_t and ε_H using the transport equations for $\overline{E'}$ and $\overline{\varepsilon'}$ is known as the $\overline{E'} - \overline{\varepsilon'}$ $(k-\varepsilon)$ model (Launder and Spalding (1972)). In most codes basing on eqn (2.4) the new unknowns are calculated by means of the $\overline{E'} - \overline{\varepsilon'}$ $(k-\varepsilon)$ model and by the Reynolds analogy.

The linear isotropic eddy-viscosity models (EVM) have two major problems associated with them: (a) They cannot account for the anisotropy and (b) the assumption that the position of maximum mean velocity and change of sign of the turbulent stresses coincide which is seldom (see e.g. Speziale (1991)). Although these deficiencies are known, the majority of turbulent flow calculations are carried out using the linear EVM. According to several authors, the full second-moment closures can overcome the limitations of the linear EVM (see e.g. Hanjalić (1999)). At the same time, this method requires six additional transport equations for the Reynolds stresses to be solved which cannot compete with the robustness and efficiency of the linear EVM. Therefore, the nonlinear EVM (see e.g. Lumley (1978), Shih et al. (1995)) and the algebraic stress models (ASM) (see e.g. Launder et al. (1975)) were developed to combine the computational robustness and efficiency of the linear EVM with the improved model accuracy of the second-moment closures. Nonlinear EVM also contains higher-order contributions from the strain and vorticity fields, e.g. product of strain and strain, vorticity and strain, and vorticity and vorticity.

Bauer et al. (2000) had applied nonlinear EVM to recalculate some of the complex flow types which include backward facing step, curved mixing layer and low-speed

internal flow in a strongly curved U-duct. They found that the nonlinear EVM are able to predict the presence of recirculation zones, flow separation etc. more precisely than the linear EVM. In this study moderate increase in the CPU-time had been observed. The computational robustness was slightly decreased in comparison to the standard $\overline{E'} - \overline{\varepsilon'}$ model.

In the above approaches the effect of buoyancy in the Reynolds stresses was not considered. Davidson (1990) had proposed a hybrid model for these Reynolds stresses which is as follows:

$$\overline{u_i' u_j'} = \left(\overline{u_i' u_j'}\right)_{\overline{E'}-\overline{\varepsilon'}} + \left(\overline{u_i' u_j'}\right)_{ASM}$$

In this model, the ASM part contains the effect of buoyancy which is anisotropic. Thereafter, Durbin (1991) had introduced an anisotropic form of the eddy viscosity which has been applied to the channel flow and boundary layer.

Grötzbach (1982a) had shown that the isotropic eddy conductivity model as in eqn (2.4) for the turbulent heat fluxes is not adequate in IHL. This is due to the presence of a wide range of the Counter Gradient Heat Flux (CGHF). Schumann (1987) had given a detailed account of the occurrence of CGHF in the stably stratified part of different flow types. In order to overcome such limitations, Launder (1988) had proposed an algebraic model for the turbulent heat fluxes, which is as follows:

$$\overline{\hat{u}_i' \hat{T}'} = -c_\theta \hat{\tau} \left(\overline{\hat{u}_i' \hat{u}_k'} \frac{\partial \overline{\hat{T}}}{\partial \hat{x}_k} + \overline{\hat{u}_k' \hat{T}'} \frac{\partial \overline{\hat{u}_i}}{\partial \hat{x}_k} - \hat{\gamma} \hat{g}_i \overline{\hat{T}'^2} \right)$$

The above model in a non-dimensional form using the present length, velocity, time and temperature scales reduces to,

$$\overline{u_i' T'} = -c_\theta \tau \left(\overline{u_i' u_k'} \frac{\partial \overline{T}}{\partial x_k} + \overline{u_k' T'} \frac{\partial \overline{u_i}}{\partial x_k} - \overline{T'^2} \delta_{i3} \right). \qquad (2.5)$$

Here $\tau = \dfrac{\overline{E'}}{\overline{\varepsilon'}}$ is a time scale and c_θ is an empirical coefficient. This model requires for buoyant flow an additional transport equation for $\overline{T'^2}$ and for even better prediction at Pr deviating from 1 the transport equation for $\overline{\varepsilon'_T}$ is necessary. This results in a $\overline{E'} - \overline{\varepsilon'} - \overline{T'^2} - \overline{\varepsilon'_T}$ model which is a 4-equation model (see e.g. Nagano and Kim (1988), Hanjalić et al. (1996)). Seki et al. (2003) have proposed a model which satisfies the linearity principle as in Lai and So (1990), and also the near-wall asymptotes for the turbulent heat transfer in the channel flow.

So far some of the well known models have been presented. All use the transport equations for $\overline{E'}$ and $\overline{\varepsilon'}$. Therefore, these equations will be considered as the next.

The transport equation for $\overline{E'}$ (see e.g. Rotta (1951), Hossain and Rodi (1974) etc.) in the non-dimensional form is given by,

$$\left.\begin{aligned} \underbrace{\frac{\partial \overline{E'}}{\partial t}}_{\text{Rate of Change}} + \underbrace{\frac{\partial}{\partial x_j}\left(\overline{u_j}\,\overline{E'}\right)}_{\text{Convection}} = \underbrace{-\overline{u_i' u_j'}\frac{\partial \overline{u_i}}{\partial x_j} + \delta_{j3}\overline{u_j' T'}}_{P_E} \underbrace{- \frac{1}{\sqrt{Gr}}\overline{\left(\frac{\partial u_i'}{\partial x_j}\right)^2}}_{\overline{\varepsilon'}} \\ + \underbrace{\frac{\partial}{\partial x_j}\left\{\frac{1}{\sqrt{Gr}}\frac{\partial \overline{E'}}{\partial x_j}\right\}}_{D_{E,m}} \underbrace{- \frac{\partial}{\partial x_j}\left\{\overline{u_j' E'} + \overline{u_j' p'}\right\}}_{D_{E,t}} . \end{aligned}\right\} \qquad (2.6)$$

In eqn (2.6), P_E is the production of $\overline{E'}$ due to the mean shear and turbulent heat fluxes (buoyancy), $\overline{\varepsilon'}$ is the dissipation of $\overline{E'}$, $D_{E,m}$ is its molecular diffusion and $D_{E,t}$ is its turbulent diffusion.

The flow types, IHL and RBC, are shear free, i.e. the production of $\overline{E'}$ is only due to the buoyancy along the vertical direction $(j = 3)$. This can be calculated using the approximations as explained above. Therefore, the closure terms that remain in the transport equation for $\overline{E'}$ are $\overline{\varepsilon'}$ and $D_{E,t}$. The eqn (2.6) shows that $D_{E,t}$ consists of $\overline{u_j' E'}$ and $\overline{u_j' p'}$. They are generally modeled together in the gradient diffusion model which is as follows (Launder and Spalding (1972)),

$$\overline{u'_j E'} + \overline{u'_j p'} \approx -\left(\frac{\nu_t}{\sigma_k} \frac{\partial \overline{E'}}{\partial x_j} \right), \text{ with } j = 1, 2, 3. \tag{2.7}$$

Here, σ_k is the turbulent Prandtl number of $\overline{E'}$. The model as in eqn (2.7) has been used in the standard RANS models which are available in different commercial codes. In these codes one uses $\sigma_k = 1.0$, in general. Some of the problems which are associated with the above model for $D_{E,t}$ have been discussed in the introduction. One of the most important problems is that this model does not account for the counter gradient transport of $\overline{E'}$ (see e.g. Lumley et al. (1978) and Moeng and Wyngaard (1989)).

As explained, $\overline{\varepsilon'}$ is one of the closure terms in the transport equation for $\overline{E'}$ (see eqn (2.6)). In order to calculate $\overline{\varepsilon'}$, its transport equation is employed within the $\overline{E'} - \overline{\varepsilon'}$ framework. In the non-dimensional form it is as follows (see e.g. Daly and Harlow (1970)),

$$\begin{aligned}
\underbrace{\frac{\partial \overline{\varepsilon'}}{\partial t}}_{\text{Rate of change}} + \underbrace{\overline{u}_j \frac{\partial \overline{\varepsilon'}}{\partial x_j}}_{\text{Convection}} = & \underbrace{-\frac{1}{\sqrt{Gr}} \left\{ \frac{\partial \overline{u_i}}{\partial x_j} \left(\overline{\frac{\partial u'_i}{\partial x_k} \frac{\partial u'_j}{\partial x_k}} \right) + \frac{\partial^2 \overline{u_i}}{\partial x_j \partial x_k} \left(\overline{u'_j \left(\frac{\partial u'_i}{\partial x_k} \right)} \right) + \right.}_{P_{\varepsilon,1}} \\
& \left. \frac{\partial \overline{u_j}}{\partial x_k} \left(\overline{\frac{\partial u'_i}{\partial x_j} \frac{\partial u'_i}{\partial x_k}} \right) \right\} \\
& \underbrace{-\frac{1}{\sqrt{Gr}} \left\{ \left(\overline{\frac{\partial u'_i}{\partial x_k} \frac{\partial u'_i}{\partial x_j} \frac{\partial u'_j}{\partial x_k}} \right) + \left(\overline{\frac{\partial u'_i}{\partial x_j} \frac{\partial T'}{\partial x_j}} \right) \delta_{i3} \right\}}_{P_{\varepsilon,2}} \\
& \underbrace{-\frac{1}{\mathrm{Gr}} \overline{\left(\frac{\partial^2 u'_i}{\partial x_j \partial x_k} \right)^2}}_{\chi_\varepsilon} + \underbrace{\frac{1}{\mathrm{Gr}} \frac{\partial^2 \overline{\varepsilon'}}{\partial x^2_j}}_{D_{\varepsilon,m}} \\
& \underbrace{-\frac{1}{\sqrt{Gr}} \frac{\partial}{\partial x_j} \left(\overline{u'_j \left(\frac{\partial u'_i}{\partial x_k} \right)^2} + 2 \overline{\left(\frac{\partial u'_j}{\partial x_k} \frac{\partial p'}{\partial x_k} \right)} \right)}_{D_{\varepsilon,t}}.
\end{aligned} \tag{2.8}$$

To obtain the non-dimensional form the scaling as already explained is used (see e.g. Hiltner (1993)). In eqn (2.8) $P_{\varepsilon,1}$ is the production of $\overline{\varepsilon'}$ due to the mean shear, $P_{\varepsilon,2}$ is the production of $\overline{\varepsilon'}$ due to the velocity and temperature fluctuations, χ_ε is the destruction of $\overline{\varepsilon'}$, $D_{\varepsilon,m}$ is its molecular diffusion and $D_{\varepsilon,t}$ is its turbulent diffusion. As the flow types are shear free, the production of $\overline{\varepsilon'}$ is only due to $P_{\varepsilon,2}$. The closure terms in eqn (2.8) are modeled as follows (see e.g. Rodi (1972), Hossain and Rodi (1974)):

$$
\begin{aligned}
P_{\varepsilon,2} &\approx c_{\varepsilon 1} \frac{\overline{\varepsilon'}}{\overline{E'}}(P_E), \\
\chi_\varepsilon &\approx c_{\varepsilon 2} \frac{\overline{\varepsilon'}^2}{\overline{E'}}, \\
D_{\varepsilon,t} &\approx \frac{\partial}{\partial x_j}\left(\frac{\nu_t}{\sigma_\varepsilon}\frac{\partial \overline{\varepsilon'}}{\partial x_j}\right)
\end{aligned}
$$

Here, σ_ε is called the turbulent Prandtl number of $\overline{\varepsilon'}$. Using the above approximation it is possible to solve the eqn (2.4). Therefore, the system of equations (eqn (2.3)) is closed in the framework of the $\overline{E'}-\overline{\varepsilon'}$ model.

In this chapter some of the standard RANS models have been explained. All these RANS models, whether it is the 1-equation Kolmogorov-Prandtl Energy-length model (Prandtl (1945)), 2-equation $\overline{E'}-\overline{\varepsilon'}$ model; all use the transport equation for $\overline{E'}$ (eqn (2.6)). So far the models as implemented in most of the commercial codes use the above framework. On the other hand, the investigations in meteorology and in astro-physics recommend the use of eqn (2.5) for computing the turbulent heat fluxes. This model needs additional transport equations for the temperature variance $\overline{T'^2}$ and for even better prediction with Pr deviating from 1 the transport equation for the dissipation of $\overline{T'^2}$ $\left(\overline{\varepsilon'_T}\right)$. This results in a 3-equation $\left(\overline{E'}-\overline{\varepsilon'}-\overline{T'^2}\right)$ or in a 4-equation $\left(\overline{E'}-\overline{\varepsilon'}-\overline{T'^2}-\overline{\varepsilon'_T}\right)$ model. The following is the transport equation for $\overline{T'^2}$ in dimensional form (see e.g. Rodi (1972)),

$$\underbrace{\frac{\partial \overline{\hat{T}'^2}}{\partial \hat{t}}}_{\text{Rate of change}} + \underbrace{\overline{\hat{u}_i}\frac{\partial \overline{\hat{T}'^2}}{\partial \hat{x}_i}}_{\text{convection}} = \underbrace{-2\overline{\hat{u}_i'\hat{T}'}\frac{\partial \overline{\hat{T}}}{\partial \hat{x}_i}}_{P_T} \underbrace{-2\hat{\kappa}\overline{\frac{\partial \hat{T}'}{\partial \hat{x}_i}\frac{\partial \hat{T}'}{\partial \hat{x}_i}}}_{\overline{\hat{\varepsilon}_T'}} + \underbrace{\frac{\partial}{\partial \hat{x}_i}\left(\hat{\kappa}\frac{\partial \overline{\hat{T}'^2}}{\partial x_i}\right)}_{D_{T,m}} \underbrace{-\frac{\partial \overline{\hat{u}_i'\hat{T}'^2}}{\partial \hat{x}_i}}_{D_{T,t}}. \qquad (2.9)$$

In the above equation P_T is the production of $\overline{\hat{T}'^2}$, $\overline{\hat{\varepsilon}_T'}$ is its dissipation, $D_{m,t}$ is its molecular diffusion and $D_{T,t}$ is its turbulent diffusion. In this equation only P_T can be calculated using eqn (2.5) as explained, whereas $\overline{\varepsilon_T'}$ can be calculated using the model form of the transport equation for $\overline{\hat{\varepsilon}_T'}$ as explained by Hossain and Rodi (1974). A new model for the remaining closure term $D_{T,t}$ is proposed by Otić et al. (2005) which is as follows:

$$\overline{u_i'T'^2} = -C_{\theta 2}\left[\frac{2}{\sqrt{Gr\,Pr}}\tau_{new}\,\Delta_x\overline{u_i'T'^2} + \frac{\overline{E'^2}}{\overline{\varepsilon'}}\frac{\partial \overline{T'^2}}{\partial x_i}\right] \qquad (2.10)$$

Here $C_{\theta 2}$ is an empirical coefficient and Δ_x is the Laplacian operator. In eqn (2.10) τ_{new} denotes a time-scale which is calculated as follows:

$$\tau_{new} = \sqrt{\frac{\overline{E'}}{\overline{\varepsilon'}}\frac{\overline{T'^2}}{\overline{\varepsilon_T'}}}$$

The time scale τ_{new} is the geometrical mean of the thermal time scale $\frac{\overline{T'^2}}{\overline{\varepsilon_T'}}$ and mechanical time scale $\frac{\overline{E'}}{\overline{\varepsilon'}}$. The model for $\overline{u_3'T'^2}$ as given in eqn (2.10) was successfully validated with RBC.

Even the 3 or 4-equation models involve the transport equation for $\overline{E'}$. Therefore, any model improvements in the $\overline{E'}$-equation will also improve all the other more complicated models. Thus, in the subsequent chapter the terms in this transport equation will be investigated using the DNS data of IHL and RBC.

3 DNS and analysis of a RANS model for $D_{E,t}$

This chapter deals with the DNS data of IHL and RBC, and the standard gradient-diffusion RANS model for $D_{E,t}$, and is arranged as follows:

The first section defines the problem and introduces some of the important literature for such flow types. Subsequently, a short mathematical description of DNS, validation of a DNS of IHL, and some statistical features of IHL and RBC are analyzed from the DNS data and are presented. Finally, the terms in the transport equation for $\overline{E'}$ and the gradient-diffusion model for $D_{E,t}$ will be analyzed using the DNS data.

3.1 The flow types

3.1.1 Internally heated fluid layers (IHL)

Natural convection and heat transfer in a fluid layer of height $\hat{D}$ which is heated internally by a homogeneous volumetric energy source $\hat{q}_v$ are of interest in certain geophysical, astrophysical, and technological problems. For example, it is also important in the safety analysis of nuclear reactors to explain the phenomena of cooling of a molten core. In this case the fluid is bounded between the two isothermal parallel plates (its own solid crust) at a temperature lower than the molten core (the freezing temperature), see figure 3-1.

The important dimensionless numbers which characterize the physical problem are the internal Rayleigh number Ra_I and the Prandtl number $Pr = \nu / \kappa$. The critical internal Rayleigh number for the onset of convection is 3.74×10^4 (see e.g. Kulacki and Richards (1985)). In practical applications Ra_I can attain very high values and simulations of IHL get their importance in these cases only at high Ra_I.

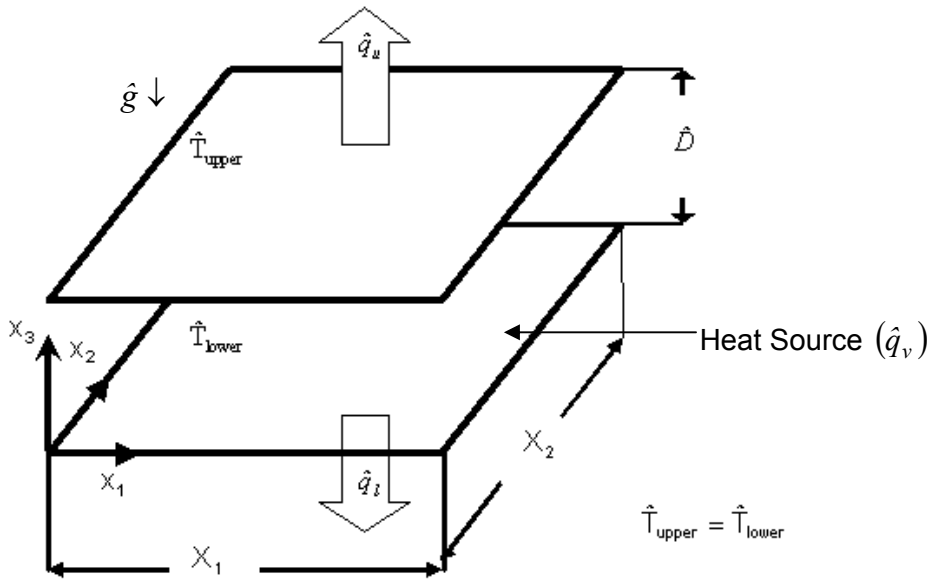

Fig. 3-1 Geometry as in TURBIT to describe internally heated fluid layers (IHL).

In IHL the maximum temperature difference across the height of the channel $\Delta\hat{T}_0$ is not known a priori for a given $\hat{q}_v$, and hence Da is also not known (see section 2.1). For fully developed convection, where $\int_V \hat{q}_v dV$ is completely removed at the top and bottom wall, it follows by an energy balance that Da equals the sum of the Nusselt numbers (Nu), i.e. $Da = Nu_{upper} + Nu_{lower}$. This is used as a measure for $\Delta\hat{T}_0$. Another dependent dimensionless number is the Grashof number $Gr = Ra_I / (Pr\, Da)$.

Kulacki and Goldstein (1972) had experimentally investigated this flow type. They obtained correlations between Nu and Ra_I at the upper and lower walls. These are as follows,

$$\left.\begin{aligned} Nu_{lower} &= 1.428\, Ra_I^{\,0.094}, \\ Nu_{upper} &= 0.329\, Ra_I^{\,0.236}. \end{aligned}\right\} \qquad (3.1)$$

Regarding the measurement of turbulent quantities in IHL, no reliable information is available so far for the fluid layer with equal temperature at the lower and upper wall.

Among the numerical studies of IHL, Grötzbach (1982a, 1987, 1989) and Schmidt et al. (1997) had performed several accurate DNS with water (Pr =7) up to $Ra_I = 10^8$

which is fully turbulent. Dinh and Nourgaliev (1997) had found that the standard Reynolds model $\overline{E'} - \overline{\varepsilon'} - Pr_t$ fails seriously in reproducing the corresponding mean temperature or Nu. This is due to the presence of counter gradient heat flux and counter gradient $\overline{E'}$ flux. Thus, DNS and LES are regarded as the promising alternatives. Recently, Tasaka and Takeda (2005) have studied the effects of a non-uniform internal heat source distribution on the onset of convection. They have considered an isothermal upper wall and an adiabatic lower wall. Based on the linear analysis, they have investigated the conditions for the onset of convection, namely, the critical Rayleigh number and the critical wave number.

In the previous simulation of IHL it was already tried to reach $Ra_I = 10^9$ and Pr=7 (see Schmidt et al. (1997)), but the periodic length ($X_{1,2}$) was not enough to record all the large scale structures. Therefore, during the present work a new DNS of IHL with $Ra_I = 10^9$ and Pr=7 has been performed. Here a larger domain size has been used and the resolution has been adapted. This will be presented in the subsequent section.

3.1.2 Rayleigh-Bénard convection (RBC)

Turbulent RBC occurs in a horizontal layer of fluid submitted to a gravity field, heated from the bottom and cooled from the top (see figure 3-2). In this case the fluid layer is unstably stratified throughout the height of the channel.

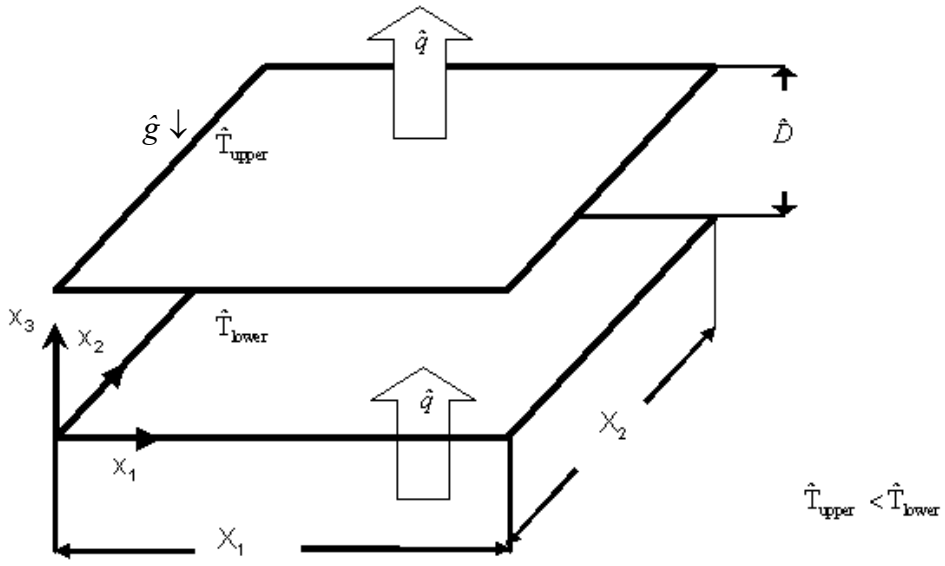

Fig. 3-2 Geometry as in TURBIT to describe Rayleigh-Bénard convection (RBC).

The independent dimensionless numbers which characterize this physical problem are the external Rayleigh number (Ra_E) and the Prandtl number (Pr). Another dependent dimensionless number is the Grashof number $Gr = \frac{Ra_E}{Pr}$. For Ra_E less than a critical value of about 1700 the fluid layers is at rest. At a higher Ra_E slightly greater than the critical value, steady laminar convection in the form of cells and rolls occurs. Increase in Ra_E causes the flow to become unsteady and complex (see e.g. Clever and Busse (1974)). It is generally accepted that the flow is fully turbulent for $Ra_E \geq 10^5$ at moderate Pr.

Krishnamurti (1970a, 1970b) had experimentally investigated this flow type for a wide range of Pr and Ra_E. She reported the occurrence of distinct transitions before the flow becomes turbulent. Later on, Clever and Busse (1974, 1981) had carried out a detailed theoretical study of this flow type even at low Pr. According to the authors, transition from the steady convection to time-dependent convection depends strongly on the wave-number of the structures.

Among the numerical studies, Grötzbach (1982b) had reported the first DNS of turbulent RBC with air (Pr=0.71). He achieved $Ra_E = 3.8 \times 10^5$ and presented a detailed account of the structures which appear in this flow type. He compared the DNS data with the experimental data of Deardorff and Willis (1967). He had also reported the reversal in the mean temperature profile in the central region at low Ra_E. This was attributed to the coalescence of larger number of warm 'blobs' near the cold wall and of cold 'blobs' near the warm wall. It was not observed at higher $Ra_E = 3.8 \times 10^5$. Afterwards, Eidson (1985) had performed a LES study of RBC up to $Ra_E = 2.5 \times 10^6$. In this study, he used a modified version of the Smagorinsky model. He compared the simulation results also with the experimental measurements of Deardorff and Willis (1967).

At a later stage Domaradzki and Metcalfe (1988) had investigated the effect of shear on turbulent RBC in a plane Couette flow with DNS. They found that at moderate $Ra_E (\approx 10{,}000 - 50{,}000)$ shear tends to organize the flow into quasi-two dimensional

rolls parallel to the mean flow which enhances the heat transfer. While at a higher $Ra_E (> 150{,}000)$, shear tends to disrupt the formation of convective plumes which reduces the heat transfer. Nieuwstadt (1990) in a review paper had discussed some of the performed DNS and LES of free convection which also includes RBC. He concluded that the modeling studies are quite successful in simulating the characteristic features of these buoyant flow types. This is because of the fact that the large-scale flow structures like rolls, cells or thermals can be accurately resolved. Later on, Wörner (1994) had carried out DNS of RBC with Pr =0.006 at $Ra_E = 3{,}000$, 6,000, 12,000 and 24,000.

Based on a DNS study of RBC with an aspect ratio (length/height) of 6:6:1, Kerr (1996) had explained the transition from the soft to hard turbulence regime. He found that in the hard turbulence regime $Nu \sim Ra_E^{2/7}$. Kimmel and Domaradzki (2000) had presented LES of RBC up to $Ra_E = 10^8$ based on an estimation model. According to the authors, this approach is more accurate than the Smagorinsky model. Further, they showed that it did not require any wall function for correct near wall behavior of the flow. It has been observed that, at a lower Ra_E the plumes are continuous. But with the increase of Ra the plumes break up into smaller scales. Hartlep et al. (2003) had reported diverse DNS of RBC up to $Ra_E = 10^7$ with $Pr = 0.7$ and 7. They found that the structures can be classified as large or small scale as a result of a gap in the spatial spectra of the heat flux. Moreover, they showed that, with the increase of Ra_E the spectral gap is more pronounced. Recently, Otić and Grötzbach (2004) have reported a DNS of RBC with $Ra_E = 10^5$ and Pr =0.025. They found that the temperature field even at this Ra_E and Pr is considerably influenced by the conduction. They used their data for intensive statistical analysis of closure terms and model development.

In this section some of the important literature for IHL and RBC is discussed. The dimensionless numbers which characterize these flow types are also presented. Hereafter, instead of Ra_I or Ra_E they will be simply referred to as Ra.

3.2 Description of DNS

3.2.1 Basic equations

In order to perform a DNS of IHL with $Ra = 10^9$ and Pr = 7 the TURBIT code is used (see e.g. Grötzbach (1987), Wörner (1994) and others.). This solves the time-dependent, three-dimensional conservation equations of mass, momentum and energy. The Boussinesq approximation is adopted. The non-dimensional form of these equations are integrated over the mesh volume $V = \Delta x_1 \Delta x_2 \Delta x_3$, which results in the volumetric average for any variable y,

$$ {}^{v}\bar{y} = \frac{1}{\Delta x_1 \Delta x_2 \Delta x_3} \iiint_{\Delta x_1 \Delta x_2 \Delta x_3} y(x_1' x_2' x_3')\, dx_3' dx_2' dx_1'. \tag{3.2} $$

Using the Gaussian theorem, the volume average of the partial derivatives is transformed into a finite-difference form of the surface averaged values ${}^{i}\bar{y}$, where i denotes the index of the direction normal to the respective mesh cell surface ${}^{i}F = V / \Delta x_i$ (Schumann (1973, 1975)),

$$ {}^{v}\overline{\frac{\partial y}{\partial x_i}} = \frac{1}{\Delta x_i}\left[{}^{i}\bar{y}\left(x_i + \frac{\Delta x_i}{2} \right) - {}^{i}\bar{y}\left(x_i - \frac{\Delta x_i}{2} \right) \right] = \delta_i {}^{i}\bar{y}. \tag{3.3} $$

Application of the operators (3.2) and (3.3) to the well known conservation equations provides the following formulae,

$$ \left.\begin{aligned} \delta_i {}^{i}\overline{u_i} &= 0, \\ \frac{\partial {}^{v}\overline{u_i}}{\partial t} + \delta_j {}^{j}\overline{u_i u_j} &= \frac{1}{\sqrt{Gr}} \delta_j {}^{j}\overline{\left(\frac{\partial u_i}{\partial x_j} + \frac{\partial u_j}{\partial x_i} \right)} - \delta_i {}^{j}\bar{p} + \delta_{i3} {}^{v}\overline{(T - T_{ref})}, \; i = 1,2,3, \\ \frac{\partial {}^{v}\overline{T}}{\partial t} + \delta_j {}^{j}\overline{T u_j} &= \frac{1}{Pr\sqrt{Gr}} \delta_j \left\{ {}^{j}\overline{\frac{\partial T}{\partial x_j}} \right\} + \frac{Da}{Pr\sqrt{Gr}}. \end{aligned}\right\} \tag{3.4} $$

In the above equation, δ_{i3} is the Kronecker delta which gives 1 if $i = 3$ and 0 otherwise. The averaged non-linear terms can be rewritten using the definitions implied by the volume-averaging procedure. The averaging operator as explained in eqn (3.2), splits the velocity and temperature into spatial averages directly resolved by the grid, ${}^{j}\overline{u_j}$, ${}^{v}\overline{T}$, with typical wavelengths larger than Δx_i and into 'sub-grid scale' parts, not resolved by the grid which are denoted by $u_j^{'} = u_j - {}^{j}\overline{u_j}$ and $T' = T - {}^{v}\overline{T}$, respectively, with typical wavelengths smaller than Δx_i . Thus, using this operator one obtains a formally identical expression as in eqn (2.2) i.e.

$$\left.\begin{aligned} {}^{j}\overline{u_i u_j} &= {}^{j}\overline{u_i}\,{}^{j}\overline{u_j} + {}^{j}\overline{u_i' u_j'}\,, \\ {}^{j}\overline{u_j T} &= {}^{j}\overline{u_j}\,{}^{j}\overline{T} + {}^{j}\overline{u_j' T'} \end{aligned}\right\}. \tag{3.5}$$

The first term on the right hand side of eqn (3.5) represents the spatially resolvable part of the instantaneous turbulent stresses and heat fluxes, respectively. The second term represents the sub-grid scale (SGS) parts to be modeled. An important point need to be noted that, unlike the common volume-averaging procedure without application of Gaussian theorem, in the Schumann approach the sub-grid scale fluxes are not averaged over the mesh cell volumes but over single surfaces of mesh cells. This has an important advantage, to deal with anisotropic grids (Grötzbach (1977)). The other advantage, in contrast to Leonard's filtering procedure, no Leonard terms, in other words, no cross correlations between sub-grid scale and resolved scale variables appear, because of the linear filter function; in addition it has the advantage of Galilean invariance property (Speziale (1985)).

3.2.2 Turbulence assumptions for DNS

The unknown SGS stresses ${}^{j}\overline{u_i' u_j'}$ and heat fluxes ${}^{j}\overline{u_j' T'}$ in the eqn (3.5) are those, which are not resolved by the grids. Thus they tend to zero if the resolution is high enough or $\Delta x_i \to 0$. This is true in particular for the flows with low Ra , where the size of smaller vortices are not much smaller than the channel width and hence can be resolved better than that of flows with high Ra , where the size of vortices varies from very large (comparable with the channel width) to a very small one. In DNS the SGS

terms are neglected which means ${}^{j}\overline{u_i'u_j'}$ = ${}^{j}\overline{u_j'T'}$ =0. As a result, the entire system of eqn (3.4) does not contain a single adjustable parameter except for problem-identifying parameters Gr and Pr. Numerically, there exist open parameters that are the domain size and the mesh width. It must be ensured that the mesh-width resolves even the smallest relevant turbulence elements to justify neglecting the SGS-terms and that the domain size records the largest turbulent scales (Grötzbach (1981, 1983)).

3.2.3 Boundary and initial conditions

Using the above assumptions in eqn (3.4) results in a closed system of the five coupled partial differential equations. These equations need to be solved for $\underline{u} = (u_1, u_2, u_3), p$ and T. The no-slip conditions for the velocity field at both impermeable horizontal walls are used, i.e.

$$\underline{u}(x_1, x_2, x_3 = 1, t) = \underline{u}(x_1, x_2, x_3 = 2, t) = 0 .$$

For the temperature field in IHL equal wall temperatures are used i.e.

$$T(x_1, x_2, x_3 = 1, t) = T(x_1, x_2, x_3 = 2, t) = 0 .$$

In RBC,

$$T(x_1, x_2, x_3 = 1, t) = 1 \text{ and } T(x_1, x_2, x_3 = 2, t) = 0 .$$

In the above description $x_3 = 1$ indicates the lower wall and $x_3 = 2$ indicates the upper wall.

The discretization of these boundary conditions in the convection term of the conservation equations as given in eqn (3.4) creates no serious problem as they fulfill on a staggered grid these equations. On the other hand the viscous and thermal diffusion terms require special care. The boundary conditions for the gradient of velocities for the wall shear stresses, gradient of temperature for the wall heat fluxes are defined as follows (from eqn (3.4)),

$$\overline{{}^{3}\tau_{i3}}\Big|_{l,u} = -\frac{1}{\sqrt{Gr}}\,\overline{{}^{3}\frac{\partial u_i}{\partial x_3}}\Big|_{l,u}, \text{ with } i = 1, 2, 3.$$

$$\overline{{}^{3}q}\Big|_{l,u} = -\frac{1}{Pr\sqrt{Gr}}\,\overline{{}^{3}\frac{\partial T}{\partial x_3}}\Big|_{l,u}.$$

In the above equations 'l' and 'u' stands for the lower and upper wall, respectively. As the fine grid resolves the viscous and thermal boundary layer, the above operator can be numerically calculated with first order finite difference approximations.

To simulate the convection in a fluid layer with a large horizontal extension, periodic boundary conditions are used. Let us consider N_1 and N_2 are the number of mesh cells in x_1 and x_2 directions, respectively. Assuming $X_i (i = 1,2)$ as the size of the computational domain along the horizontal directions $x_i (i = 1,2)$ which are defined as,

$$\begin{aligned} X_1 &= N_1\ \Delta x_1, \\ X_2 &= N_2\ \Delta x_2 \end{aligned}.$$

Here $\Delta x_{1,2}$ indicate the grid widths in the $x_i (i = 1,2)$ direction. In the TURBIT code the periodic boundary conditions are used along the horizontal directions for any variable y:

$$y(x_1, x_2, x_3) = y(x_1 + m\,X_1,\ x_2 + n\ X_2,\ x_3) \text{ with } m, n \in Z \qquad (3.6)$$

Where Z denotes the set of non-negative integer.

In order to perform a DNS of IHL with $Ra = 10^9$ and Pr =7, the simulation results from a similar problem with $Ra = 10^8$ and Pr =7 at time $t_i = 264.29$ from Schmidt et al. (1997) have been used as the initial condition. These results are interpolated to the new grid. Such initial values are very close to realistic fields and need short computing time for redistribution and redevelopment of an equilibrium state. Also the IHL with $Ra = 10^8$ and Pr =7 has been further simulated starting with the results for this case at time $t_i = 264.29$.

3.3 Selection of grid widths for a DNS of IHL and case specifications

The spatial discretization required for DNS is explained in Grötzbach (1981, 1983). In case of IHL with $Pr = 7.0$ the thickness of thermal boundary layers are smaller than that of the viscous boundary layers. Hence, the vertical grid widths near the upper and lower walls $\Delta x_{3,\,lower\,/\,upper}$ should be adequate to resolve the thermal boundary layers. With increasing Ra the thickness of upper and lower thermal boundary layers decreases (see figure 3-10). Therefore $\Delta x_{3,\,lower\,/\,upper}$ have to be accordingly reduced to resolve the steep temperature gradients near the walls. According to Grötzbach (1987) in order to record adequately the wall heat fluxes the allowable vertical grid widths near the lower wall $h_{3,lower}$ and near the upper wall $h_{3,upper}$ are given by,

$$\Delta x_{3,lower} \le h_{3,lower} = \frac{\hat{D}}{3Nu_{lower}} \quad \text{and} \quad \Delta x_{3,upper} \le h_{3,upper} = \frac{\hat{D}}{3Nu_{upper}}. \tag{3.7}$$

The eqn (3.7) was deduced by discretizing the thermal boundary layers by three nodes. To analyze closure terms, much finer grids near the walls may be required. According to the same author the maximum allowable mean grid width $h_{max} = \left(\Delta x_1 \Delta x_2 \Delta x_3\right)^{1/3}$ for an isotropic grid in IHL is given by,

$$h_{max} = 3.45\left(\frac{\kappa^3}{\overline{\varepsilon'}_{max}}\right)^{0.25}, \text{ with } \overline{\varepsilon'}_{max} \approx \left(Nu_u - Nu_l\right)\frac{Ra}{Re^3\, Pr^2\, Da}. \tag{3.8}$$

In eqn (3.8) $\overline{\varepsilon'}_{max}$ indicates the maximum value of dissipation which is calculated near the upper wall.

The grid widths of the DNS of IHL with different Ra and Pr =7 performed by Schmidt et al. (1997) and in this thesis are shown in the figure 3-3. The lines indicate the maximum allowable mean grid width h_{max} as in eqn (3.8) and $h_{3,lower}$ and $h_{3,upper}$ as in eqn (3.7).

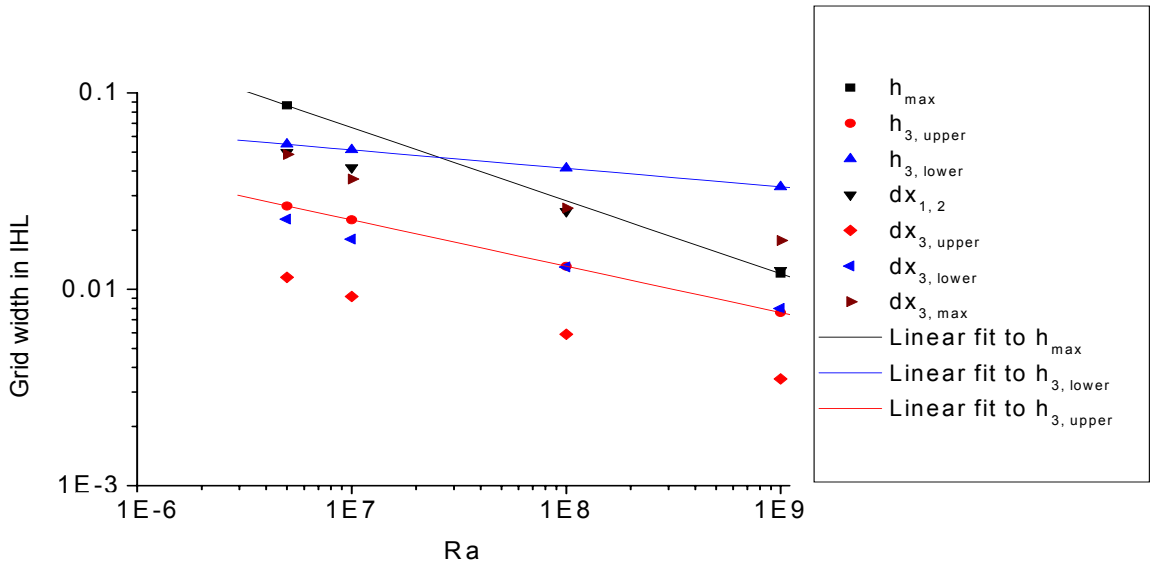

Fig. 3-3 Plot of the grid widths for DNS of IHL with different Ra and Pr =7 (dx_i is used instead of Δx_i).

The figure 3-3 also shows that all the selected grid widths are either smaller than or equal to the corresponding limiting values except the maximum value of the grid width $\Delta x_{3,\max}$ in the vertical direction. In contrast, $\Delta x_{3,lower} < h_{3,lower}$ and $\Delta x_{3,lower} < h_{3,lower}$ indicate that the presence of more than 3 nodes in the thermal boundary layers close to the lower and upper walls is achieved.

Table 1 shows the different cases of IHL which are explained in sub-section (3.2.3).

IHL	Ra	Pr	$X_{1,2}/\hat{D}$	$\Delta x_{1,2}$	$\Delta x_{3,lower/upper}$	$N_1 = N_2$	N_3	t_{final}
IN1E8	10^8	7	4	0.025	lower: 0.012 upper: 0.0057	160	55	450.714
IN1E9	10^9	7	4	0.0125	lower: 0.008 upper: 0.0035	320	77	361.86

Table 1: Case specification of IHL.

Here, the node numbers $N_{1,2}$ required at least in the $x_{1,2}$ directions are:

$$N_{1,2} \geq \frac{X_{1,2}}{h_{max}}.$$

The node number N_3 required in the x_3 direction can be estimated for a non-equidistant grid by starting with $h_{3,lower/upper}$ from the walls and slowly increasing the grid width up to h_{max}. The last column in table 1 shows the final non-dimensional time up to which the simulations are performed starting from the corresponding initial data. The DNS of IHL with $Ra = 10^8$ and Pr =7 requires about 13 hours of computational time on the Fujitsu/Siemens VPP5000 to proceed from $t_i = 264.29$ to t_{final} = 450.714. On the other hand, the DNS of IHL with $Ra = 10^9$ and Pr =7 needs 37 hours of computational time on the VPP5000 to proceed from $t_i = 264.29$ to t_{final} =361.86.

Table 2 shows the DNS datasets of IHL and RBC which will be used in the subsequent sections and chapters.

Flow Type	Ra	Pr	**Source of the DNS data**
RBC	10^5	0.025	Otić, Grötzbach and Wörner (2005)
RBC	6.3×10^5	0.71	Wörner (1994)
IHL	$5\times10^6, 10^7, 10^8$	7	Wörner, Schmidt and Grötzbach (1997)
IHL	10^9	7	new simulation

Table 2. DNS datasets used in the analysis.

Some of the cases as mentioned in table 2 are discussed in the context of table 1. The sources of the DNS datasets of IHL and RBC are given in the last column of this table. These include the DNS data of RBC from Otić et al. (2005) with liquid metal Pr =0.025 and from Wörner (1994) with a standard fluid like air Pr =0.71.

3.4 Statistical evaluation of DNS data

In the statistical analysis modules of the TURBIT code $\langle\ \rangle$ has been employed to average the variables over the homogeneous horizontal planes and over time and

$( )''$ indicates their fluctuating parts. From application of these operators to any variable y follows,

$$y = \langle y \rangle + y'' .$$

Due to horizontal averaging, $\langle y \rangle$ and y'' depend only on x_3.

Flow Type	Ra	N_{time}	t_{max}	N_{tav}	Δt_{av}
RBC	10^5	27,000	617.265	16	86.502
RBC	6.3×10^5	5,200	204.425	20	20.155
IHL	5×10^6	16,560	78.228	12	46.007
IHL	10^7	8,800	111.258	36	17.594
IHL	10^8	21,620	450.714	30	82.299
IHL	10^9	21,560	360.01	11	40.903

Table 3. DNS Data used for the statistical evaluation

In table 3, N_{time} is the number of time steps of the performed DNS within the final time interval Δt_{av} up to the maximum time t_{max}. N_{tav} is the number of time steps distributed within the time interval Δt_{av} over which mean values have been taken. In the analysis, physical variables at every analyzed time points are averaged over the horizontal plane. In the time averaging these surface averaged quantities are averaged over N_{tav}.

3.5 Validation of the new DNS of IHL

This section deals with the validation of the DNS of IHL with $Ra = 10^9$ and Pr=7. Only Nu is available from experiments for this set of parameters; there is no reliable information regarding the mean temperature or any other turbulent quantities. Therefore, the validation is based on the previous experience of this flow type at lower Ra (Grötzbach (1982a) and (1987)). Considering these studies as the basis and the criteria that are used, validation of the DNS of IHL has been carried out as follows.

3.5.1 Time development

Starting with the initial data as explained, the time integration of IHL has been carried out. This generates a restart-file which is further integrated in time until the flow becomes steady. During this procedure the time dependent integral quantities e.g. the surface averaged heat fluxes close to the upper and lower walls ${}^{3}\overline{q}_{l}$ and ${}^{3}\overline{q}_{u}$, the volume averaged (over complete channel) kinetic energy and temperature , ${}^{v}\langle E \rangle$ and ${}^{v}\langle T \rangle$ are obtained. These can be used to characterize the steady state of the flow field.

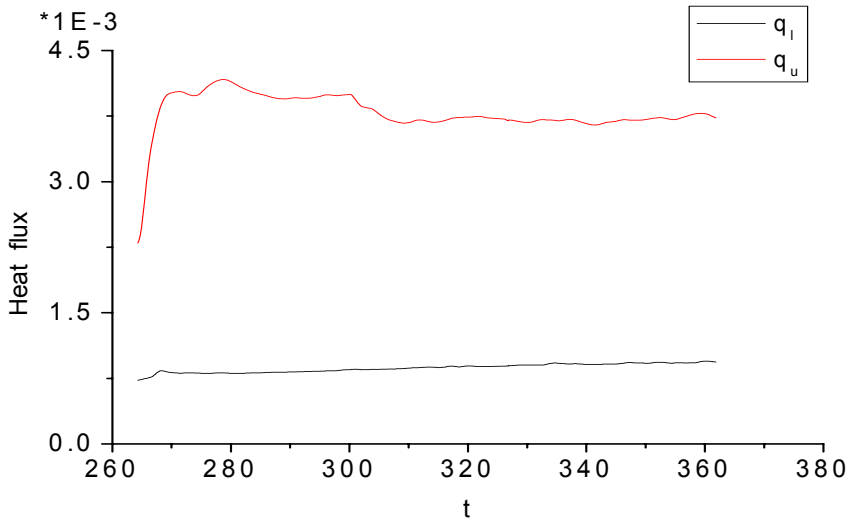

Fig. 3-4 Time development of the surface averaged wall heat fluxes evaluated from the DNS data of IHL with $Ra = 10^9$.

Figures 3-4, 3-5 and 3-6 show the time development of the surface averaged wall heat fluxes, the volume averaged total kinetic energy and temperature in IHL. In each of these curves 843 values are plotted beginning at the time 264.29 and ending at the time 361.86. Starting from the initial condition the development of the flow field is represented by the sharp rise in the heat flux at the upper wall, kinetic energy, and a small increase in temperature. After $t \approx 270$ the flow field tends towards the steady state.

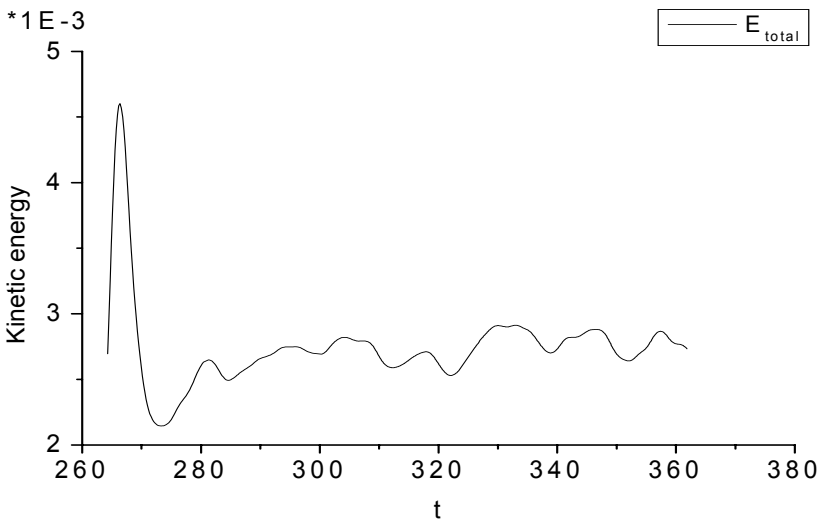

Fig. 3-5 Time development of the volume averaged total kinetic energy evaluated from the DNS data of IHL.

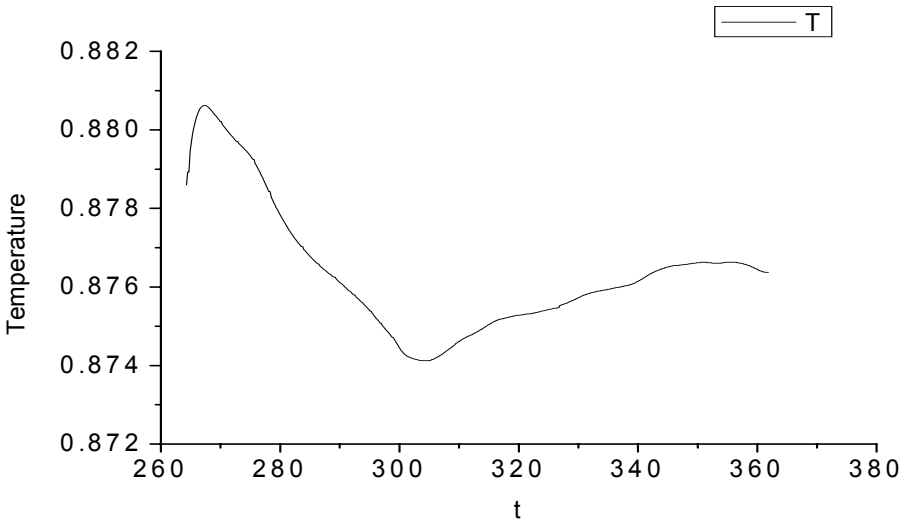

Fig. 3-6 Time development of the volume averaged temperature of IHL.

In the figures 3-5 and 3-6, the slight increase in the volume averaged kinetic energy and temperature with time (t) indicates that for more accurate analyses the simulation should be proceeded to achieve the accurate fully developed steady state.

This DNS of IHL was performed to develop and analyze an extended model for the turbulent diffusion of $\overline{E'}$ which will be discussed in the subsequent chapters. On the other hand, the time development of the different characteristic integral quantities shows that the flow field in this case has not yet fully reached the steady state. Further simulation of this case was not possible during the course of the present work. As a result, the available DNS data of IHL with $Ra = 10^9$ and $Pr = 7.0$ may not be accurate enough for the statistical evaluation of the RANS model for the turbulent

diffusion of $\overline{E'}$. Hence, the existing DNS data of IHL at a lower $Ra\left(10^7, 10^8\right)$ at same Pr will be used for the deduction and evaluation of the model for the turbulent diffusion of $\overline{E'}$.

3.5.2 Domain size for resolving the large scales

In order to investigate the domain size which is required to resolve the large scale structures the two-point correlations of the velocity fluctuations are considered. These correlations in the x_1 direction are defined as follows:

$$R_{[i][i]}(\Delta x_1) = \frac{\left\langle {}^{i}\overline{u_{[i]}}'(x_1, x_2, x_3)\, {}^{i}\overline{u_{[i]}}'(x_1 + \Delta x_1, x_2, x_3)\right\rangle}{\left\langle {}^{i}\overline{u_{[i]}}'^{2}(x_1, x_2, x_3)\right\rangle}.$$

[ ] indicates no Einstein-summation over i.

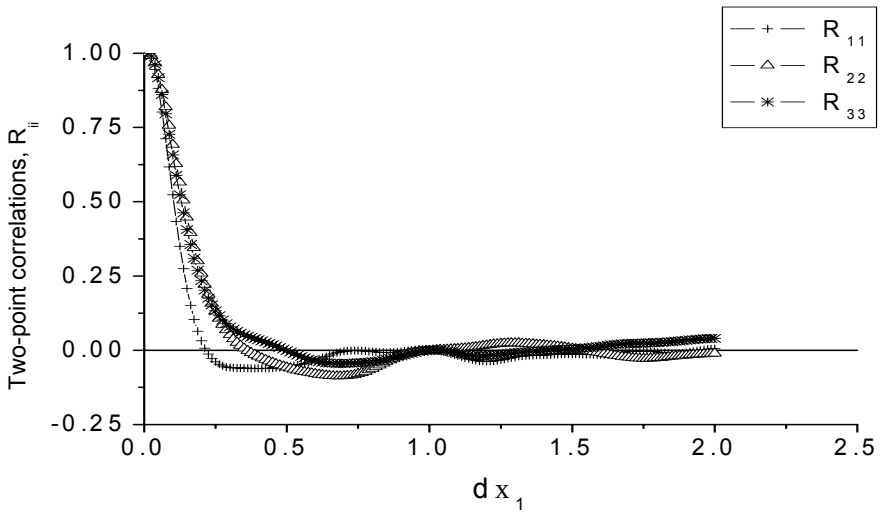

Fig. 3-7 Two-point correlations R_{ii} of the velocity fluctuations in IHL at $x_3 = 1.52$ (here 'd' is used instead of Δ).

The figure 3-7 depicts that the two-point correlations near the mid-plane at $x_3 = 1.52$ are very close to zero over a wide range in the x_1 direction up to half the periodic length $\frac{X_1}{2}$. This implies that the assigned periodic length $X_1 = 4$ (see Table 1) is large enough to reach statistical independence within the different zones of the recorded flow volume. Therefore, the selected domain size $X_{1,2}$ is considered as sufficient.

3.5.3 Vertical grid width for resolving the thermal boundary layers

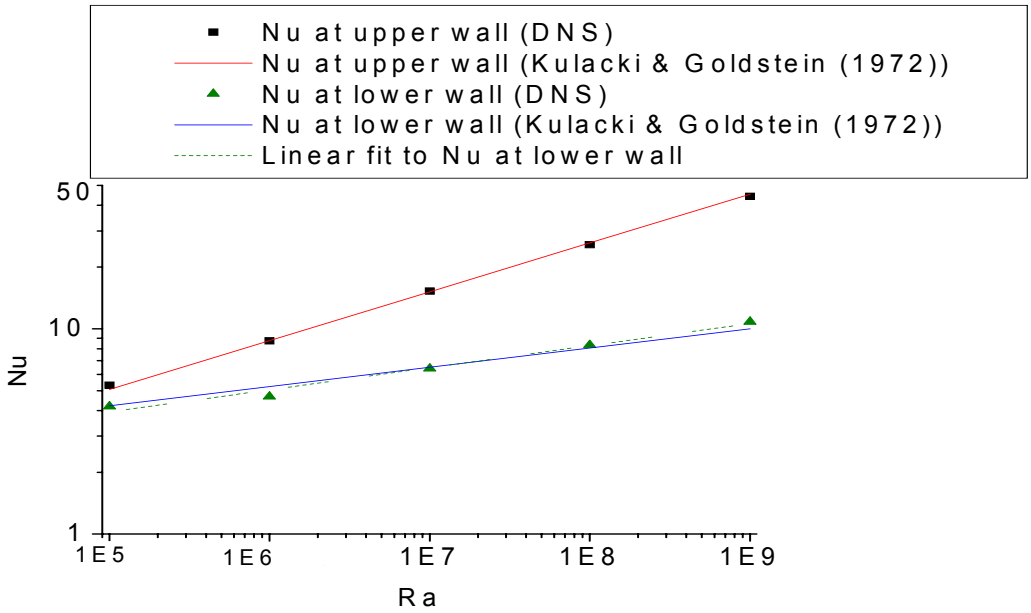

Fig. 3-8 Nusselt number over Rayleigh number in IHL.

Figure 3-8 shows the comparison between the data analyzed from the DNS and the experimental value of Nu represented by the correlations as in eqn (3.1) at the upper and lower walls. The Nu analyzed from the DNS data of IHL with $Ra = 10^9$ and Pr =7 is in good agreement with the experimental value of Nu at the upper wall. This indicates that the selected vertical grid resolution is sufficient for resolving the steep temperature gradient near the upper wall. The linear fit (dotted line) of Nu at the lower wall indicates the slight difference between the slopes of the experimental and DNS analyzed values of Nu. The difference of about 8% between the DNS and the experimental value of Nu at the lower wall may be attributed to the higher value of $\Delta x_{3,\max}$ in comparison to h_{max} or that the $\Delta x_{1,2}$ should really be somewhat smaller than h_{max} and not only equal to h_{max} (see figure 3-3). A third reason could be due to the still not fully developed flow state.

3.5.4 Grid width for resolving the smallest scales

One of the important tools to analyze the adequacy of the grid resolution for the small scale turbulent fluctuations for a DNS is the one-dimensional energy spectrum of the turbulent fluctuations. The one-dimensional energy spectra of the different velocity fluctuation components at $x_3 = 1.27$ analyzed from the DNS data are shown in figure 3-9.

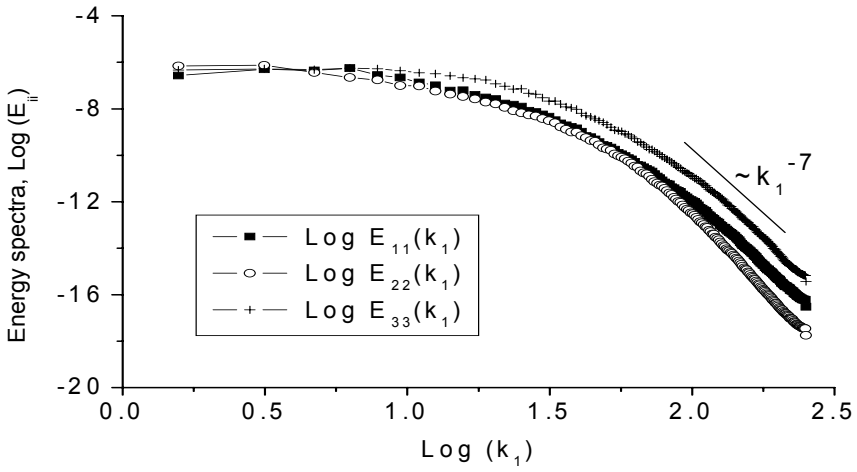

Fig. 3-9 One-dimensional energy spectra of the different velocity fluctuations evaluated from the data of IHL with $Ra = 10^9$ at $x_3 = 1.27$ with $k_1 = 2\pi/x_1$.

Here, k_1 is the wave-number in the x_1 direction. The figure 3-9 shows that most of the energy of the different velocity fluctuations is associated with low wave numbers. The anisotropy between the different velocity fluctuations can be observed except the lowest wave number region close to the lower wall. This figure also reveals that at higher wave-numbers the energy spectra of the velocity fluctuations are having a slope ~ k_1^{-7}. In the highest wave-numbers the energy spectra of the velocity fluctuations are even steeper. This indicates that the selected grid is fine enough to resolve the smallest scales in IHL, because $\int_0^\infty k^2 E(k) dk$ gives the maximum contribution to the dissipation at $E(k) \sim k^{-3}$; this integral converges for a steeper spectrum, i.e. with a slope much steeper than k_1^{-3} it is expected that the dissipation scales are sufficiently resolved. So far the experience shows that a slope ~ k_1^{-7} means that the small scales are very well resolved (see e.g. Grötzbach (1987) for IHL with lower Ra). Thus, it can be excluded that the problem with Nu at the lower wall as in figure 3-8 may be due to large $\Delta x_{1,2}$ values.

These investigations show that the present DNS is better than the previous DNS of IHL with $Ra = 10^9$. It is not perfect, but for basic analysis of the principle behavior of the different closure terms and of related turbulence models it should be applicable.

3.6 DNS results for IHL and RBC

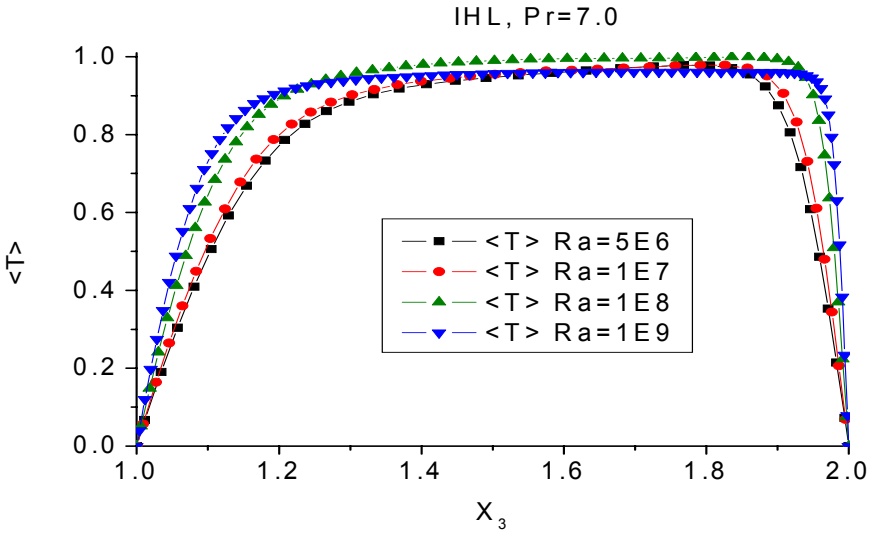

Fig. 3-10 Vertical profiles of the time mean temperature <T> in IHL.

The time mean temperature profiles in IHL with water (Pr=7.0) and at different Ra indicate that the thickness of the upper and lower thermal boundary layers decrease with increasing Ra, see figure 3-10. Moreover, the thickness of the upper thermal boundary layer is smaller than that of the lower thermal boundary layer. The maximum value of the mean temperature occurs near the edge of the upper boundary layer. This thin upper boundary layer is unstably stratified and thus drives the turbulent heat and momentum exchange. Whereas the rest of the region along the vertical direction (downward) is stably stratified that attenuates the turbulent exchange.

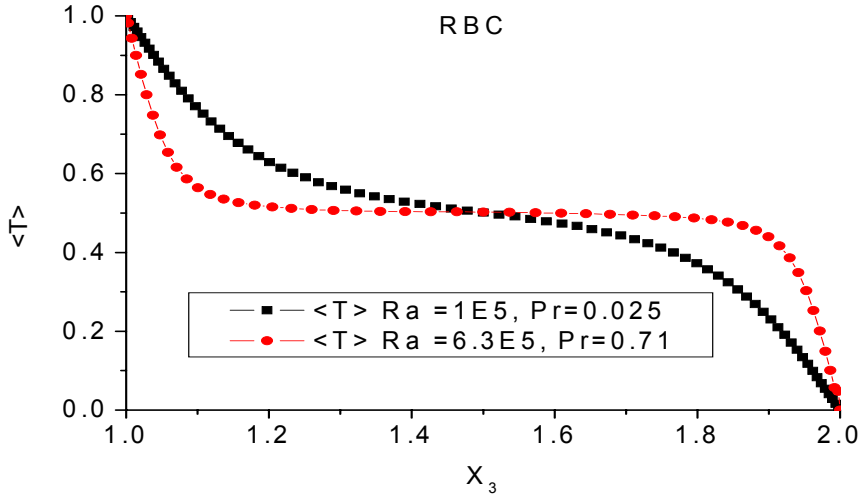

Fig. 3-11 Vertical profiles of the time mean temperature <T> in RBC.

The time mean temperature profiles in RBC at different Ra and Pr show that the fluid layer in RBC is unstably stratified as in figure 3-11. The thickness of thermal boundary layers in RBC with liquid metal (Pr =0.025) are greater than that of RBC with air (Pr =0.71). This indicates that the temperature field in RBC with liquid metal is considerably influenced by conduction even at this large Ra . This can be attributed to the dominance of the large thermal conductivity in the thermal boundary layer and due to the strong damping of the temperature fluctuations in low Pr flows. With further increase of Ra , the vertical profile of the mean temperature in RBC with liquid metal should move towards the profile in RBC with air.

Moreover, Gr in RBC with liquid metal is higher $\left(Gr = 4 \times 10^6\right)$ than that of RBC with air $\left(Gr = 9 \times 10^5\right)$. The statistical features of the velocities including the scales are comparable at about same value of Gr as shown in Wörner (1994). He referred it as the Grashof analogy. Thus, the velocity scales in case of RBC with liquid metal are smaller in comparison to RBC with air. This implies that the dissipation of turbulent kinetic energy in the RBC with liquid metal will extend to higher wave-numbers in comparison to RBC with air and therefore, finer grids are required in the liquid metal case.

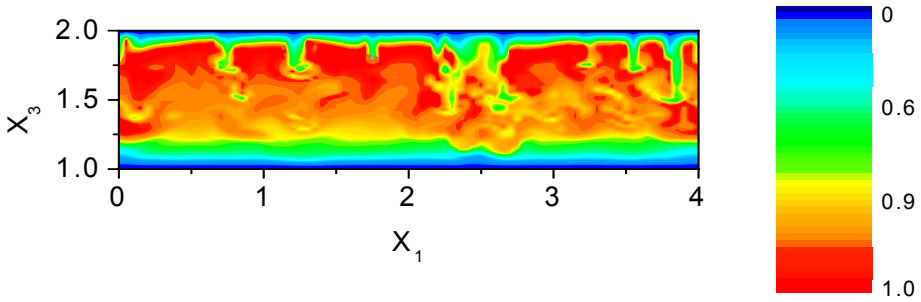

Fig. 3-12 Vertical cut through the calculated temperature field in IHL with $Ra = 10^9$ and Pr =7 at $x_2 = 2.3438$ and t = 361.86.

A snap-shot of the vertical cut of the calculated temperature field in IHL as in figure 3-12 shows the cold fluid close to the upper and lower isothermal walls. The fluid which is confined in between these layers has higher temperature. Due to the Rayleigh-Taylor instability plumes are generated close to the upper wall. These plumes plunge down from the unstable layer deeply into the stable layer.

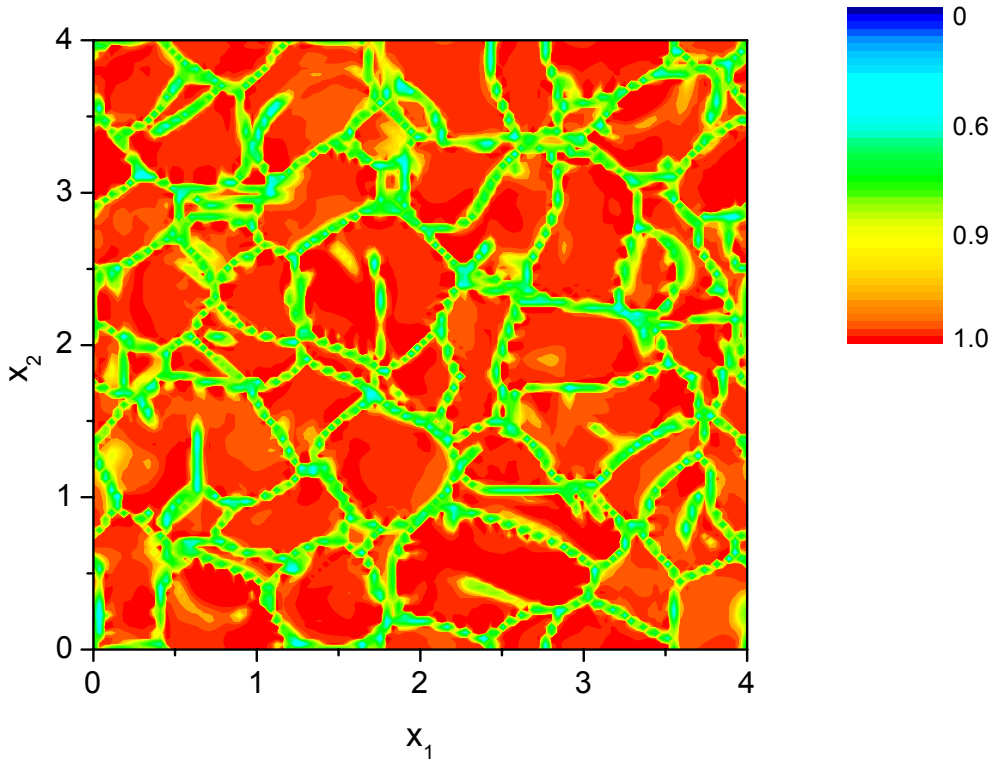

Fig. 3-13 Horizontal cut through the calculated temperature field in IHL with $Ra = 10^9$ and Pr =7 at $x_3 = 1.9483$ and t = 361.86.

In the horizontal cut through the temperature field within the upper thermal boundary layer at the same time in figure 3-13 it can be detected that the plumes form open and closed cells. As the time progresses, new cells or parts of them are formed. Smaller cells finally contract to knots. Some of the plumes have sufficient kinetic energy to reach even the lower stably stratified thermal boundary layer (see figure 3-12). There they re-distribute along the horizontal direction close to the lower wall as a result of continuity, later called “wall damping”.

The cell structures as shown in figure 3-13 can only be found in the upper third of the channel including the upper thermal boundary layer. The critical wavelength of these cell structures at Ra_c is $\lambda_c = \pi / 2$, see Tveitereid (1978). The experiments by Kulacki and Goldstein (1972) and Jahn (1975) reveal that the largest scale of this type of flow decrease with increasing Ra. Based on DNS investigation, Schimdt et al. (1997) had shown that the size of the cells decreases with increasing Ra in IHL with $Pr = 7.0$. Therefore, this aspect can also be used as a qualitative validation of the DNS of IHL.

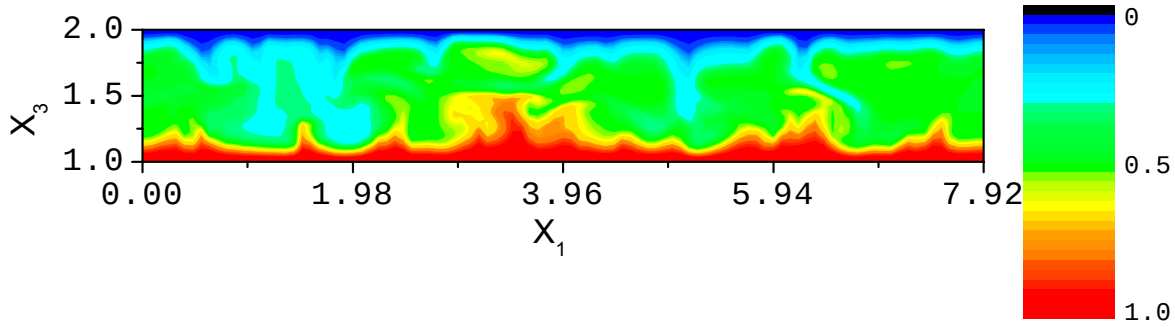

Fig. 3-14 Vertical cut of the calculated temperature field in RBC with $Ra = 6.3 \times 10^5$ and Pr =0.71 at $x_2 = 7.5042$ and t = 203.18.

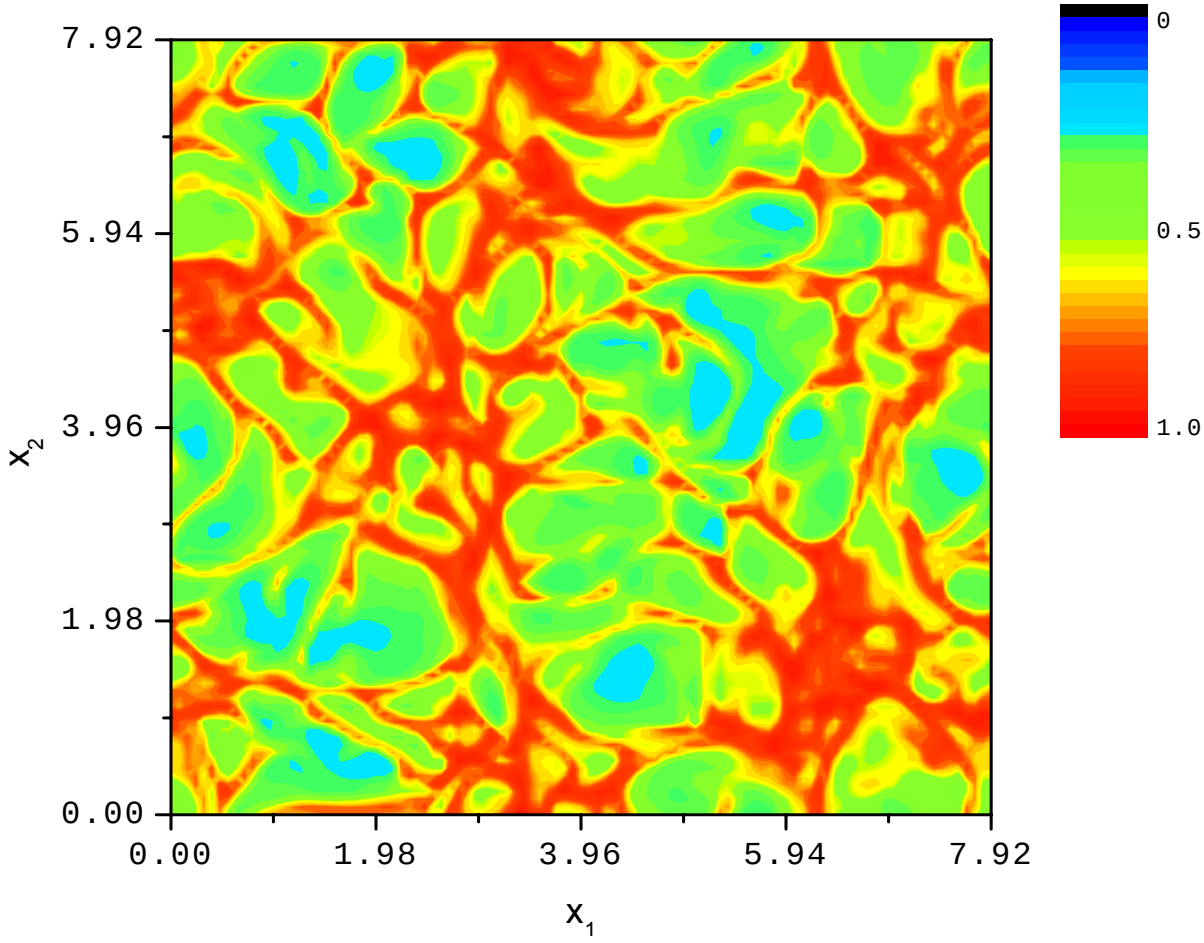

Fig. 3-15 Horizontal cut of the calculated temperature field in RBC with $Ra = 6.3 \times 10^5$ and Pr =0.71 at $x_3 = 1.07$ and t = 203.18.

A snap-shot of the vertical cut of the calculated temperature field in RBC of air as in figure 3-14 shows the cold boundary layer near the upper wall and the hot boundary layer near the lower wall. Hot plumes rise from the lower wall and cold plumes fall from the upper wall. Both plunge into the opposite boundary layers. In this cut the spatial arrangement does not indicate any regular horizontal structures.

The horizontal cut of the instantaneous calculated temperature field which is close to the lower wall is shown in figure 3-15 for the same time. This reveals the presence of cellular structures. These are quite unlikely to be detectable at the mid-plane because of the interpenetration of the plumes coming from both boundary layers (see Grötzbach (1990)). The knots indicate the upward rise of warm fluid and the relatively calm region in between these knots indicates the downward fall of cold fluid which redistributes along the horizontal direction close to the lower wall.

The anisotropy between the RMS velocity fluctuations $u_{rms} = \langle u''^2 \rangle^{1/2} = \langle (u - \langle u \rangle)^2 \rangle^{1/2}$ evaluated from the DNS data of IHL and RBC can be observed in figures 3-16 and 3-17. The anisotropy between these RMS velocity fluctuations is attributed to both the effect of buoyancy and presence of wall in both flow types.

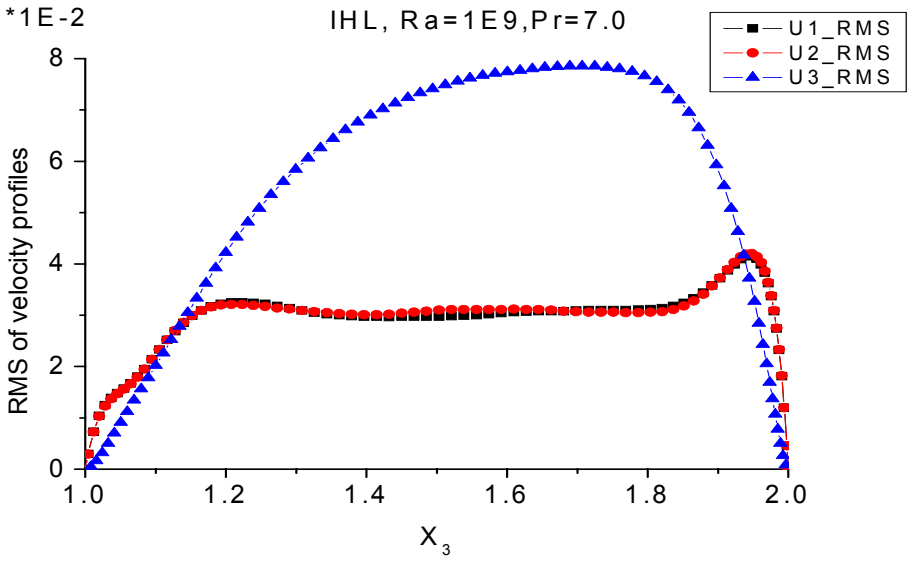

Fig. 3-16 Vertical profiles of the Root Mean Square (RMS) velocity fluctuations in IHL with $Ra = 10^9$.

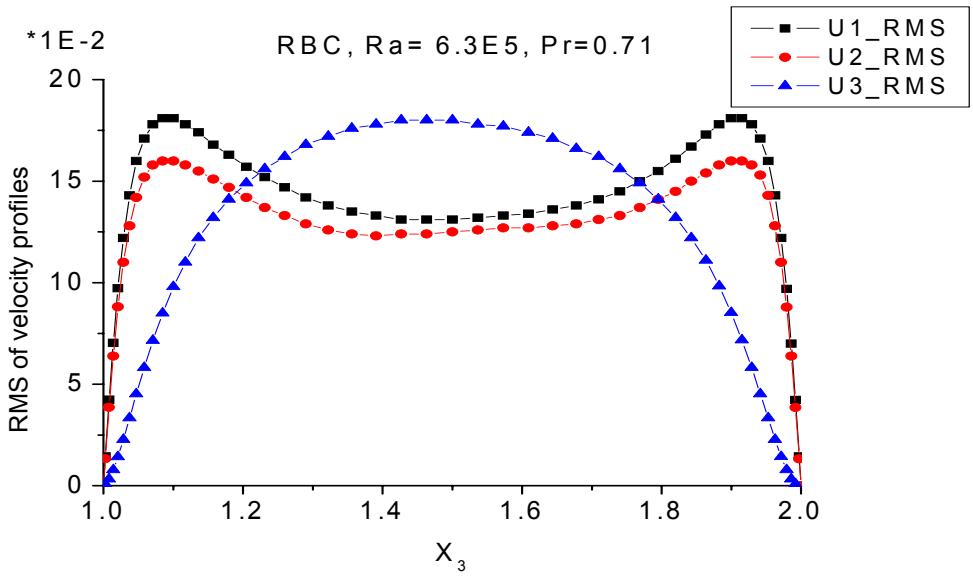

Fig. 3-17 Vertical profiles of the Root Mean Square (RMS) velocity fluctuations in RBC of air.

In IHL, most of the turbulent kinetic energy is produced in the vertical velocity component away from the walls due to the effect of buoyancy (see figure 3-16). The maximum in each of the horizontal components of the RMS values can be observed close to the upper wall in this flow type. Further, there appear small extrusions in the horizontal components close to the lower wall. These extrusions were not prominent in the earlier studies of IHL with $Pr = 7.0$ at lower Ra. With the increase of Ra these extrusions may grow further in IHL. Both the presence of the maximum and the extrusions indicate a considerable amount of energy transfer from the vertical velocity component to the horizontal components close to the walls in IHL. This can be attributed to the pressure strain term in the transport equation for the auto-correlation of the velocity fluctuations (see Grötzbach (1989)).

Similarly, in RBC of air there appear maxima close to the walls in each of the horizontal velocity components. These can also be attributed to the energy transfer from the vertical to the horizontal velocity components in this flow type. Perot and Moin (1995) had given an explanation of this inter-component energy transfer close to the walls based on a DNS investigation of the shear-free turbulent boundary layer. They consider this event is due to the presence of a local region of stagnation that arises from the fluid impinging on the boundary. This region influences the pressure strain term in

the transport equation for auto-correlation which is responsible for the inter-component energy transfer.

The RMS velocity fluctuations of the two horizontal components are not equal in RBC, see figure 3-17. These differences are regarded as a result of the presence of large scale roll structures which could be interpreted from the band-like arrangement of the knots with rising warm fluid and of the more calm areas with down coming cold fluids in figure 3-15. Presence of such structures was observed in Grötzbach (1990) and more recently Hartlep et al. (2003) had described the classification of these structures based on a spectral analysis.

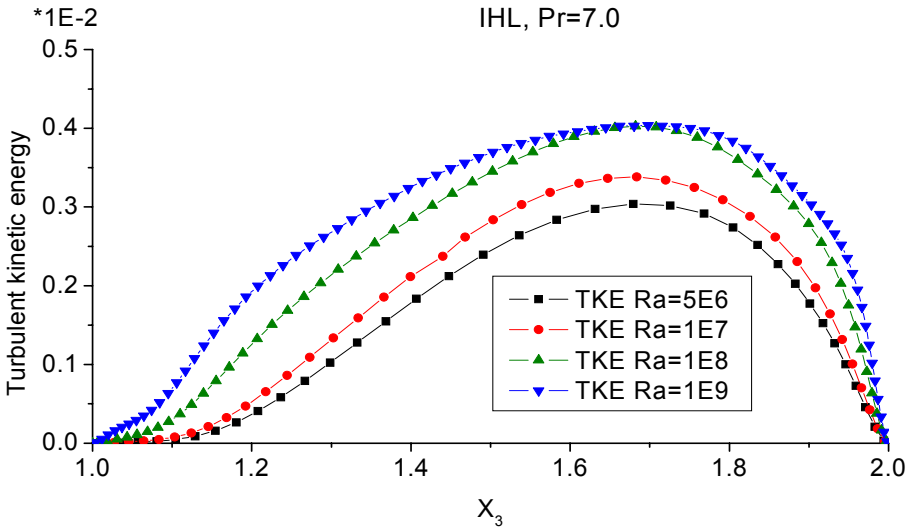

Fig. 3-18 Vertical profiles of $\langle E'' \rangle$ (TKE) evaluated from the DNS data of IHL.

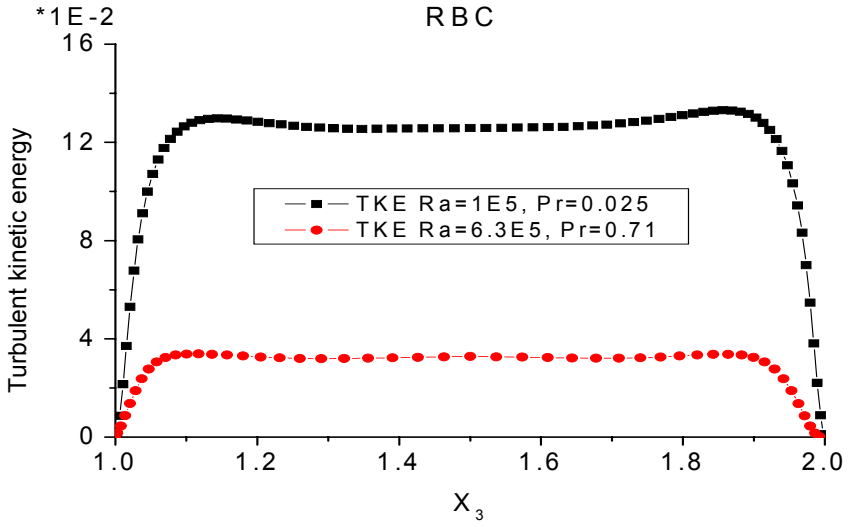

Fig. 3-19 Vertical profiles of $\langle E'' \rangle$ (TKE) evaluated from the DNS data of RBC.

The vertical profiles of $\langle E'' \rangle$ evaluated from the DNS data of IHL as in figure 3-18 show the increase of the maximum value of $\langle E'' \rangle$ with the increasing Ra. This increase in the maximum value depicts a kind of transition regime. Whereas, after certain Ra the maximum value of $\langle E'' \rangle$ is almost the same. However, presence of small extrusions in the horizontal components of the RMS velocity fluctuations as in figure 3-16 indicates that the flow has not reached the fully turbulent regime in which the distribution of statistical turbulence data is qualitatively independent from Ra. It can be concluded from these observations that the flow is tending towards the fully turbulent regime. On the contrary, in RBC with liquid metal higher values of $\langle E'' \rangle$ in comparison to RBC with air are observed. These reveal both the regime in which the flow is not fully turbulent and presence of the large scale structures in RBC with liquid metal. Therefore, with further increase of Ra the values of $\langle E'' \rangle$ in RBC with liquid metal should move towards the values of $\langle E'' \rangle$ in RBC with air.

Hereafter, for simplicity the standard notations for the mean $\overline{(\,)}$ and fluctuations components $(\,)'$ of any variable are preserved in writing instead of $\langle\ \rangle$ and $(\,)''$, respectively. These are already used in several equations (see e.g. eqn (2.6)).

3.7 Analysis of the $\overline{E'}$ equation for IHL and RBC

This section deals with the analysis of the terms in the transport equation for $\overline{E'}$ (eqn (2.6)) in IHL and RBC based on the DNS data. Subsequently, the gradient-diffusion model results and the DNS data of the turbulent diffusion of $\overline{E'}\left(D_{E,t}\right)$ will be compared in both flow types.

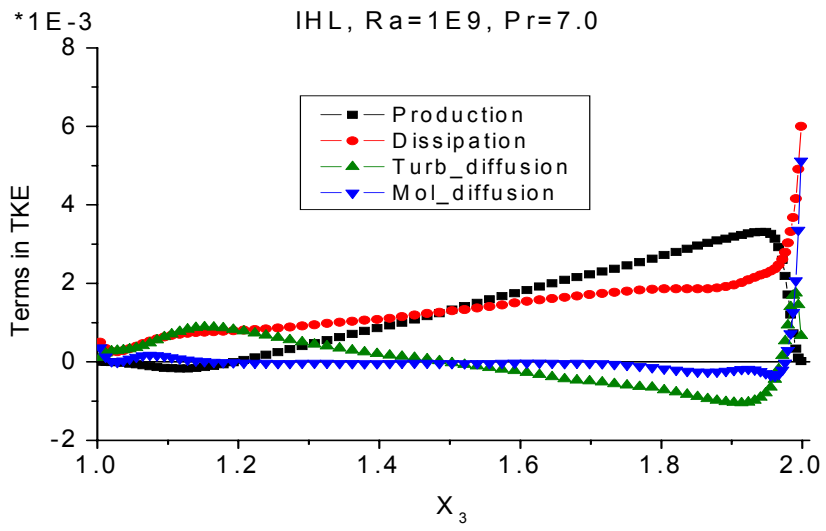

Fig. 3-20 Vertical profiles of the terms in the transport equation for $\overline{E'}$ (TKE) in IHL with $Ra = 10^9$.

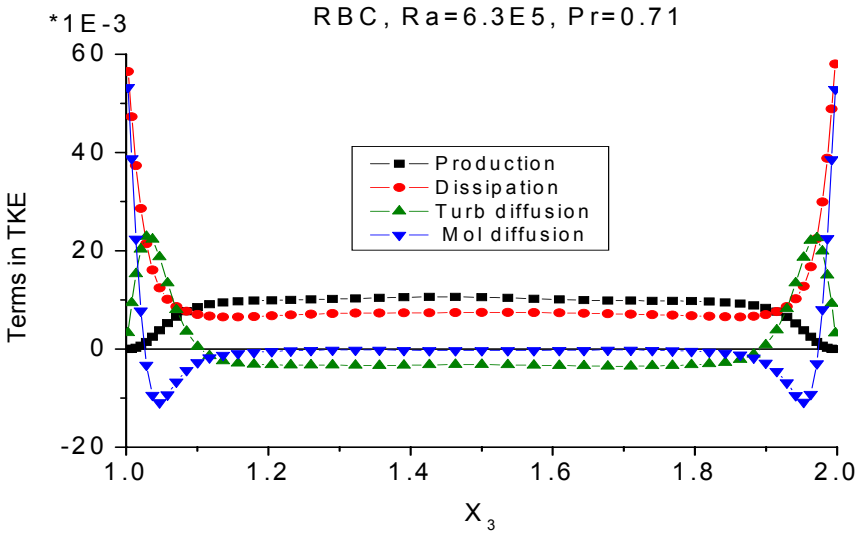

Fig. 3-21 Vertical profiles of the terms in the transport equation for $\overline{E'}$ (TKE) in RBC of air.

The terms in the transport equation for $\overline{E'}$ (see eqn (2.6)) in IHL and RBC show their different behavior in these flow types, see figures 3-20 and 3-21. In the present case the flow types do not have any imposed mean flow, e.g. wind, as a result the mean values of the velocities averaged over horizontal plane vanish. Therefore the flow types are shear free. Thus, the production of $\overline{E'}$ (P_E) is exclusively due to the buoyancy along $j = 3$ which is represented by the turbulent heat flux. In RBC this is al-

ways positive, whereas in IHL it has even negative values in the strongly stably stratified lower thermal boundary layer.

In RBC, dissipation $\left(\overline{\varepsilon'}\right)$ has the maxima close to the walls along $j=3$, where the fluid layers are strongly unstably stratified. In IHL, this shows a monotonically increasing tendency along $j=3$. In this case the maximum value is close to the upper wall. The above figures depict that the criterion of local equilibrium between P_E and $\overline{\varepsilon'}$ is fulfilled only at certain points in both flow types but not in most areas along $j=3$. In IHL the deviation from local equilibrium is strongly position dependent, whereas in RBC it is widely constant in the inner part of the channel.

The molecular diffusion $\left(D_{E,m}\right)$ is not significant in the central region $\left(\approx 1.2 \leq x_3 \leq 1.8\right)$ in both flow types. In IHL it has the maximum close to the upper wall and has a small contribution close to the lower wall. Whereas in RBC it has the maxima close to the upper and lower walls.

The turbulent diffusion $\left(D_{E,t}\right)$ distributes $\overline{E'}$ within different regions along $j=3$. The negative values indicate the extraction and positive values indicate the supply of energy to the respective region. The above figures show that $D_{E,t}$ is the balance between production and dissipation in the central region, not only that, it is quite significant close to the upper and lower walls in both flow types. Therefore, it is concluded that $D_{E,t}$ is very important in both flow types, and that it requires special attention. Hereafter, $D_{E,t}$ which consists of $\overline{u_3' E'}$ and $\overline{u_3' p'}$ will be investigated. They are usually modeled together in the gradient-diffusion model as given in eqn (2.7) (see e.g. Launder and Spalding (1972)).

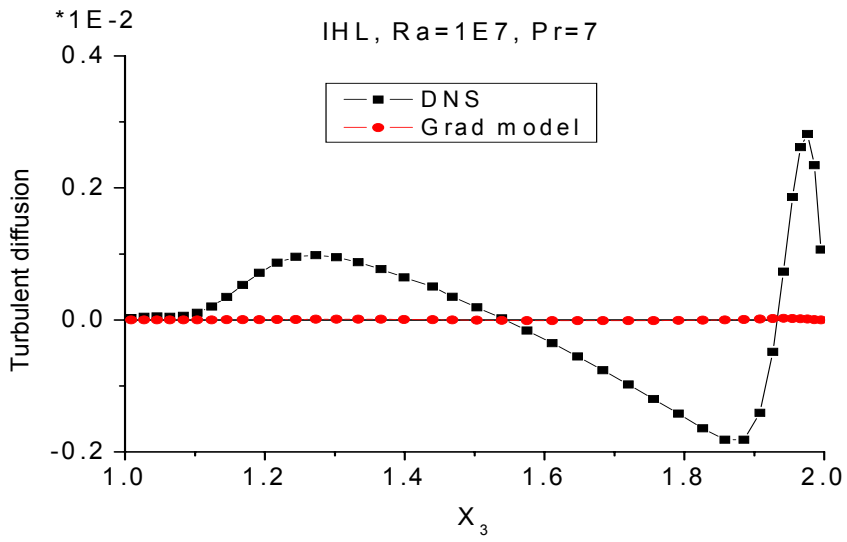

Fig. 3-22 Vertical profiles of $D_{E,t}$ and its model analyzed from the DNS data of IHL, $Ra = 10^7$.

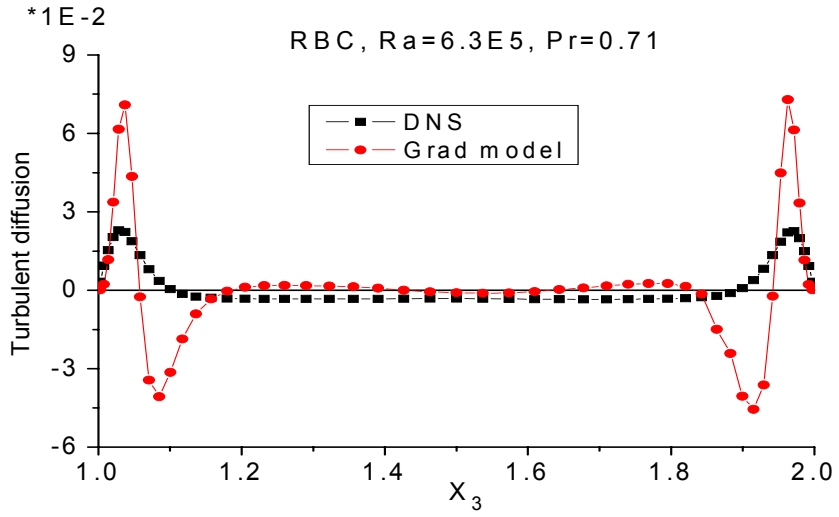

Fig. 3-23 Vertical profiles of $D_{E,t}$ and its model analyzed from the DNS data of RBC of air.

Figures 3-22 and 3-23 show the comparisons between $D_{E,t}$ and its gradient-diffusion model according to Launder and Spalding (1972) as in eqn (2.7), along $j = 3$ in IHL and RBC. These depict that the gradient-diffusion model for $D_{E,t}$ is not adequate in these flow types and its improvement is inevitable. This deficiency is considerable in RBC, but it is completely unacceptable in IHL. This can be regarded as one of the reasons that the standard $\overline{E'} - \overline{\varepsilon'}$ type RANS model fails completely as it was already experienced by Dinh and Nourgaliev (1997) to describe such thermally stratified flow types like IHL.

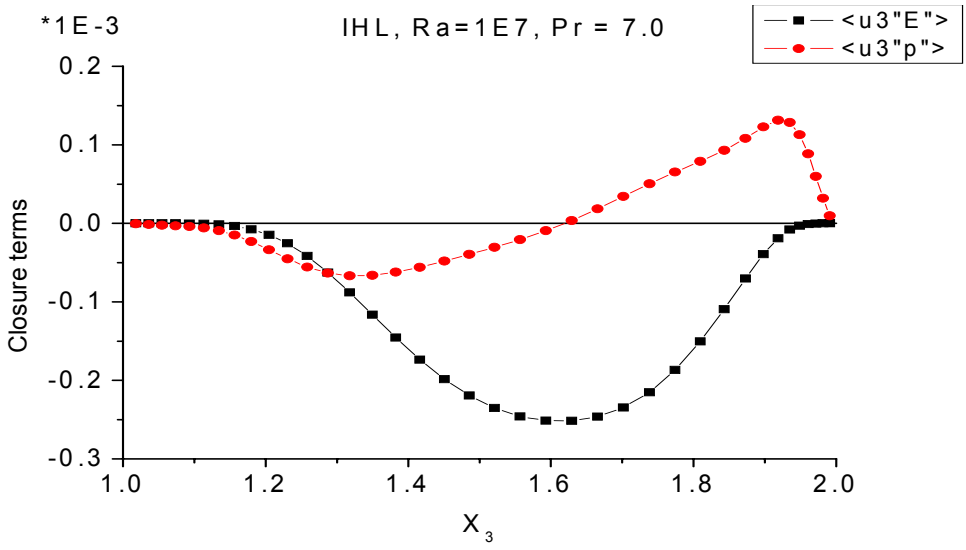

Fig. 3-24 Vertical profile of the closure terms of $D_{E,t}$ analyzed from the DNS data of IHL, $Ra = 10^7$.

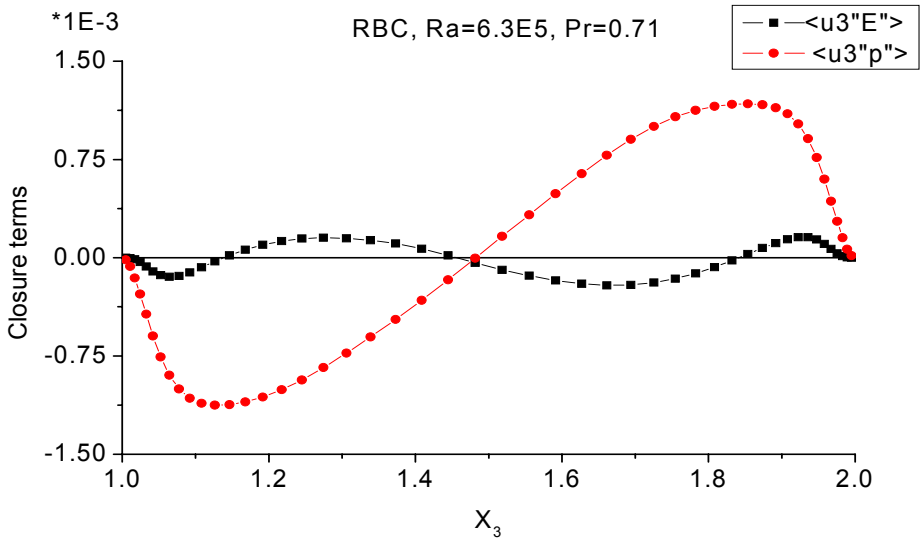

Fig. 3-25 Vertical profile of the closure terms of $D_{E,t}$ analyzed from the DNS data of RBC of air.

The gradient-diffusion model for $D_{E,t}$ assumes that $\overline{u_j' p'}$ and $\overline{u_j' E'}$ can be modeled together. On the contrary, figures 3-24 and 3-25 show their different behavior and importance in IHL and RBC along $j = 3$. These figures also reveal that $\overline{u_3' p'}$ is significant close to the upper and lower walls in both flow types. This is due to deceleration or acceleration of the upward and downward moving plumes in these flow types (see Grötzbach (1982a) and Wörner and Grötzbach (1998)). In IHL $\overline{u_3' E'}$ have larger values away from the walls, whereas in RBC the values are lower than that of $\overline{u_3' p'}$.

In $D_{E,t}$ not the size of the terms as given in figures 3-24 and 3-25 is of interest but their vertical derivative; but this will behave similarly. This means, the contributions of both correlations in the flow types is even qualitatively quite different. Based on a DNS study of the effects of shear on turbulent RBC, Domaradzki and Metcalfe (1988) had also explained the importance of $\overline{u_3' p'}$. They indicated towards a need of careful modeling of this term. Considering these studies, in the next chapter an extended version of the gradient-diffusion model for $D_{E,t}$ will be derived.

4 Mathematical modeling of $D_{E,t}$

In this chapter extended versions of the existing gradient diffusion model for the turbulent diffusion of $\overline{E'}$ ($D_{E,t}$) will be deduced. The development will be based on the DNS data of IHL and RBC.

4.1 Modeling approach

One approximation for linking the two contributions to $D_{E,t}$ was developed by Lumley (1978). He showed that $-\overline{u_j' p'} = \frac{1}{5}\overline{u_j' E'}$ holds in homogeneous turbulence. DNS analyzed values of $D_{E,t}$ in RBC indicate that apart from the thermal boundary layers $D_{E,t}$ is roughly constant, which indicates towards homogeneous turbulent energy transfer, see figure 3-21. However, in the case of IHL the vertical distribution of $D_{E,t}$ is strongly non-constant, so that the turbulent energy transfer is hardly locally homogeneous between the walls, see figure 3-20. This may explain why this Lumley (1978) approximation holds only at certain height points in this flow type. It has already been explained that the gradient-diffusion model for $D_{E,t}$ as in eqn (2.7) assumes that $\overline{u_j' p'}$ and $\overline{u_j' E'}$ can be modeled together. On the other hand, figures 3-24 and 3-25 reveal that $\overline{u_j' E'}$ is having higher importance in comparison to $\overline{u_j' p'}$ in most of the central region $(\approx 1.25 \leq x_3 \leq 1.8)$ in IHL. Whereas $\overline{u_j' p'}$ is the dominant term in RBC, in contrast to the approximation by Lumley. Further, $\overline{u_j' p'}$ is significant close to the walls in both flow types. This different behavior and importance of $\overline{u_j' E'}$ and $\overline{u_j' p'}$ in IHL and RBC were already reported and explained by the differences in the driving mechanisms by e.g. Wörner and Grötzbach (1998). Therefore, in the present study $\overline{u_j' E'}$ and $\overline{u_j' p'}$ are modeled separately. Afterwards these models will be joined. This results in an extended RANS model 1 for $D_{E,t}$. Using this strategy also an extended RANS model 2 for $D_{E,t}$ will be obtained. These models for $D_{E,t}$ include both effects of buoyancy and of $\overline{u_j' p'}$.

In order to obtain the separate RANS models for $\overline{u_j' E'}$ and $\overline{u_j' p'}$ the following assumptions are used:

- The flow types are horizontally homogeneous and there is no mean flow so that the flows are shear free. In this study, $x_{1,2}$ indicates the horizontal and x_3 is the vertical direction.

- The cross-correlations of the velocity fluctuations are smaller than their auto-correlations i.e. $\overline{u_i' u_j'} << \overline{u_j'^2} \quad for \quad i \neq j,$ with $i, j = 1, 2, 3$.

4.2 Derivation of a RANS model for $\overline{u_j' E'}$

Additionally, following strategy and assumptions are employed to derive the RANS model for $\overline{u_j' E'}$:

- Starting point for the model development is a non-dimensional form of the transport equation for $\overline{u_j' E'}$.

- In the transport equation for $\overline{u_j' E'}$ some of the closure terms are approximated according to the available literature.

- Following Weinstock (1989) $\overline{u_j'^2} \dfrac{\partial \overline{u_j'^2}}{\partial x_j} \sim \overline{E' \dfrac{\partial p'}{\partial x_j}}$ is used with a coefficient of magnitude greater than or equal to 1. Following this author, this approximation is also applicable in case of horizontally homogeneous fluid layer. It has been used in the present work to obtain a simplified extension of the gradient-diffusion approximation.

Considering $\overline{E'} = \dfrac{1}{2} \overline{u_i'^2}$, the non-dimensional form of the transport equation for $\overline{u_j' E'}$ (see Hanjalić and Launder (1972) and Moeng and Wyngaard (1989)) is as follows,

$$
\begin{aligned}
\frac{\partial \overline{u'_j E'}}{\partial t} = &\underbrace{-\left(\overline{u_l} \frac{\partial \overline{u'_j E'}}{\partial x_l} \right)}_{\text{Convection}} + \underbrace{\left(\overline{u'_i u'_j} \frac{\partial \overline{u'_i u'_l}}{\partial x_l} + \overline{E'} \frac{\partial \overline{u'_j u'_l}}{\partial x_l} \right)}_{\text{Production due to Rey. stresses and its gradient}} \\
&\underbrace{- \left(\overline{E' u'_l} \frac{\partial \overline{u_j}}{\partial x_l} + \overline{u'_j u'_i u'_l} \frac{\partial \overline{u_i}}{\partial x_l} \right)}_{\text{Production due to mean shear}} - \underbrace{\left(\frac{\partial \overline{u'_j u'_l E'}}{\partial x_l} \right)}_{\text{Turbulent transport}} \\
&\underbrace{+ \frac{Ra}{Re^2 Pr} \left(\overline{E'T'} + \overline{u'^2_j T'} \right) \delta_{j3}}_{\text{Buoyancy}} \\
&+ \left(\underbrace{\frac{1}{Re} \left\{ \frac{\partial^2 \overline{u'_j E'}}{\partial x_l^2} \right\}}_{\text{Mol. diff}} - \underbrace{\frac{1}{Re} \left(2\overline{u'_j \frac{\partial u'_i}{\partial x_l} \frac{\partial u'_i}{\partial x_l}} + \overline{u'_i \frac{\partial u'_i}{\partial x_l} \frac{\partial u'_j}{\partial x_l}} \right)}_{\text{Dissipation (Dis)}} \right) \\
&\underbrace{- \left\{ \overline{E' \frac{\partial p'}{\partial x_j}} - \overline{p' \left(\frac{\partial u'_j u'_l}{\partial x_l} \right) \delta_{jl}} \right\}}_{\text{Pressure term}} - \underbrace{\frac{\partial \overline{p' u'_j u'_l}}{\partial x_l} \delta_{jl}}_{\text{Pressure transport}} .
\end{aligned}
\tag{4.1}
$$

In eqn (4.1) all terms except the convection and the production due to Reynolds stresses and its gradient are the closure terms. In the present case, both flow types are shear free. Therefore, the convection and production due to mean shear vanish, i.e.

$$
\overline{u_l} \frac{\partial \overline{u'_j E'}}{\partial x_l} = 0 = \overline{E' u'_l} \frac{\partial \overline{u_j}}{\partial x_l} + \overline{u'_j u'_i u'_l} \frac{\partial \overline{u_i}}{\partial x_l} . \tag{4.1a}
$$

The contribution of buoyancy $\frac{Ra}{Re^2 Pr} \left(\overline{E'T'} + \overline{u'^2_j T'} \right) \delta_{j3}$ is non-zero only along $j = 3$.

The turbulent diffusion of $\overline{u'_j E'}$ consists of the pressure and turbulent transport,

$$
\text{Turbulent diffusion of } \overline{u'_j E'} = -\frac{\partial}{\partial x_l} \left(\overline{u'_j u'_l E'} + \overline{p' u'_j u'_l} \delta_{jl} \right).
$$

δ_{jl} denotes the Kronecker delta. The fourth-order velocity fluctuation correlations in the turbulent transport are approximated according to Millionshtchikov (1941) i.e. that when the triple-correlations are small and their distribution do not differ substantially

from those of a Gaussian one, the fourth-order correlations may be approximated in terms of second-order correlations, which is as follows,

$$\overline{u'_i u'_j u'_k u'_l} \approx \left(\overline{u'_i u'_j}\right)\left(\overline{u'_k u'_l}\right) + \left(\overline{u'_i u'_k}\right)\left(\overline{u'_j u'_l}\right) + \left(\overline{u'_i u'_l}\right)\left(\overline{u'_k u'_j}\right). \qquad (4.2)$$

The proof of this simplification of the fourth-order correlations in terms of the second-order correlations is available in Monin and Yaglom (1971).

Using the above relation gives,

$$\overline{u'_j u'_l u'^2_i} \approx \left(\overline{u'_l u'_j}\right)\left(\overline{u'^2_i}\right) + 2\left(\overline{u'_i u'_j}\right)\left(\overline{u'_i u'_l}\right).$$

Considering $\overline{u'_i u'_j} << \overline{u'^2_j}$ or $\overline{u'_i u'_l} << \overline{u'^2_l}$ *for* $i \neq l \neq j$, with $i, j, l = 1, 2, 3$ results in,

$$\left(\overline{u'_i u'_j}\frac{\partial \overline{u'_i u'_l}}{\partial x_l} + \overline{E'}\frac{\partial \overline{u'_j u'_l}}{\partial x_l}\right) - \left(\frac{\partial \overline{u'_j u'_l E'}}{\partial x_l}\right) \approx -\overline{u'^2_j}\frac{\partial \overline{u'^2_j}}{\partial x_l}\delta_{jl} - \overline{u'^2_j}\frac{\partial \overline{E'}}{\partial x_l}\delta_{jl}. \qquad (4.2a)$$

The molecular diffusion $\frac{1}{Re}\left\{\frac{\partial^2 \overline{u'_j E'}}{\partial x_l^2}\right\}$ can be neglected at high Re. Following the approach of Hanjalić and Launder (1972) and Weinstock (1989), the pressure contribution is modeled as in Rotta (1951); the dissipation term is approximated with Zeman and Lumley (1976) model. These results in,

$$\underbrace{-\left\{\frac{1}{Re}\left(2\overline{u'_j \frac{\partial u'_i}{\partial x_l}\frac{\partial u'_i}{\partial x_l}} + \overline{u'_i \frac{\partial u'_i}{\partial x_l}\frac{\partial u'_j}{\partial x_l}}\right)\right\}}_{\text{Dissipation}} \underbrace{-\left\{c\overline{E'\frac{\partial p'}{\partial x_j}} - \overline{p'\left(\frac{\partial u'_j u'_l}{\partial x_l}\right)}\delta_{jl}\right\}}_{\text{Pressure contribution}} \approx -C'_1\frac{\overline{u'_j E'}}{\tau}. \qquad (4.3)$$

Here, C'_1 is a coefficient and τ is a time scale, $\tau = \frac{\overline{E'}}{\overline{\varepsilon'}}$, a coefficient c is introduced to account for $\overline{u'^2_j}\frac{\partial \overline{u'^2_j}}{\partial x_j} + \overline{E'\frac{\partial p'}{\partial x_j}} \approx c\overline{E'\frac{\partial p'}{\partial x_j}}$ in accordance with the approximation as in Weinstock (1989). Following this author, this is also applicable in horizontal homogeneous fluid layer. This simplification may also satisfy a criterion of the above approximation, that the magnitude of the pressure contribution is greater than that of

the dissipation term as in eqn (4.3). However, the proof of this is not available at present. The right hand side of this equation is known as the relaxation term i.e. triple-correlation divided by the time scale (see e.g. Lumley et al. (1978)).

Buoyancy $\left(\overline{E'T'} + \overline{u_j'^2 T'}\right)\delta_{j3}$ acts along the vertical direction which results in strong anisotropy between the vertical and horizontal components of the velocity fluctuations. The figures 3-16 and 3-18 indicate that most of the turbulent kinetic energy $\overline{E'}$ is produced in the vertical component of the velocity fluctuations. Thus, it can be concluded that the buoyancy term may be simplified to,

$$\left(\overline{E'T'} + \overline{u_j'^2 T'}\right)\delta_{j3} \approx 2\overline{u_j'^2 T'}\delta_{j3}. \qquad (4.4)$$

Eqn (4.4) further reduces the number of unknowns that appear in the transport equation for $\overline{u_j' E'}$ as given in eqn (4.1). This assumption may not be sufficient in case of RBC. In the present case, the priority to achieve a better modeling for IHL is higher than RBC.

Considering fully developed flow, that means the steady state i.e. $\frac{\partial \overline{u_j' E'}}{\partial t}$=0, using $\overline{u_i' u_j'} << \overline{u_j'^2}$ or $\overline{u_i' u_l'} << \overline{u_l'^2}$ *for* $i \neq l \neq j$, with $i, j, l = 1, 2, 3$ and introducing eqn (4.1a), (4.2a) and (4.4) in eqn (4.1) gives,

$$0 \approx -\overline{u_j'^2}\frac{\partial \overline{E'}}{\partial x_l}\delta_{jl} + \frac{Ra}{Re^2\, Pr}\left(2\overline{u_j'^2 T'}\right)\delta_{j3} - \frac{\partial \overline{p' u_j'^2}}{\partial x_l}\delta_{jl} -$$
$$\left\{\frac{1}{Re}\left(2\overline{u_j'\frac{\partial u_i'}{\partial x_l}\frac{\partial u_i'}{\partial x_l}} + \overline{u_i'\frac{\partial u_i'}{\partial x_l}\frac{\partial u_j'}{\partial x_l}}\right)\right\} - \left\{\overline{cE'\frac{\partial p'}{\partial x_j}} - \overline{p'\left(\frac{\partial u_j'^2}{\partial x_l}\right)}\delta_{jl}\right\}.$$

Introducing the sink term model from eqn (4.3) in the above equation one obtains,

$$0 \approx -\overline{u_j'^2}\frac{\partial \overline{E'}}{\partial x_l}\delta_{jl} + \frac{Ra}{Re^2\, Pr}\left(2\overline{u_j'^2 T'}\right)\delta_{j3} - \frac{\partial \overline{p' u_j'^2}}{\partial x_l}\delta_{jl} - C_1'\frac{\overline{u_j' E'}}{\tau}.$$

Rearrangement of the above equation and $\tau = \dfrac{\overline{E'}}{\overline{\varepsilon'}}$ (see e.g. Launder et al. (1975) results in results in the required model for the triple-correlation,

$$\overline{u_j' E'} \approx C_1 \frac{\overline{E'}}{\overline{\varepsilon'}} \left(\underbrace{-\overline{u_j'^2} \frac{\partial \overline{E'}}{\partial x_l} \delta_{jl}}_{\text{Grad. Approx.}} + 2 \frac{Ra}{Re^2 Pr} \underbrace{\overline{u_j'^2 T'} \delta_{j3}}_{\text{Buoyancy}} - \underbrace{\frac{\partial \overline{p' u_j'^2}}{\partial x_l} \delta_{jl}}_{\text{Press. Transport}} \right). \qquad (4.5)$$

Here $C_1 \approx \dfrac{1}{C_1'}$ is a coefficient with $0.04 \le C_1 \le 0.17$ (see figures B-3 and B-4 in Appendix B). The range of this coefficient is expected to reduce in IHL with a very high Ra as a result of homogeneity away from the walls as in RBC along the vertical direction. Eqn (4.5) is a new RANS model for $\overline{u_j' E'}$. In this model, the first term can be regarded as an anisotropic form of the gradient-diffusion approximation for $\overline{u_j' E'}$ which includes the velocity fluctuations. The second term is the buoyancy contribution which is non-zero along $j = 3$. The last term is the pressure-transport. All three still contain closure terms. These will be approximated or discussed in the sections 4.4 and 4.5. Thus, this RANS model for $\overline{u_j' E'}$ as in eqn (4.5) compared to the standard model by Launder (1989) has two additional terms along with an anisotropic form of the gradient-diffusion approximation for $\overline{u_j' E'}$.

4.3 A modified RANS model for $\overline{u_j' p'}$

In order to obtain a modified RANS model for $\overline{u_j' p'}$, this correlation is represented as in Donaldson (1969), which is as follows,

$$\overline{u_j' p'} \approx -C_2' \left(\overline{E'}^{1/2} l \frac{\partial \overline{u_l' u_j'}}{\partial x_l} \right). \qquad (4.6)$$

According to this author the RANS model as in eqn (4.6) is a redistribution term. Here, C_2' is a coefficient and l is a length scale.

Using the Rotta (1951) dissipation model for high Reynolds number flows, l is defined as a function of $\overline{E'}$ and $\overline{\varepsilon'}$ i.e. $l = \frac{\overline{E'}^{3/2}}{\overline{\varepsilon'}}$. Daly and Harlow (1970) indicates that C_2' is a function of the turbulent Reynolds number Re_t (see Appendix A for the vertical profiles) which is usually employed in the near-wall damping functions. Wörner et al. (1997) had found that some of the model coefficients for the closure terms in the transport equations for $\overline{E'}$ and turbulent heat fluxes have to be increased by a large factor in IHL. Based on these observations and figure B-1 in Appendix B, $C_2' = \frac{C_2}{Re_t^{\alpha}}$ has been introduced here with $\alpha = 0.8$. In this approximation C_2 is a positive coefficient. Moreover, using $\overline{u_l' u_j'} << \overline{u_j'^2}$ *for* $l \neq j = 1, 2, 3$ in eqn (4.6) results in the required modified RANS model for $\overline{u_j' p'}$ which is as follows,

$$\overline{u_j' p'} \approx -\frac{C_2}{Re_t^{\alpha}} \left(\frac{\overline{E'}^2}{\overline{\varepsilon'}} \frac{\partial \overline{u_j'^2}}{\partial x_l} \right) \delta_{jl}. \qquad (4.7)$$

It is possible to calculate the coefficients C_1 and C_2, which are involved in the above RANS models (see eqn (4.5) and (4.7)) using the DNS data. The vertical profiles of these coefficients in IHL and RBC are given in the Appendix B (see figures B-3 to B-6). $1.5 \leq C_2 \leq 7$ is used in the present work.

In flow types like RBC, where the contribution of $\overline{u_j' E'}$ to $D_{E,t}$ is small, a better model for the derivative of $\overline{u_j' p'}$ which appears in $D_{E,t}$ may be needed. Therefore, another way to model the derivative of $\overline{u_j' p'}$ is explained in the Appendix C.

4.4 RANS model for $D_{E,t}$

In accordance with the sub-section 4.1, the separate RANS models for $\overline{u_j' E'}$ and $\overline{u_j' p'}$ have been presented. The RANS model for the terms appearing in $D_{E,t}$ is derived by adding eqn (4.5) and (4.7), which is as follows,

$$\overline{u_j' E'} + \overline{u_j' p'} \approx$$

$$\left.\begin{aligned} &\underbrace{-C_1 \frac{\overline{E'}}{\overline{\varepsilon'}} \overline{u_j'^2} \frac{\partial \overline{E'}}{\partial x_l} \delta_{jl}}_{\text{Grad. Approx.}} + \underbrace{2 C_1 \frac{\overline{E'}}{\overline{\varepsilon'}} \frac{Ra}{Re^2\, Pr} \overline{u_j'^2 T'} \delta_{j3}}_{\text{Buoyancy term}} \underbrace{- C_1 \frac{\overline{E'}}{\overline{\varepsilon'}} \frac{\partial \overline{p' u_j'^2}}{\partial x_l} \delta_{jl}}_{\text{Pressure term}} \\ &- \frac{C_2}{Re_t^{\alpha}} \left(\frac{\overline{E'}^2}{\overline{\varepsilon'}} \frac{\partial \overline{u_j'^2}}{\partial x_l} \right) \delta_{jl} \end{aligned}\right\} . \quad (4.8a)$$

In this RANS model for $D_{E,t}$ using the present scaling results in $\frac{Ra}{Re^2\, Pr}$=1. This model for $D_{E,t}$ includes the contribution of buoyancy and a higher-order pressure term. The first and last term in the RHS of eqn (4.8a) without their coefficients indicates to follow the approximation as in eqn (4.2). The Einstein-summation is not applicable to the index j which appears also in the LHS of eqn (4.8a).

4.4.1 Analysis of buoyancy and higher-order pressure term

In the RANS model for $D_{E,t}$ as in eqn (4.8a) the buoyancy term and the pressure term need to be modeled. Among these terms, the pressure term is problematic. Its importance and behavior in IHL and RBC are supposed to be different due to the different mechanisms in IHL and RBC leading to pressure and velocity fluctuations (see e.g. Wörner and Grötzbach (1998)). Such higher order correlations between pressure and velocity fluctuations are not very well understood in both flow types.

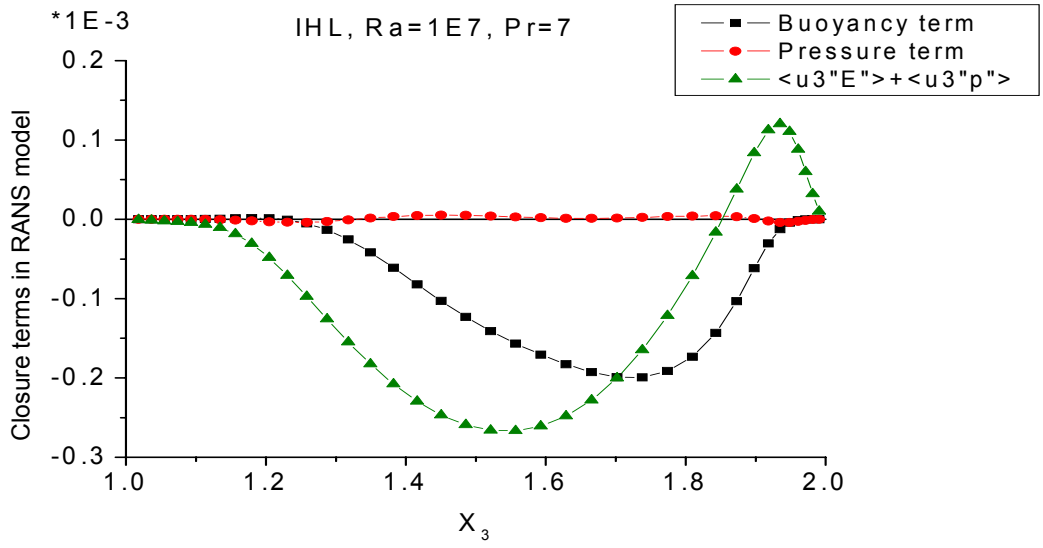

Fig. 4-1 Vertical profiles of the terms in RANS model as in eqn (4.8a) evaluated from the DNS data of IHL with $Ra = 10^7$, $C_1 = 0.17$.

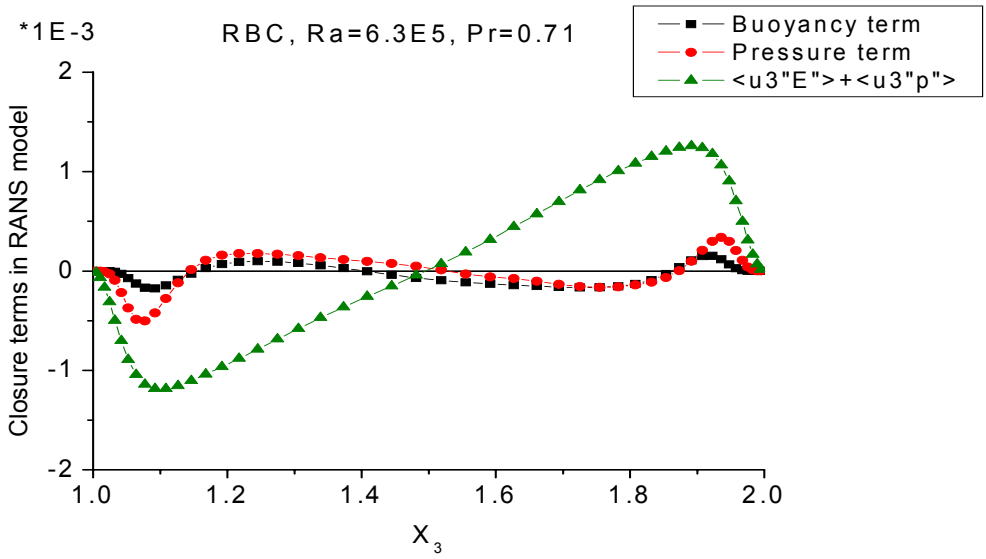

Fig. 4-2 Vertical profiles of the terms in RANS model as in eqn (4.8a) evaluated from the DNS data of RBC of air, $C_1 = 0.08$.

In order to understand the importance of the buoyancy term and the pressure term in the modeling of $D_{E,t}$, their contributions to $\overline{u_j' E'} + \overline{u_j' p'}$ (terms appearing in $D_{E,t}$) are analyzed from the DNS data of IHL and RBC along $j = 3$ as in figures 4-1 and 4-2. The results indicate that the buoyancy term and the pressure term have different nature in IHL and RBC. These also reveal the small contribution of the pressure term to $\overline{u_3' E'} + \overline{u_j' p'}$ in IHL. On the other hand, the pressure-term is not negligible in RBC. In the present work the primary goal is to obtain a RANS model for $D_{E,t}$ in IHL. Since there is no reliable model available at present for the pressure term, it will be neglected in the final form of RANS model for $D_{E,t}$ i.e. $-C_1 \frac{\overline{E'}}{\overline{\varepsilon'}} \frac{\partial \overline{p' u_j'^2}}{\partial x_l} \delta_{jl}$ will be set to zero in eqn (4.8a) which results in,

$$\overline{u_j' E'} + \overline{u_j' p'} \approx -C_1 \frac{\overline{E'}}{\overline{\varepsilon'}} \overline{u_j'^2} \frac{\partial \overline{E'}}{\partial x_l} \delta_{jl} + \underbrace{2\, C_1 \frac{\overline{E'}}{\overline{\varepsilon'}} \frac{Ra}{Re^2\, Pr} \overline{u_j'^2 T'} \delta_{j3}}_{\text{Buoyancy term}} - \frac{C_2}{Re_t^{\alpha}} \left(\frac{\overline{E'}^2}{\overline{\varepsilon'}} \frac{\partial \overline{u_j'^2}}{\partial x_l} \right) \delta_{jl} \Bigg\}. \quad \text{(4.8b)}$$

As a result of neglecting $-C_1 \frac{\overline{E'}}{\overline{\varepsilon'}} \frac{\partial \overline{p' u_j'^2}}{\partial x_l} \delta_{jl}$ some deviations between $D_{E,t}$ and its modeled values may be expected in RBC.

4.4.2 Modeling of the buoyancy term

The buoyancy term as in eqn (4.8b) contains the unknown $\overline{u_j'^2 T'}$ which can be modeled as follows:

4.4.2.1 Daly and Harlow approximation

Using the Daly and Harlow (1970) approximation and introducing the assumption $\overline{u_i' u_j'} << \overline{u_j'^2}$ *for* $i \neq j = 1, 2, 3$ results in,

$$\overline{u_j'^2 T'} \approx -C_\theta \frac{\overline{E'}}{\overline{\varepsilon'}} \left(2\overline{u_j'^2} \frac{\partial \overline{u_j' T'}}{\partial x_j} + \overline{u_j' T'} \frac{\partial \overline{u_j'^2}}{\partial x_j} \right). \tag{4.9a}$$

Here, C_θ is a coefficient. In most of the literature the values of this coefficient are assumed to be constant. On the contrary, Dol et al. (1997) had shown that this coefficient is not a constant in a buoyant flow type. Whereas, Wörner et al. (1997) had found that some of the model coefficients have to be increased by about a factor of 100 in IHL that means, the model needs improvement. There are indications in literature e.g. in Daly and Harlow (1970) that this coefficient may depend on the turbulent Reynolds number Re_t. Thus, instead of using the above values it is assumed that also this coefficient depends on Re_t which results in,

$$\overline{u_j'^2 T'} \approx -C_\theta'(Re_t) \frac{\overline{E'}}{\overline{\varepsilon'}} \left(2\overline{u_j'^2} \frac{\partial \overline{u_j' T'}}{\partial x_j} + \overline{u_j' T'} \frac{\partial \overline{u_j'^2}}{\partial x_j} \right). \tag{4.9b}$$

Here $C_\theta'(Re_t)$ represents a function of Re_t. Based on the observation in eqn (4.7) which also satisfies the finding of Wörner et al. (1997), this coefficient will be treated in an analogous manner. This will be directly tested along with the complete RANS model for $D_{E,t}$ (see e.g. eqn (4.14)). In order to differentiate between eqn (4.9a) and eqn (4.9b) in writing, they will be referred to as Daly and Harlow (DH) model for $\overline{u_j'^2 T'}$ and variable Daly and Harlow (VDH) model for $\overline{u_j'^2 T'}$, respectively.

4.4.2.2 Daly and Harlow Extended approximation

According to an assessment by Dol et al. (1997), the DH model for $\overline{u_j'^2 T'}$ needs improvement. This section deals with an extended version of the DH model. It can be observed from eqn (4.8b) that the buoyancy term is non-zero only along $j=3$, accordingly $\overline{u_3'^2 T'}$ will be discussed.

4.4.2.2.1 Analysis of the transport equation for $\overline{u_3'^2 T'}$

In order to investigate $\overline{u_3'^2 T'}$ in more details, the terms in the transport equation for $\overline{u_3'^2 T'}$ as given in Dol (1998) are analyzed using the DNS data of IHL and RBC. Based on this analysis an extended version of the DH model for $\overline{u_3'^2 T'}$ is presented. This model is referred to as the Daly and Harlow Extended (DHE) model for $\overline{u_3'^2 T'}$. The non-dimensional form of the transport equation for $\overline{u_3'^2 T'}$ is as follows,

$$\begin{aligned}
\frac{\partial \overline{u_3'^2 T'}}{\partial t} = & \underbrace{-\left(\overline{u_k} \frac{\partial \overline{u_3'^2 T'}}{\partial x_k} \right)}_{\text{Convection}} + \underbrace{\left(\overline{u_3'^2} \frac{\partial \overline{u_k' T'}}{\partial x_k} + 2\overline{u_3' T'} \frac{\partial \overline{u_3' u_k'}}{\partial x_k} \right)}_{\text{Production by Reynolds stress and turbulent heat fluxes (ProS)}} \\
& \underbrace{- \left(\underbrace{\overline{u_3'^2 u_k'} \frac{\partial \overline{T}}{\partial x_k}}_{\text{ProT}} + 2\overline{u_3' u_k' T'} \frac{\partial \overline{u_3}}{\partial x_k} \right)}_{\text{Prod. due to mean Temp. and mean shear}} - \underbrace{\left(\frac{\partial \overline{u_3'^2 u_k' T'}}{\partial x_k} \right)}_{\text{Tur. transport (TurbT)}} + \underbrace{2 \frac{Ra}{Re^2 \, Pr} \left(\overline{u_3' T'^2} \right)}_{\text{Buoyancy (ProB)}} \\
& \underbrace{+ \frac{1}{Re} \left(\frac{\partial}{\partial x_k} \left\{ 2 \overline{u_3' T'} \frac{\partial u_3'}{\partial x_k} + \frac{1}{Pr} \left\{ \overline{u_3'^2} \frac{\partial T'}{\partial x_k} \right\} \right\} \right)}_{\text{Molecular terms (M)}} + \underbrace{2 \left(\underbrace{\overline{p' \left\{ \frac{\partial u_3' T'}{\partial x_k} \right\}}}_{\substack{\text{Press. strain} \\ (Pdut)}} - \underbrace{\frac{\partial \overline{p' u_3' T'}}{\partial x_k}}_{\substack{\text{Press. transport} \\ (Dput)}} \right) \delta_{k3}}_{\text{Pressure terms (P)}} \\
& \underbrace{- \frac{2}{Re} \left(\left(\overline{\left\{ \frac{\partial u_3'}{\partial x_k} \right\}^2 T'} \right) + \left(1 + \frac{1}{Pr} \right) \left\{ \overline{u_3' \frac{\partial u_3'}{\partial x_k} \frac{\partial T'}{\partial x_k}} \right\} \right)}_{\text{Dissipative terms (D)}}.
\end{aligned} \tag{4.10}$$

Using the scaling as in section (2.1) results in $Re = \sqrt{Gr}$ and $\frac{Ra}{Re^2\, Pr}$=1. In this equation all the terms other than the convection and the production due to Reynolds stresses and turbulent heat fluxes are the closure terms. In the absence of mean shear the production is only due to the mean temperature gradient (ProT).

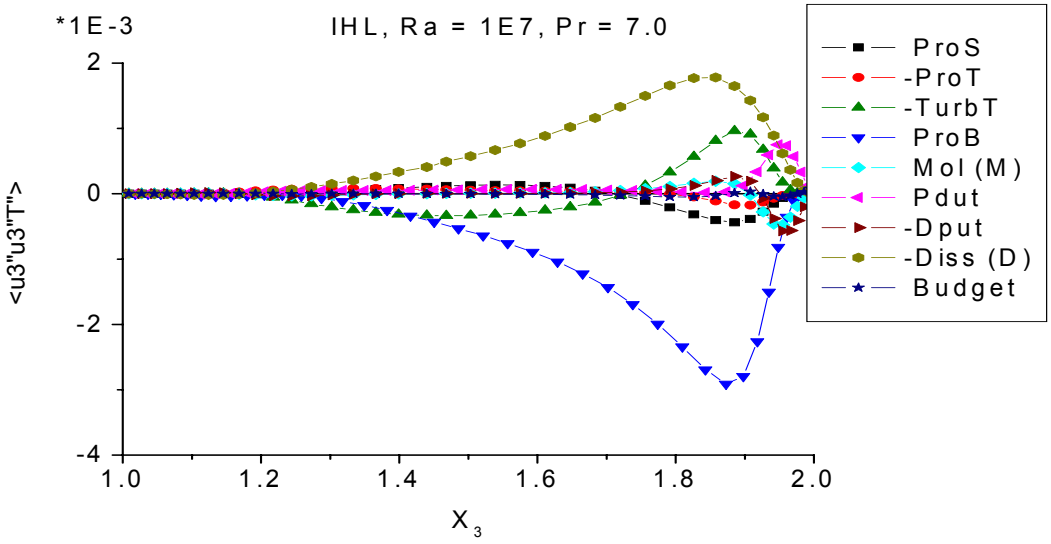

Fig. 4-3 Vertical profiles of the terms in the transport equation for $\overline{u_3'^2 T'}$ in IHL with $Ra = 10^7$.

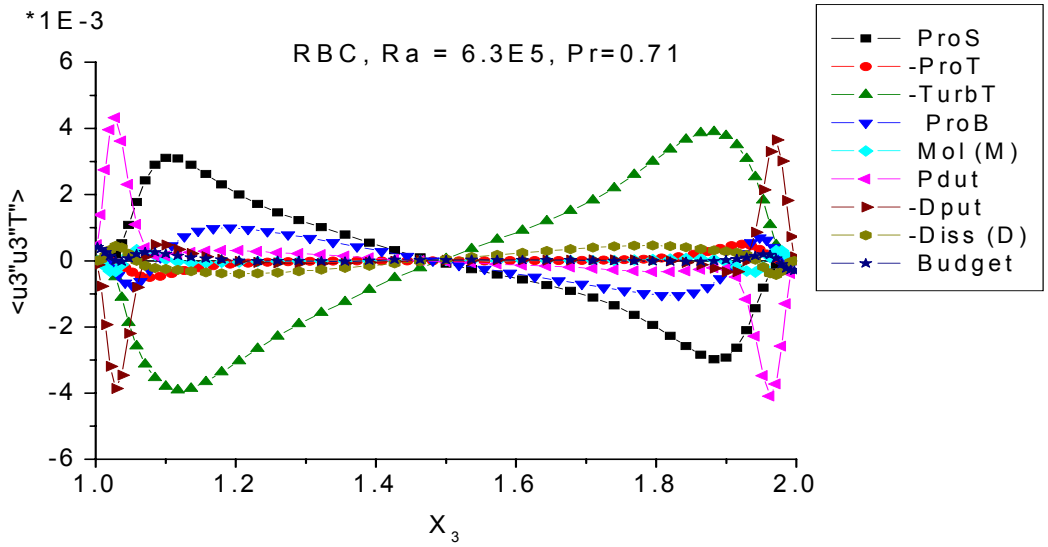

Fig. 4-4 Vertical profiles of the terms in the transport equation for $\overline{u_3'^2 T'}$ in RBC of air.

The DH model for $\overline{u_3'^2 T'}$ as in eqn (4.9a) can be derived by using the production by the Reynolds stresses and turbulent heat fluxes (ProS), the turbulent transport

(TurbT) and the dissipation terms (D). On the other hand, there are additional terms which can be important in the different flow types. Therefore, all the terms in eqn (4.10) which remain at the steady state will be analyzed.

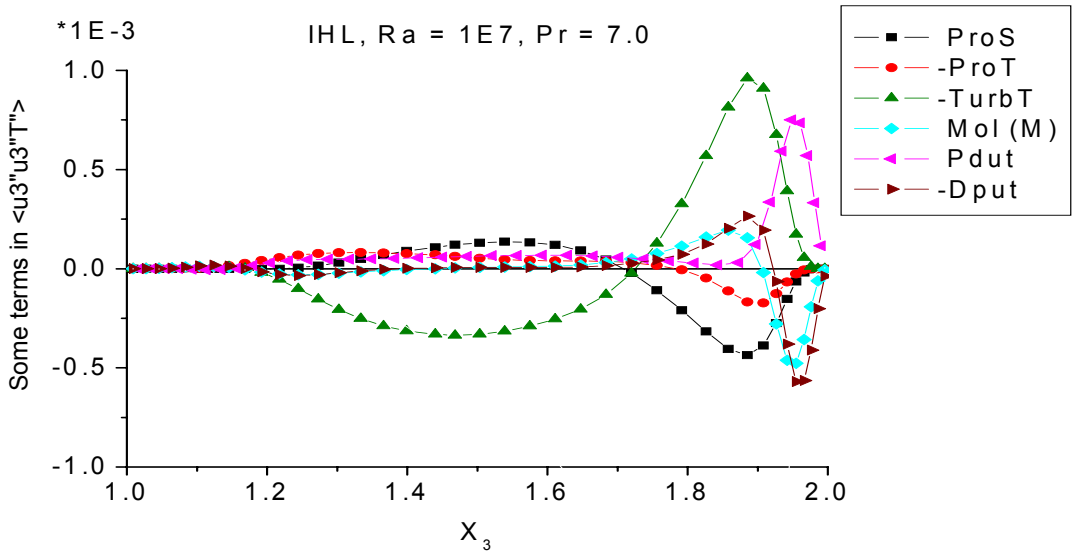

Fig. 4-5 Vertical profiles of some of the terms in the transport equation for $\overline{u_3'^2 T'}$ in IHL with $Ra = 10^7$.

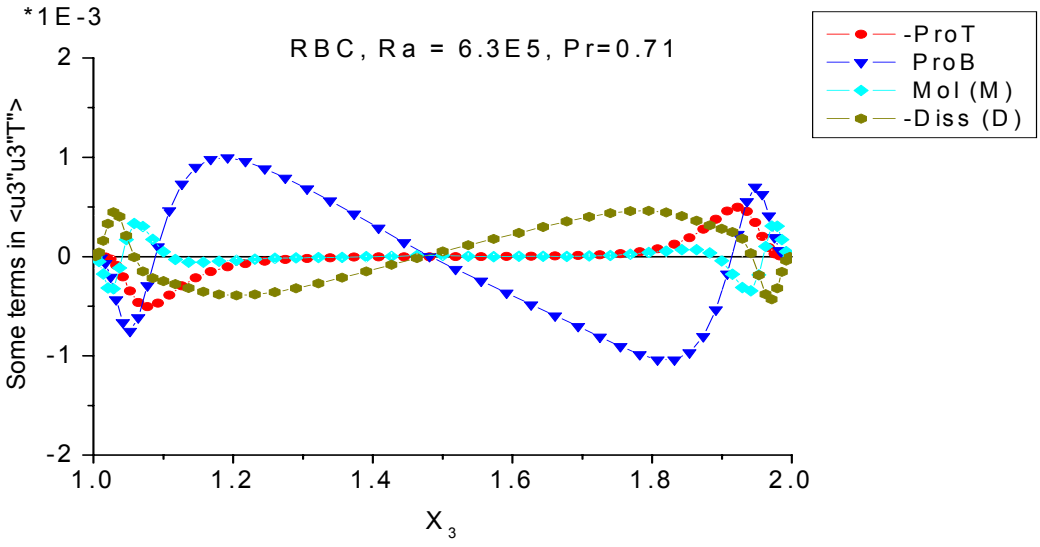

Fig. 4-6 Vertical profiles of some of the terms in the transport equation for $\overline{u_3'^2 T'}$ in RBC of air.

A software package has been developed and implemented in the analyzing program of the TURBIT code to analyze all terms in eqn (4.10). The vertical profiles of the terms in the transport equation for $\overline{u_3'^2 T'}$ analyzed from the DNS data of IHL and RBC are shown in figures 4-3 and 4-4. These also include the budget or out of bal-

ance of this equation which is calculated using all terms. This term is smaller in comparison to most of the terms. There is a second form of the transport equation $\overline{u_3'^2 T'}$ in literature which is deduced by Sander (1998). The values of the out of balance term calculated from his equation are found to be considerably larger than that of the out of balance term as calculated using the equation by Dol (1998). This could indicate to a formal problem in the equation by Sander (1998) especially in the molecular and dissipative terms.

Some of the terms in this transport equation which are having smaller values are shown in separate figures 4-5 and 4-6 for both flow types again. These show that none of the terms can simply be classified in both flow types e.g. the production due to the Reynolds stresses and heat fluxes has both positive as well as negative signs in RBC and the dissipation terms are not everywhere positive. The natures of these terms in the flow types depend on the gradients which are involved therein. The classification of these terms is only formal and not based on their real action. As the terms have different nature in these flow types, in the modeling of $\overline{u_3'^2 T'}$ it is difficult to consider the aspect of local equilibrium. The only practical way to model $\overline{u_3'^2 T'}$ is to identify the terms which may have higher importance. The production due to Reynolds stresses and turbulent heat fluxes (ProS) and the turbulent transport (TurbT) have higher significance in RBC than in IHL. The production due to the temperature gradient (ProT) is important close to the walls due to the increase of the temperature gradient with increasing Ra in both flow types (see figures 3-10 and 3-11). The contribution of the buoyancy term (ProB) is comparable to the dissipative terms (D) in IHL. The higher values of the pressure-transport (Dput) and of the pressure-strain (Pdut) close to the walls in RBC can be accounted to the presence of a local region of high values of the pressure fluctuations as well as the turbulent heat flux close to the walls. The molecular terms (M) need attention close to the walls due to the presence of strong viscous effects. The appearance of Pr in the denominator of the molecular terms of $\overline{u_3'^2 T'}$ and dissipative terms shows that their contribution will be enhanced in the liquid metal case (see eqn (4.10)). Therefore, these observations indicate that in addition to the production due to Reynolds stresses (ProS), turbulent transport (TurbT) and dissipative terms (D), the production due to the temperature

gradient (ProT), buoyancy contribution (ProB) and molecular terms (M) need to be included in a model for $\overline{u_3'^2 T'}$.

4.4.2.2.2 Modeling of $\overline{u_3'^2 T'}$

In order to obtain the RANS model for $\overline{u_3'^2 T'}$ the transport equation for $\overline{u_3'^2 T'}$ as given in eqn (4.10) has been used in which the following assumptions are employed,

- The fluid layers are horizontally homogeneous.
- As the flow types are shear free, convection and production due to mean shear vanish in eqn (4.10).
- The cross-correlations of the velocity fluctuations are smaller than their auto-correlations i.e. $\overline{u_i' u_j'} << \overline{u_j'^2} \quad for \;\; i \neq j,$ with $i, j = 1, 2, 3$.
- Following a similar approach as in Hanjalić and Launder (1972) the pressure term (P) is modeled as in Rotta (1951) and the Dissipative terms (D) in eqn (4.10) is modeled as in Zeman and Lumley (1976) as a relaxation term (see e.g. Lumley et al. (1978)) which is as follows,

$$P - D \approx -C \frac{\overline{u_3'^2 T'}}{\tau}, \text{ with } C \text{ as a coefficeint.}$$

Here, $\tau = \frac{\overline{E'}}{\overline{\varepsilon'}}$ is the typical turbulence time scale.

- The higher-order correlation in the turbulent transport TurbT in eqn (4.10) is modeled with the Millionshtchikov (1941) approximation as in Hanjalić and Launder (1972); see e.g. eqn (4.2).
- As a first extension, the contribution of buoyancy ProB and production due to temperature gradient ProT as in eqn (4.10) will be intro-

duced analogous to the turbulent diffusion of the temperature variance as in Dol et al. (1999)).

- Considering high Re and moderate Pr the molecular terms (M) are not considered.

Assuming fully developed convection in the steady state and introducing the above assumptions as explained in eqn (4.10) results in,

$$0 \approx -\left(2\overline{u_3'^2}\frac{\partial \overline{u_3'T'}}{\partial x_3} + \overline{u_3'T'}\frac{\partial \overline{u_3'^2}}{\partial x_3} \right) - \overline{u_3'^3}\frac{\partial \overline{T}}{\partial x_3} + 2\frac{Ra}{Re^2\,Pr}\overline{u_3'T'^2} - C\frac{\overline{u_3'^2T'}}{\tau}.$$

.

Rearranging the above equation gives,

$$\overline{u_3'^2T'} \approx -C'_{\theta 1}\frac{\overline{E'}}{\overline{\varepsilon'}}\left(2\overline{u_3'^2}\frac{\partial \overline{u_3'T'}}{\partial x_3} + \overline{u_3'T'}\frac{\partial \overline{u_3'^2}}{\partial x_3} + \overline{u_3'^3}\frac{\partial \overline{T}}{\partial x_3} - 2\frac{Ra}{Re^2\,Pr}\overline{u_3'T'^2} \right). \qquad (4.11)$$

Here, $C'_{\theta 1} \sim \frac{1}{C}$ is a coefficient. Analogous to the results of Dol et al. (1997) and Wörner et al. (1997) and considering figure B-2 in Appendix B it is concluded that $C'_{\theta 1} \approx \frac{C_{\theta 1}}{Re_t^{\beta}}$ with $\beta \approx 0.52$ and $C_{\theta 1} \approx 0.25$ (see figures B-7 and B-8 in Appendix B) will be used in the present work. The DH model as in eqn (4.9a) contains only the first two terms on the rhs of eqn (4.11). The DHE model for $\overline{u_3'^2T'}$ as in eqn (4.11) also includes the production due to the mean temperature gradient and the contribution of buoyancy. In this model the last two terms involves higher-order correlations $\overline{u_3'^3}$ and $\overline{u_3'T'^2}$. These are the closure terms in this model for $\overline{u_3'^2T'}$. One of the other closure terms namely $\overline{u_3'^3}$ may be modeled according to Launder (1989) as in eqn (4.16). An improved model for $\overline{u_3'T'^2}$ has been derived by Otić et al. (2005) as given in eqn (2.10). Before application of the Otić model for $\overline{u_3'T'^2}$ to the DHE model for $\overline{u_3'^2T'}$ its behavior should first be investigated and validated in IHL.

4.4.3 Extended RANS model 1 for $D_{E,t}$

Using the VDH model for $\overline{u_j'^2 T'}$ as in eqn (4.9b) in eqn (4.8b) and taking the partial derivative with respect to x_j gives,

$$\frac{\partial}{\partial x_j}\left\{\overline{u_j' E'} + \overline{u_j' p'}\right\} \approx \frac{\partial}{\partial x_j}\left\{-C_1 \frac{\overline{E'}}{\overline{\varepsilon'}}\overline{u_j'^2}\frac{\partial \overline{E'}}{\partial x_l}\delta_{jl}\right\} - \frac{\partial}{\partial x_j}\left\{\begin{array}{l} 2C_1 C_\theta'\left(\frac{\overline{E'}}{\overline{\varepsilon'}}\right)\frac{Ra}{Re^2\,Pr}\frac{\overline{E'}}{\overline{\varepsilon'}}\left(2\overline{u_j'^2}\frac{\partial \overline{u_j' T'}}{\partial x_j} + \overline{u_j' T'}\frac{\partial \overline{u_j'^2}}{\partial x_j}\right)\delta_{j3} \\ + C_2'\left(\frac{\overline{E'}}{\overline{\varepsilon'}}\right)\overline{E'}\left(\frac{\partial \overline{u_j'^2}}{\partial x_l}\right)\delta_{jl} \end{array}\right\}. \tag{4.12}$$

Here the formulation as already introduced with eqn (4.7), $C_2' = \frac{C_2}{Re_t^\alpha}$ is used. In eqn (4.12) there appear several unknown coefficients. The number of these coefficients should be reduced for practical applications. Since, C_θ' is a function of Re_t it implies $2C_1 C_\theta' = f(Re_t)$. Therefore, let us consider that there exists a coefficient C_p' such that $2C_1 C_\theta' \approx C_p' = f(Re_t) \approx C_2'$. This coupling between the VDH model for $\overline{u_j'^2 T'}$ as in eqn (4.9b) with the modified model $\overline{u_j' p'}$ as in eqn (4.7) may also compensate some of the deficiencies in the VDH model for $\overline{u_j'^2 T'}$ due to the dominant nature of $\overline{u_j' p'}$; see e.g. figures 3-24 and 3-25 in certain regions in both flow types. Using the coefficient C_p' in the RANS model as in eqn (4.12) results in,

$$\frac{\partial}{\partial x_j}\left\{\overline{u_j' E'} + \overline{u_j' p'}\right\} \approx \frac{\partial}{\partial x_j}\left\{-C_1 \frac{\overline{E'}}{\overline{\varepsilon'}}\overline{u_j'^2}\frac{\partial \overline{E'}}{\partial x_l}\delta_{jl}\right\} - \frac{\partial}{\partial x_j}\frac{C_p}{Re_t^\alpha}\left(\frac{\overline{E'}}{\overline{\varepsilon'}}\right)\left\{\frac{Ra}{Re^2\,Pr}\frac{\overline{E'}}{\overline{\varepsilon'}}\left(2\overline{u_j'^2}\frac{\partial \overline{u_j' T'}}{\partial x_j} + \overline{u_j' T'}\frac{\partial \overline{u_j'^2}}{\partial x_j}\right)\delta_{j3} + \overline{E'}\left(\frac{\partial \overline{u_j'^2}}{\partial x_l}\right)\delta_{jl}\right\}. \tag{4.13}$$

The Einstein-summation is not applicable to the index j which appears both in the lhs and rhs of eqn (4.13). Here, C_p is a coefficient. These simplifications can be re-

garded as the constraints in the extended RANS model for $D_{E,t}$ as given in eqn (4.13). In this RANS model, the effect of buoyancy and $\overline{u'_j p'}$ have been introduced. For comparison, the simple gradient-diffusion model for $D_{E,t}$ as explained in eqn (2.7) is as follows,

$$\overline{u'_j E'} + \overline{u'_j p'} \approx -\left(\frac{\nu_t}{\sigma_k} \frac{\partial \overline{E'}}{\partial x_j} \right), \text{with } j = 1, 2, 3.$$

Considering the simple gradient-diffusion approximation for $D_{E,t}$ and the extended RANS model for $D_{E,t}$ as in eqn (4.13) reveals the additional contribution in the extended RANS model for $D_{E,t}$ and how the anisotropy of the fluctuation field is introduced here.

A simplified version of the extended RANS model for $D_{E,t}$ has been deduced and validated by Chandra and Grötzbach (2005). In this model the contribution of $\overline{u'^2_j T'}$ was not introduced. Therefore, the extended RANS model for $D_{E,t}$ as given in eqn (4.13) is expected to be more accurate in thermally stratified flow types.

Not only in RANS but also in LES the gradient-diffusion model for $D_{E,t}$ requires improvement for investigating the buoyant flow types (e.g. Moeng and Wyngaard (1989)). The results of this work can also be used to deduce improved sub-grid scale (SGS) models in that case, that the variables in the LES are defined by linear filter variables. This holds for the common volume integration to deduce the equations for the resolved scales. These equations look formally identical to the RANS equations, and so are also the models very similar. The main difference between a RANS model and SGS model is typical the different length and time scales. So, to get a SGS version of the deduced model, one has mainly to consider adapting these scales to their SGS character.

The eqn (4.13) shows that the contribution of buoyancy is non-zero only along $j = 3$. Considering the horizontally homogeneous fluid layers like IHL and RBC one obtains,

$$\frac{\partial}{\partial x_3}\left\{\overline{u_3' E'} + \overline{u_3' p'}\right\} \approx \frac{\partial}{\partial x_3}\left\{\underbrace{-C_1 \frac{\overline{E'}}{\overline{\varepsilon'}}\overline{u_3'^2}\frac{\partial \overline{E'}}{\partial x_3}}_{\text{Grad. Approx.}}\right\} - \frac{\partial}{\partial x_3}\frac{C_p}{Re_t^{\alpha}}\left(\frac{\overline{E'}}{\overline{\varepsilon'}}\right)\left\{\frac{Ra}{Re^2\, Pr}\frac{\overline{E'}}{\overline{\varepsilon'}}\left(2\overline{u_3'^2}\frac{\partial \overline{u_3' T'}}{\partial x_3} + \overline{u_3' T'}\frac{\partial \overline{u_3'^2}}{\partial x_3}\right) + \overline{E'}\left(\frac{\partial \overline{u_3'^2}}{\partial x_3}\right)\right\}. \tag{4.14}$$

The applications of the RANS model for $D_{E,t}$ as given in eqn (4.14) require an additional transport equation for $\overline{u_3'^2}$. In other words, this model extends the $\overline{E'} - \overline{\varepsilon'}$ model to a $\overline{E'} - \overline{\varepsilon'} - \overline{u_3'^2}$ model which is a 3-equation model.

The transport equation for $\overline{u_3'^2}$ (see e.g. Launder et al. (1975)) in a non-dimensional form is as follows,

$$\frac{\partial \overline{u_3'^2}}{\partial t} + \underbrace{\overline{u_k}\frac{\partial \overline{u_3'^2}}{\partial x_k}}_{\text{Convection}} = \underbrace{-2\left(\overline{u_3' u_k'}\frac{\partial \overline{u_3}}{\partial x_k}\right) + 2\overline{u_3' T'}}_{P_3} \underbrace{- \frac{\partial}{\partial x_k}\left(\overline{u_k' u_3'^2} + 2\overline{u_3' p'}\delta_{3k}\right)}_{D_{3,t}} + \underbrace{2\overline{p'\frac{\partial u_3'}{\partial x_3}}}_{\Pi_3} + \underbrace{\frac{1}{\sqrt{Gr}}\frac{\partial^2 \overline{u_3'^2}}{\partial x_k^2}}_{D_{3,m}} \underbrace{- \frac{2}{\sqrt{Gr}}\overline{\left(\frac{\partial u_3'}{\partial x_k}\right)^2}}_{\varepsilon_3'}. \tag{4.15}$$

In order to obtain the non-dimensional form of the transport equation for $\overline{u_3'^2}$ the scaling as explained in section (2.1) is used. In eqn (4.15) P_3 is the production of $\overline{u_3'^2}$ due to the mean shear and turbulent heat flux (buoyancy), $D_{3,t}$ is its turbulent diffusion, Π_3 is its pressure strain or a redistribution term, $D_{3,m}$ is its molecular diffusion and $\overline{\varepsilon_3'}$ is its dissipation. In this equation except the convection and $D_{3,m}$ all are closure terms.

The information on the closure assumptions should be well known because $\overline{u_3'^2}$ is just one component of the shear stresses from a full-second order Reynolds stress model. In order to calculate P_3 the closure assumptions of the actually used turbulence models have to be applied, in the $\overline{E'} - \overline{\varepsilon'}$ model e.g. as in eqn (2.4). The veloc-

ity fluctuation triple-correlation term in $D_{3,t}$ can be modeled with the anisotropic-gradient diffusion approximation as in Launder (1989) which is as follows,

$$\overline{u_k' u_3'^2} \approx -C_\mu \overline{u_k' u_3'} \frac{\overline{E'}}{\overline{\varepsilon'}} \left(\frac{\partial \overline{u_3'^2}}{\partial x_k} \right).$$

Considering $\overline{u_i' u_j'} << \overline{u_j'^2} \quad for \; i \neq j,$ with $i, j = 1, 2, 3$ the above model can be further reduced to only one component. This is as follows,

$$\overline{u_3'^3} \approx -C_\mu \overline{u_3'^2} \frac{\overline{E'}}{\overline{\varepsilon'}} \left(\frac{\partial \overline{u_3'^2}}{\partial x_3} \right). \tag{4.16}$$

The velocity-pressure fluctuation correlation term in $D_{3,t}$ can be modeled either with the Durbin (1991) approach or by using $j = 3$ in eqn (4.7) which is recommended here for consistency.

Π_3 is generally approximated with the return to isotropy model by Rotta (1951) which is as follows,

$$\overline{p' \frac{\partial u_3'}{\partial x_3}} \approx -C_R \frac{\overline{\varepsilon'}}{\overline{E'}} \left(\overline{u_3'^2} - \frac{2}{3} \overline{E'} \right). \tag{4.17}$$

Here, $C_R = 0.326$ (as in Rotta (1951)) is a coefficient. An extended version of this Rotta model for Π_3 which also include e.g. the production term P_3, is explained in Launder (1989).

At high Re numbers $\overline{\varepsilon_3'}$ as in eqn (4.15) can be calculated by considering the following isotropic form, see e.g. Sander (1998),

$$\overline{\varepsilon_3'} \approx \frac{2}{3} \overline{\varepsilon'}. \tag{4.18}$$

The above approximations close the transport equation for $\overline{u_3'^2}$. Consequently, the extended RANS model for $D_{E,t}$ as given in eqn (4.14) can be computed in the framework of the $\overline{E'}-\overline{\varepsilon'}-\overline{u_3'^2}$ model.

If the turbulent heat flux in P_3 is calculated using the ASM model from eqn (2.5), which is according to the current understanding in the turbulence modeling community for buoyant flow a necessity, then the $\overline{E'}-\overline{\varepsilon'}-\overline{u_3'^2}$ model further extends to a $\overline{E'}-\overline{\varepsilon'}-\overline{u_3'^2}-\overline{T'^2}$ model which is a 4-equation ASM model.

4.4.4 Extended RANS model 2 for $D_{E,t}$

To derive the extended RANS model 1 for $D_{E,t}$ the VDH model for $\overline{u_j'^2 T'}$ as in eqn (4.9b) was used in eqn (4.8b). In order to obtain the extended RANS model 2 for $D_{E,t}$ the DHE model for $\overline{u_3'^2 T'}$ as given in eqn (4.11) is introduced in eqn (4.8b) for $j=3$ which results in,

$$\left\{\overline{u_3' E'}+\overline{u_3' p'}\right\}\approx -\left\{\begin{array}{l} C_1 \dfrac{\overline{E'}}{\overline{\varepsilon'}}\overline{u_3'^2}\dfrac{\partial \overline{E'}}{\partial x_3}+ \\ 2\,C_1 \dfrac{C_{\theta 1}}{Re_t^{\beta}}\dfrac{\overline{E'}}{\overline{\varepsilon'}}\dfrac{Ra}{Re^2\,Pr}\dfrac{\overline{E'}}{\overline{\varepsilon'}}\left(2\overline{u_3'^2}\dfrac{\partial \overline{u_3' T'}}{\partial x_3}+\overline{u_3' T'}\dfrac{\partial \overline{u_3'^2}}{\partial x_3}+\overline{u_3'^3}\dfrac{\partial \overline{T}}{\partial x_3}-2\dfrac{Ra}{Re^2\,Pr}\left(\overline{u_3' T'^2}\right)\right) \\ +\dfrac{C_2}{Re_t^{\alpha}}\left(\dfrac{\overline{E'}^2}{\overline{\varepsilon'}}\dfrac{\partial \overline{u_3'^2}}{\partial x_3}\right) \end{array}\right\}. \quad (4.19)$$

Taking the derivative of eqn (4.19) along $j=3$ gives,

$$\frac{\partial}{\partial x_3}\left\{\overline{u_3' E'} + \overline{u_3' p'}\right\} \approx$$

$$-\frac{\partial}{\partial x_3}\left\{\begin{array}{l} C_1 \dfrac{\overline{E'}}{\overline{\varepsilon'}}\overline{u_3'^2}\dfrac{\partial \overline{E'}}{\partial x_3} + \\ 2C_1 \dfrac{C_{\theta 1}}{Re_t^{\beta}}\dfrac{\overline{E'}}{\overline{\varepsilon'}}\dfrac{Ra}{Re^2\, Pr}\dfrac{\overline{E'}}{\overline{\varepsilon'}}\left(\begin{array}{l} 2\overline{u_3'^2}\dfrac{\partial \overline{u_3' T'}}{\partial x_3} + \overline{u_3' T'}\dfrac{\partial \overline{u_3'^2}}{\partial x_3} + \overline{u_3'^3}\dfrac{\partial \overline{T}}{\partial x_3} \\ -2\dfrac{Ra}{Re^2\, Pr}\left(\overline{u_3' T'^2}\right) \end{array}\right) \\ + \dfrac{C_2}{Re_t^{\alpha}}\left(\dfrac{\overline{E'}^2}{\overline{\varepsilon'}}\dfrac{\partial \overline{u_3'^2}}{\partial x_3}\right). \end{array}\right\} \qquad (4.20)$$

The eqn (4.20) is the extended RANS model 2 for $D_{E,t}$. The coefficients which appear in this model have already been explained in section 4.2, 4.3 and in 4.4.2.2.2 (see also Appendix B). It can be observed that also here the additional transport equation for $\overline{u_3'^2}$ is required which is already given in sub-section 4.4.3. This model includes two additional closures $\overline{u_3'^3}$ and $\overline{u_3' T'^2}$. The closure term $\overline{u_3'^3}$ can be modeled by an anisotropic gradient diffusion approximation as in eqn (4.16).The closure term $\overline{u_3' T'^2}$ occurred already in eqn (4.11). Here it could also be modeled by the gradient diffusion approximation as in e.g. Hossain and Rodi (1974) or by an improved model as in Otić et al. (2005). In order to validate this model (eqn (4.20)) the closure terms will be analyzed from the DNS data of IHL and RBC. In this model the same values of the coefficients and parameters as in eqn (4.5), (4.7) and (4.11) will be used.

4.5 Model summary

The turbulent diffusion of $D_{E,t}$ as in eqn (2.6) is defined as,

$$D_{E,t} = -\frac{\partial}{\partial x_j}\left(\overline{u_j' E'} + \overline{u_j' p'}\right).$$

Table 4 shows the different RANS models for $\overline{u_j' E'}$ and $\overline{u_j' p'}$ and $\overline{u_3'^2 T'}$ which are involved in the present work for developing the extended RANS models for $D_{E,t}$.

Different closure terms	**RANS Models for the closure terms**
$\overline{u_j' E'}$	RANS model as in eqn (4.5).
$\overline{u_j' p'}$	Modified RANS model as in eqn (4.7).
RANS model for $D_{E,t}$	Sum of eqn (4.5) and (4.7) and neglecting higher-order pressure term results in eqn (4.8b).
$\overline{u_3'^2 T'}$ (closure term in eqn (4.8b))	(1) VDH model as in eqn (4,9b) (2) DHE model as in eqn (4.11).

Table 4. RANS models for the different closure terms.

Table 5 shows the different extended RANS models for $D_{E,t}$ which are based on the different models for $\overline{u_3'^2 T'}$. In these models $\overline{u_j' E'}$ and $\overline{u_j' p'}$ are calculated according to eqn (4.5) and eqn (4.7), respectively (see table 4). In order to derive the model 1 for $D_{E,t}$ the VDH model as in eqn (4.9b) is used in eqn (4.8b). To obtain the model 2 for $D_{E,t}$ the DHE model as in eqn (4.11) is employed in (4.8b).

Extended RANS models for $D_{E,t}$	**RANS model for** $\overline{u_3'^2 T'}$
Extended model 1, eqn (4.14)	VDH model as in eqn (4.9b) is used in eqn (4.8b).
Extended model 2, eqn (4.20)	DHE model as in eqn (4.11) is used in eqn (4.8b).

Table 5. Different Extended RANS models for $D_{E,t}$.

5 Validation of proposed models

This chapter deals with the validation of the RANS models for $\overline{u_j' E'}$ as in eqn (4.5), for $\overline{u_j' p'}$ as in eqn (4.7), Daly and Harlow Extended (DHE) model for $\overline{u_j'^2 T'}$ as in eqn (4.11), extended RANS model 1 for $D_{E,t}$ as in eqn (4.14), and a extended RANS model 2 for $D_{E,t}$ as in eqn (4.20). In the present case, the horizontal plane and time averaged variables depends only on x_3 . Therefore, in the validation the RANS models are considered only in this direction.

The validation will be based on the DNS data of IHL and RBC. In addition to the DNS-data used in the development of the models, here additional DNS data of IHL at $Ra = 10^8$ and DNS data of RBC of liquid metal at $Ra = 10^5$ and $Pr = 0.025$, for the validation of the model 1 for $D_{E,t}$ will be used. To validate the model 2 for $D_{E,t}$ in addition to the DNS data that are used in the development of the different model terms DNS data of IHL at $Ra = 10^8$ will be used.

As explained, $D_{E,t}$ is defined by eqn (2.6),

$$D_{E,t} = -\frac{\partial}{\partial x_j}\left(\overline{u_j' E'} + \overline{u_j' p'}\right), \text{ with } j = 1, 2, 3.$$

This implies that the derivatives (here it means partial derivatives) of $\overline{u_j' E'}$ and $\overline{u_j' p'}$ will be the deciding factors regarding their importance in different flow types.

5.1 Validation of the RANS model for $\overline{u_3' E'}$

In order to validate the RANS model for $\overline{u_3' E'}$ as given in eqn (4.5), the coefficient C_1 is set to 0.17 for IHL and 0.08 for RBC.

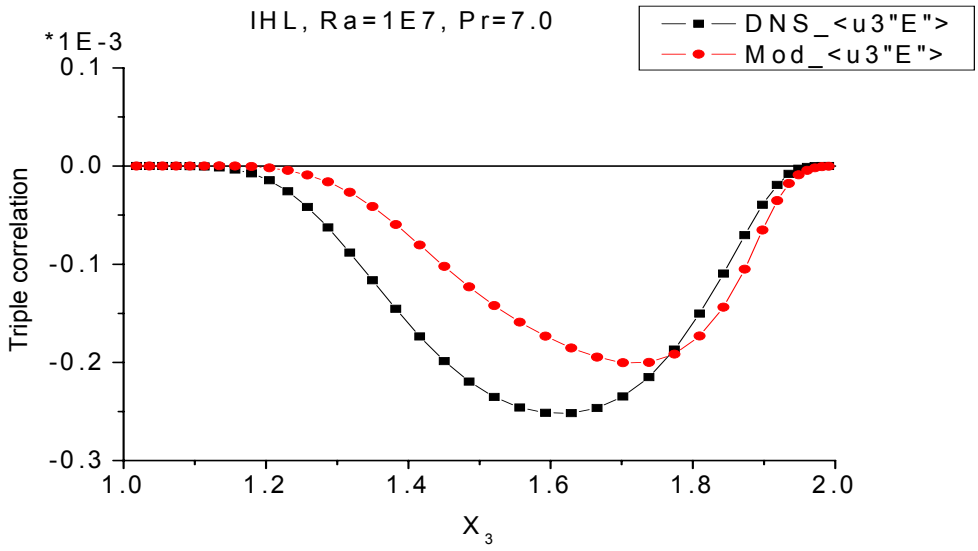

Fig. 5-1 Vertical profiles of $\overline{u_3' E'}$ and its model analyzed from the DNS data of IHL with $Ra = 10^7$, $C_1 = 0.17$.

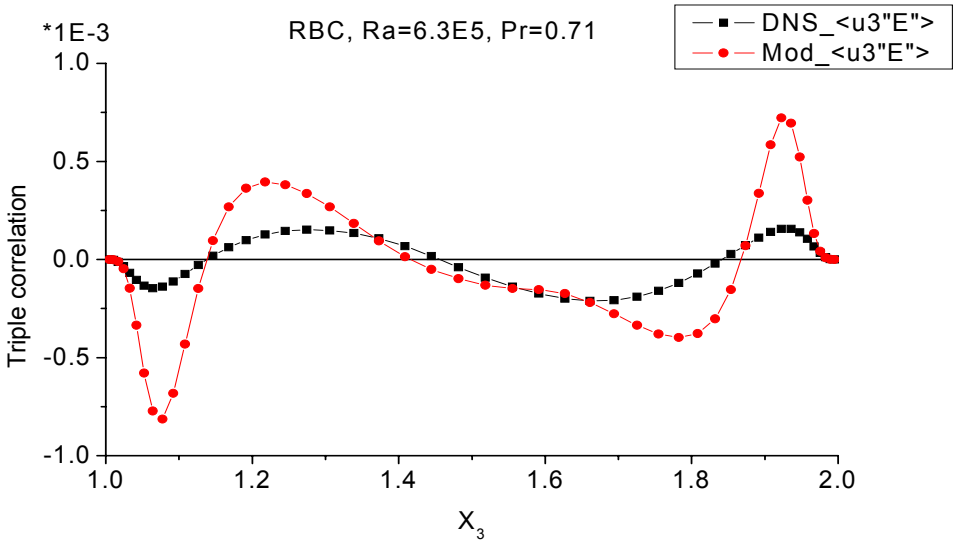

Fig. 5-2 Vertical profiles of $\overline{u_3' E'}$ and its model analyzed from the DNS data of RBC of air, $C_1 = 0.08$.

The comparisons between the vertical profiles of $\overline{u_3' E'}$ and its model analyzed from the DNS data of IHL and RBC are shown in figures 5-1 and 5-2. In IHL the modeled values show an acceptable agreement with $\overline{u_3' E'}$. In RBC the RANS model over-predicts values of $\overline{u_3' E'}$. However, the modeled values have roughly the required qualitative distribution. In IHL figure 3-24 indicates that the derivative of $\overline{u_3' E'}$ is greater than the derivative of $\overline{u_3' p'}$ in most of the central region $(\approx 1.25 \le x_3 \le 1.8)$.

Therefore, $\overline{u_3' E'}$ is more significant in this flow type. Further, the derivative of $\overline{u_3' E'}$ is very small close to the walls in IHL. Consequently, in this flow type its contribution to $D_{E,t}$ is not significant in this region. In RBC figure 3-25 indicates that the derivative of $\overline{u_3' E'}$ is smaller than the derivative of $\overline{u_3' p'}$. Therefore, $\overline{u_3' E'}$ is less significant in this case.

5.2 Validation of the modified RANS model for $\overline{u_3' p'}$

In order to validate the modified RANS model for $\overline{u_3' p'}$ as in eqn (4.7) the coefficient C_2 is set to 1.5 for IHL and 3.0 for RBC and the parameter $\alpha = 0.8$.

The comparisons between the vertical profiles of $\overline{u_3' p'}$ and its model analyzed from the DNS data of IHL and RBC are shown in figures 5-3 and 5-4.

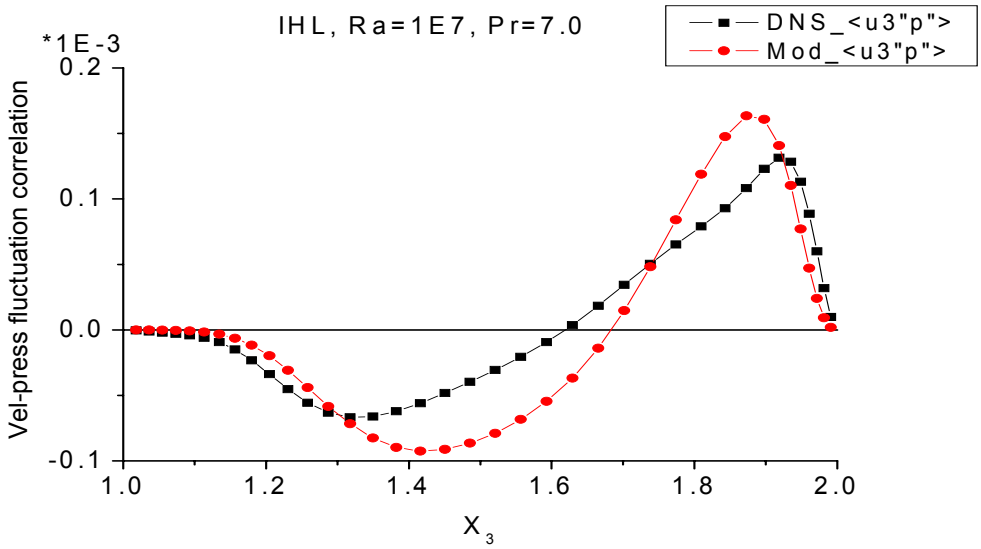

Fig. 5-3 Vertical profiles of $\overline{u_3' p'}$ and its model analyzed from the DNS data of IHL with $Ra = 10^7$, $C_2 = 1.5$, $\alpha = 0.8$.

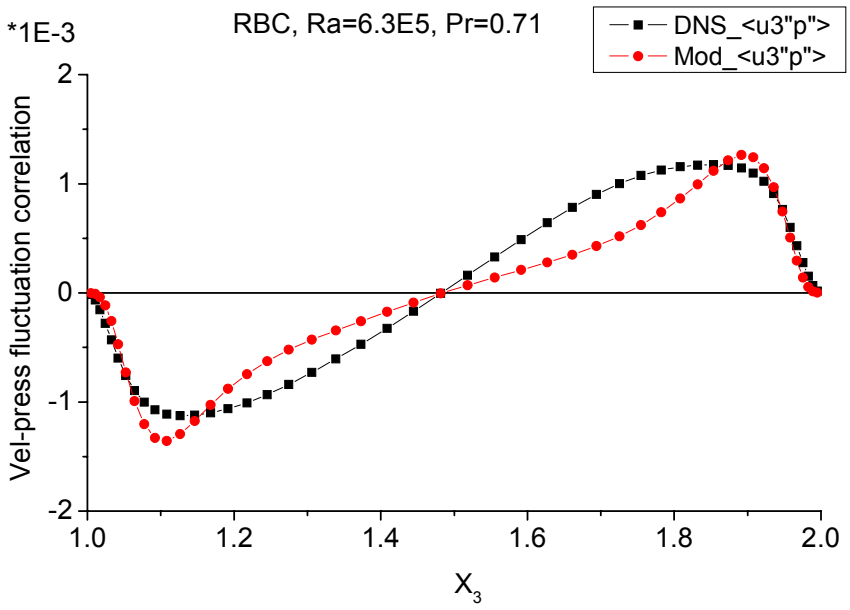

Fig. 5-4 Vertical profiles of $\overline{u_3' p'}$ and its model analyzed from the DNS data of RBC of air, $C_2 = 3.0$, $\alpha = 0.8$.

These results indicate an acceptable qualitative and quantitative agreement between $\overline{u_3' p'}$ and its modeled values in both flow types. Moreover, $\overline{u_3' p'}$ is very significant close to the walls in both flow types. In IHL, figure 3-24 indicates that the derivative of $\overline{u_3' p'}$ is smaller than the derivative of $\overline{u_3' E'}$ in most of the central region $(\approx 1.25 \leq x_3 \leq 1.8)$. It implies, $\overline{u_3' p'}$ has a lower contribution to $D_{E,t}$ in this region for this flow type. As a consequence, the model for $\overline{u_3' p'}$ will not play a significant role in this region. In RBC, figure 3-25 indicates that the derivative of $\overline{u_3' p'}$ is greater than the derivative of $\overline{u_3' E'}$. It implies, $\overline{u_3' p'}$ has a higher contribution to $D_{E,t}$ in this flow type.

So far, each of the RANS models for the closure terms in $D_{E,t}$ was found to model roughly acceptable its contributions especially in those areas in which the corresponding terms are relevant in both flow types.

5.3 Validation of the DHE model for $\overline{u_3'^2 T'}$

In order to validate the DHE model for $\overline{u_3'^2 T'}$ as in eqn (4.11) the coefficients, $C_{\theta 1}$=0.25 and β=0.52 is used in IHL and RBC. For this study $\overline{u_3'^3}$ and $\overline{u_3' T'^2}$ are analyzed from DNS data of both flow types.

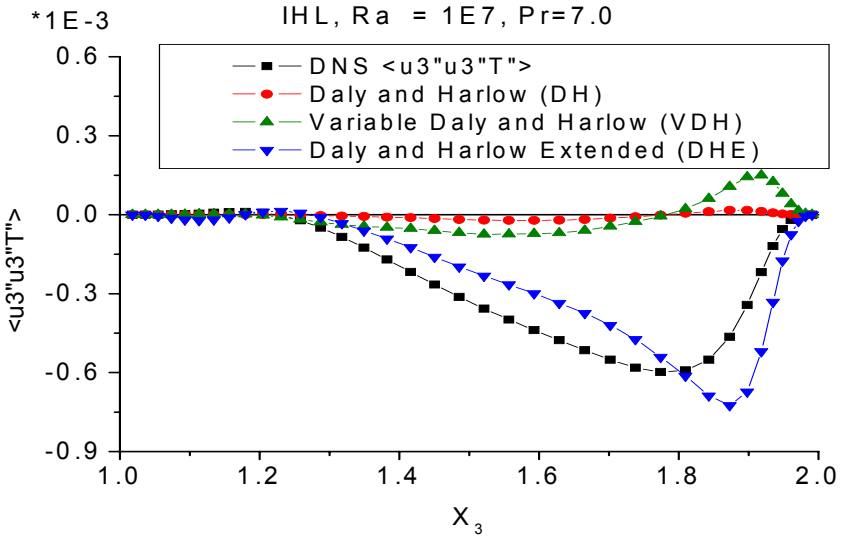

Fig. 5-5 Vertical profiles of $\overline{u_3'^2 T'}$ and its models analyzed from the DNS data of IHL with $Ra = 10^7$.

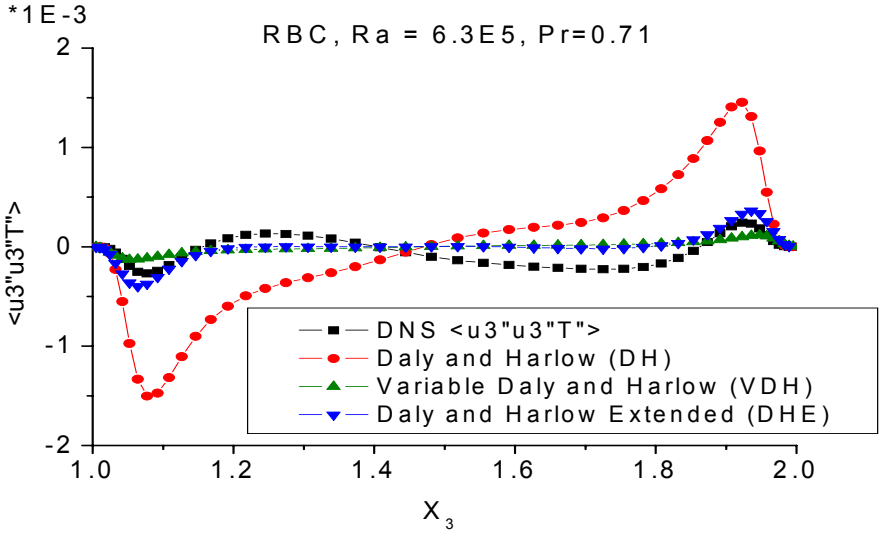

Fig. 5-6 Vertical profiles of $\overline{u_3'^2 T'}$ and its models analyzed from the DNS data of RBC of air.

The comparisons between $\overline{u_3'^2 T'}$ and its models in IHL and RBC are shown in figures 5-5 and 5-6. These figures indicate that DH model as in eqn (4.9a) with $C_\theta \approx 0.11$

and VDH model as in eqn (4.9b) with $C'_\theta \approx \frac{0.35}{Re^{0.8}}$ need improvement in both flow types. The Daly and Harlow Extended (DHE) model as given in eqn (4.11) shows a small improvement in the prediction of $\overline{u_3'^2 T'}$ in IHL except close to the lower wall. In RBC the DHE model shows an acceptable agreement close to the walls.

5.4 Validation of the RANS models for $D_{E,t}$

This section deals with the validation of the RANS models for $D_{E,t}$. For the extended RANS model 1 for $D_{E,t}$ as in eqn (4.14), $C_1 = 0.17, C_p = 0.7$ (see figures B-9 and B10 in Appendix B) and $\alpha = 0.8$ is used. For the extended RANS model 2 for $D_{E,t}$ as in eqn (4.20) the coefficients and parameters $C_1 = 0.17, C_{\theta 1} = 0.25, C_2 = 2,$ $\alpha = 0.8$ and $\beta = 0.52$ is used.

5.4.1 Validation of the extended RANS model 1 for $D_{E,t}$

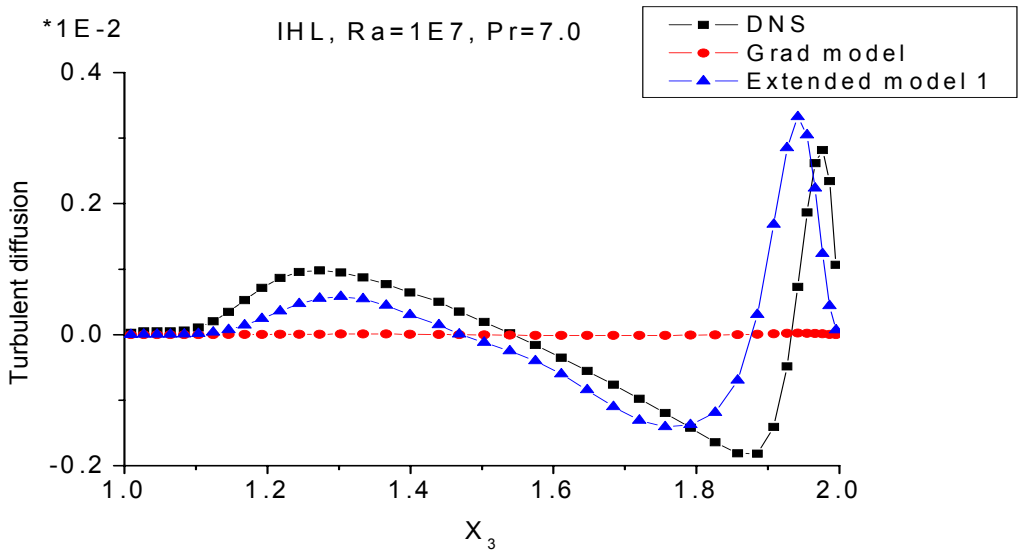

Fig. 5-7 Vertical profiles of $D_{E,t}$ and its models analyzed from the DNS data of IHL with $Ra = 10^7$.

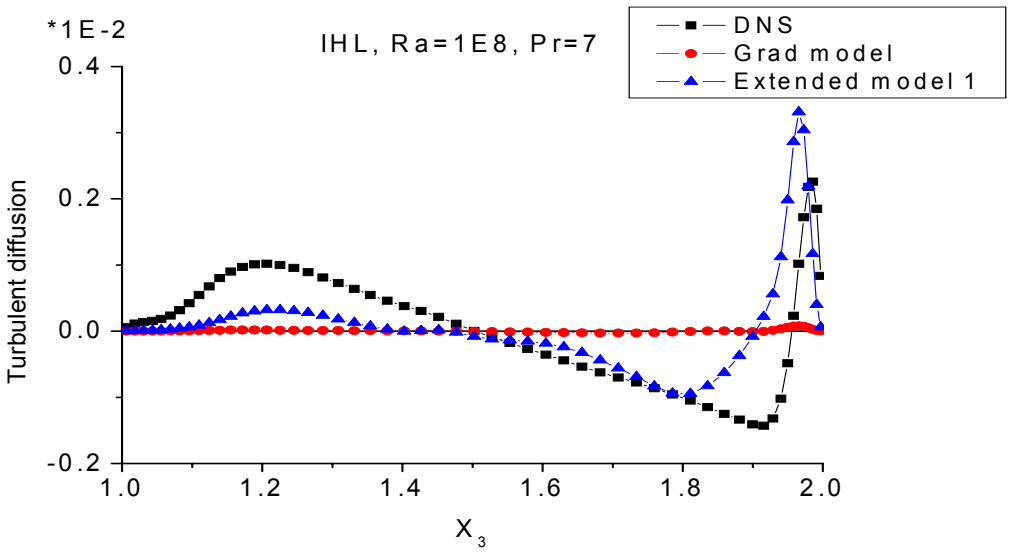

Fig. 5-8 Vertical profiles of $D_{E,t}$ and its models analyzed from the DNS data of IHL with $Ra = 10^8$.

The comparisons between vertical profiles of $D_{E,t}$ and its models analyzed from the DNS data of IHL with water and at different Ra are shown in figures 5-7 and 5-8. These depict that the model 1 for $D_{E,t}$ has significant improvement in the prediction of $D_{E,t}$ in comparison to the standard gradient-diffusion model for $D_{E,t}$ (see eqn (2.7)) in this flow type. The model gives acceptable results at both Ra. Therefore, the application of this model in CFD codes may provide more accurate results for such flow types.

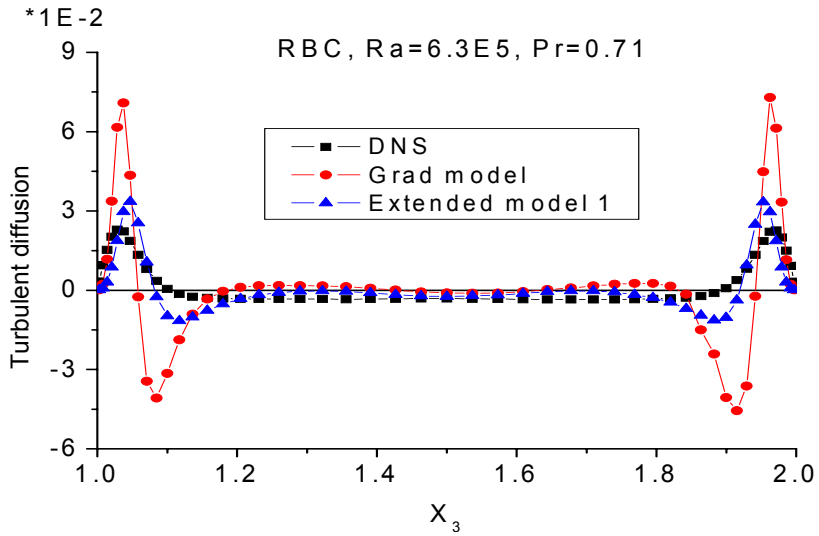

Fig. 5-9 Vertical profiles of $D_{E,t}$ and its models analyzed from the DNS data of RBC with air.

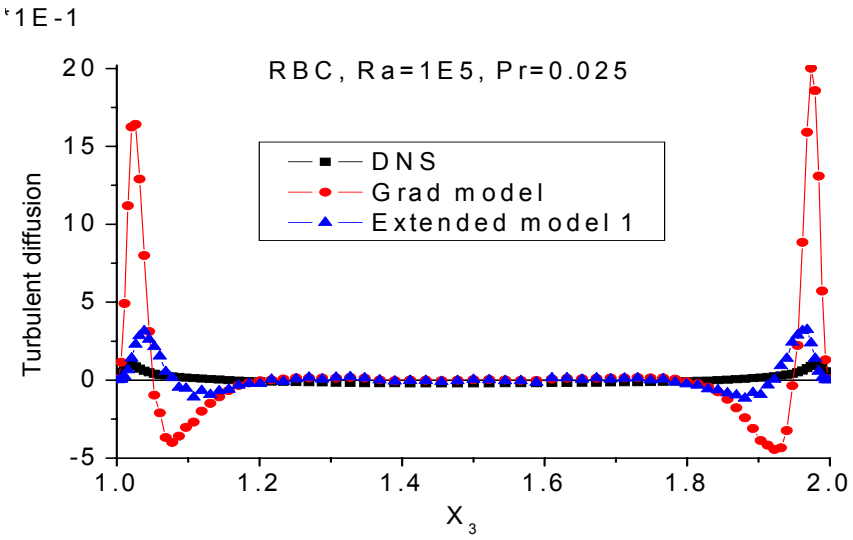

Fig. 5-10 Vertical profiles of $D_{E,t}$ and its models analyzed from the DNS data of RBC with liquid metal.

The comparisons between the vertical profiles of $D_{E,t}$ and its models analyzed from the DNS data of RBC at different Ra and Pr (air and liquid metal) are shown in figures 5-9 and 5-10. These reveal that the extended RANS model 1 for $D_{E,t}$ has roughly the required distribution as $D_{E,t}$ in RBC with liquid metal. The deviations between $D_{E,t}$ and its modeled values are smaller in the model 1 in comparison to the gradient-diffusion model. These deviations can be attributed to both the use of VDH model for $\overline{u_3'^2 T'}$ and the pressure term in eqn (4.8a) which is neglected in this extended RANS model for $D_{E,t}$.

From these validations it can be concluded that the extended RANS model 1 for $D_{E,t}$ as given in eqn (4.14) gives a considerable improvement in comparison to the gradient-diffusion model for $D_{E,t}$ as in eqn (2.7). In RBC this model shows small improvement in comparison to the standard gradient-diffusion model for $D_{E,t}$.

5.4.2 Validation of the extended RANS model 2 for $D_{E,t}$

To validate this model the closure terms $\overline{u_3'^3}$ and $\overline{u_3'T'^2}$ are analyzed from the DNS data of IHL and RBC.

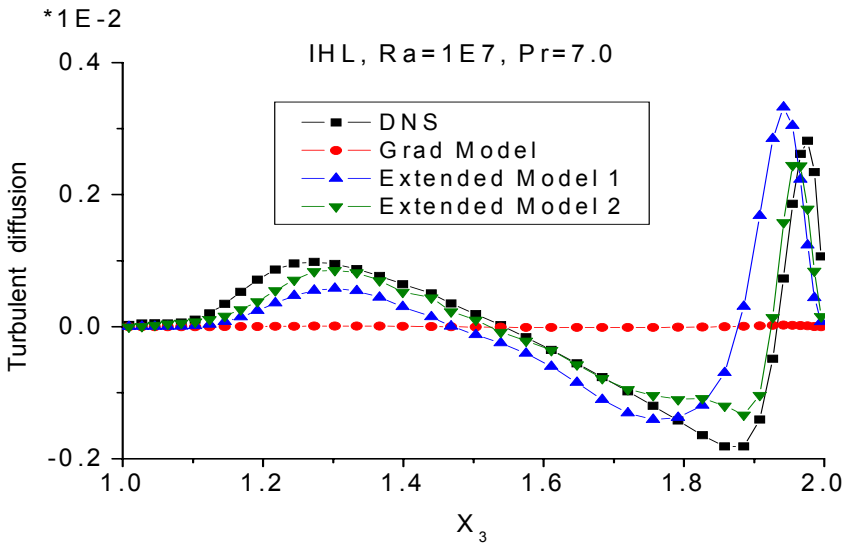

Fig. 5-11 Vertical profiles of $D_{E,t}$ and its models analyzed from the DNS data of IHL with $Ra = 10^7$.

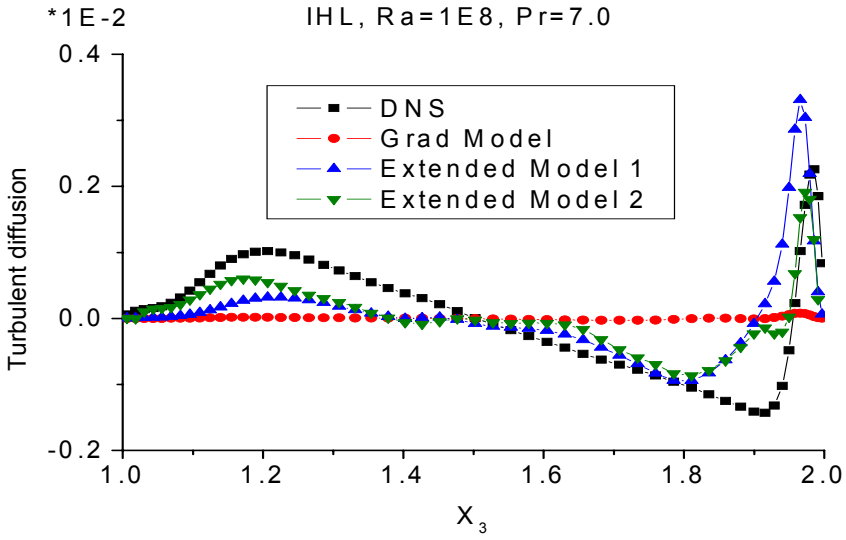

Fig. 5-12 Vertical profiles of $D_{E,t}$ and its models analyzed from the DNS data of IHL with $Ra = 10^8$.

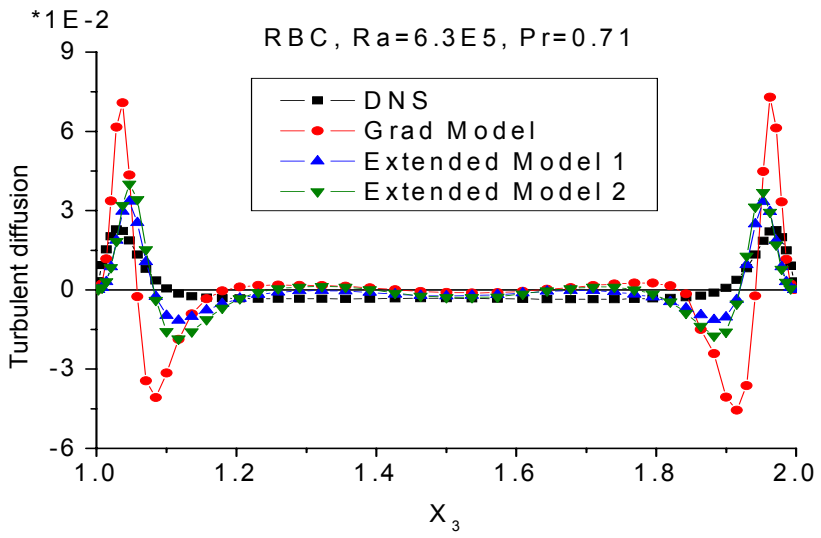

Fig. 5-13 Vertical profiles of $D_{E,t}$ and its models analyzed from the DNS data of RBC with air.

Comparison between $D_{E,t}$ and its models analyzed from the DNS data reveals that the model 2 as given in eqn (4.20) has even better predictive capability than the extended model 1 for $D_{E,t}$ as in eqn (4.14) in IHL with $Ra = 10^7$ and 10^8 especially close to the upper wall, see figures 5-11 and 5-12. Thus, the application of the model 2 for $D_{E,t}$ may provide more accurate results in such thermally stratified flow types. In RBC of air the model 2 for $D_{E,t}$ shows almost no difference close to the walls comparison to the model 1, see figure 5-13. At certain points the model 2 shows slightly better agreement with $D_{E,t}$ compared to the model 1.

6 Conclusions and Outlook

The literature review shows that the standard Reynolds Averaged Navier Stokes (RANS) models, like the $\overline{E'}-\overline{\varepsilon'}$ model, are not adequate for investigating certain buoyant flow types (e.g. Dinh and Nourgaliev (1997)). Different strategies to improve the standard RANS models use the transport equation for the turbulent kinetic energy $\overline{E'}$. In this transport equation the turbulent diffusion appears as one of the closure terms. This term consists of velocity-fluctuation triple correlation $\overline{u_j' E'}$ and velocity-pressure fluctuation correlation $\overline{u_j' p'}$. They are generally modeled together in the standard gradient diffusion approximation as given in eqn (2.7). Based on a large eddy simulation (LES) investigation in meteorology Moeng and Wyngaard (1989) had shown that the gradient-diffusion model for the turbulent diffusion of the turbulent kinetic energy is not adequate in buoyant flow types. In order to improve this model, they recommended the inclusion of the effect of buoyancy. These studies provide the basis for the present work which deals with the extensions of the gradient-diffusion model for the turbulent diffusion of the turbulent kinetic energy.

For this purpose, two different buoyant flow types have been considered as a vehicle, namely, internally heated fluid layers and Rayleigh Bénard convection. In Rayleigh-Bénard convection the fluid layers are unstably stratified along the complete height of the channel. Whereas in internally heated fluid layers the presence of both unstably and stably stratified fluid layers make it more difficult in RANS modeling compared to Rayleigh-Bénard convection. Hence, in this study the priority to achieve a better modeling for internally heated fluid layers is higher than for Rayleigh-Bénard convection.

Direct numerical simulation (DNS) investigations of internally heated fluid layers at $Ra = 10^9$, $Pr = 7$ and Rayleigh-Bénard convection of air at $Ra = 6.3 \times 10^5$, $Pr = 0.71$ reveal that the criterion of local equilibrium between the production and dissipation of turbulent kinetic energy is fulfilled only at certain points, at other heights it is not fulfilled in both flow types. Anisotropy between the different components of the root mean square values of the velocity fluctuations are also observed in both flow types. This can be attributed to the effect of buoyancy and the presence of the walls. Analy-

sis of the closure terms $\overline{u_j' E'}$ and $\overline{u_j' p'}$ using the DNS data show their different importance and behavior in internally heated fluid layers with $Ra = 10^7$ and in Rayleigh-Bénard convection of air. This was already reported by Wörner and Grötzbach (1998) and the mechanisms leading to this difference were discussed. Therefore, in the present study the closure terms in the turbulent diffusion are modeled separately in order to extend the gradient-diffusion model for the turbulent diffusion.

In order to derive a RANS model for the triple-correlation $\overline{u_j' E'}$, the transport equation for this closure term has been used. In this equation the turbulent transport term is modeled according to Milionshtchikov (1941). Following the approach of Hanjalić and Launder (1972) and Weinstock (1989), the pressure contribution is modeled as in Rotta (1951) and the dissipation term is modeled as in Zeman and Lumley (1976). The new RANS model for the triple-correlation incorporates the contribution of buoyancy and pressure transport along with an anisotropic gradient-diffusion approximation. Starting with the Donaldson (1969) approximation for the velocity-pressure correlation $\overline{u_j' p'}$ and introducing that the cross-correlations of the velocity fluctuations are smaller than their auto-correlations, a modified RANS model for the velocity-pressure correlation is obtained. The RANS models for the triple-correlation and the velocity-pressure correlation are joined to deduce the model for the turbulent diffusion. This model includes a buoyancy term which contains $\overline{u_j'^2 T'}\,\delta_{j3}$, a higher-order pressure term and the velocity-pressure correlation. Analysis of the buoyancy and higher-order pressure term using DNS data reveal that in internally heated fluid layers the higher-order pressure term is having a small contribution to the turbulent diffusion of turbulent kinetic energy which consists of $\left(\overline{u_j' E'} + \overline{u_j' p'}\right)$. Due to non availability of a reliable model for the higher-order pressure term, and in accordance with the priority of obtaining better modeling of internally heated fluid layers compared to Rayleigh-Bénard convection in the present work, it is neglected in the RANS model for turbulent diffusion of turbulent kinetic energy as given in eqn (4.8b). Of course the contribution of buoyancy term $\overline{u_j'^2 T'}$ is non-zero only along the vertical direction $j = 3$.

According to the existing literature, the Daly and Harlow model for the buoyancy term needs improvement. In order to obtain more detailed information for its vertical component $\overline{u_3'^2 T'}$ all the terms in its transport equation are analyzed using the DNS data of internally heated fluid layers and Rayleigh-Bénard convection. Based on these investigations, a Daly and Harlow Extended (DHE) model for the buoyancy term as in eqn (4.11) is obtained. This model includes both the effect of buoyancy and the production due to the temperature gradient. In this model buoyancy term $\overline{u_3' T'^2}$ and $\overline{u_3'^3}$ are the additional closure terms. Otić et al. (2005) have recently proposed an improved model for the buoyancy term. In this model, the contribution of the molecular fluid properties is introduced in addition to the gradient-approximation. This model was successfully validated using the DNS data of Rayleigh-Bénard convection. As a result, one of the closure problems of the DHE model can be solved at least for RBC. The second closure term $\overline{u_3'^3}$ in the DHE model can be modeled with the anisotropic gradient approximation as in Launder (1989).

By incorporating a variable Daly and Harlow (VDH) model for $\overline{u_j'^2 T'}$ in the RANS model for the turbulent diffusion of turbulent kinetic energy as in eqn (4.8b) results in an extended model 1 for the turbulent diffusion as given in eqn (4.13). By introducing the DHE model in eqn (4.8b) results in an extended model 2 for the turbulent diffusion of turbulent kinetic energy as given in eqn (4.20). Both the models 1 and 2 for the turbulent diffusion include the effect of buoyancy and velocity-pressure correlation. According to e.g. Lumley et al. (1978) and Moeng and Wyngaard (1989), inclusion of the effect of buoyancy may explain the counter gradient transport of $\overline{E'}$ .s

The DNS data of internally heated fluid layers and Rayleigh-Bénard convection are used to validate the RANS models for the triple-correlation, velocity-pressure correlation, buoyancy term and turbulent diffusion of turbulent kinetic energy along the vertical direction. In internally heated fluid layers with $Ra = 10^7$, the model values show an acceptable agreement with the triple-correlation. In this flow type the contribution of triple-correlation to the turbulent diffusion is greater than that of the velocity-pressure correlation in most of the central region $(\approx 1.25 \leq x_3 \leq 1.8)$. Whereas, the triple-correlation is having a very small contribution to the turbulent diffusion close to

the walls in this flow type. The comparison between the triple-correlation and its model shows the over prediction of the triple-correlation in Rayleigh-Bénard convection of air. However the modeled values have roughly the required qualitative distribution in this flow type. A comparative study between the triple-correlation and the velocity-pressure correlation reveals the higher importance of the velocity-pressure correlation in the turbulent diffusion in this flow type. The comparisons between the velocity-pressure correlation and its model show an acceptable qualitative and quantitative agreement in internally heated fluid layers and Rayleigh-Bénard convection. The analysis of the velocity-pressure correlation using the DNS data depicts its higher contribution to the turbulent diffusion compared to the triple-correlation in Rayleigh-Bénard convection. Further, the velocity-pressure correlation is more significant in comparison to the triple-correlation close to the walls in both flow types. These studies show that the RANS models for the triple-correlation and the velocity-pressure correlation can roughly explain these quantities especially in those areas in which they are relevant in both flow types along the vertical direction. The comparison between the buoyancy term $\overline{u_3'^2 T'}$ and its model in internally heated fluid layers show an improvement in DHE model in comparison to the DH and VDH model except close to the lower wall. In Rayleigh-Bénard convection the DHE modeled values have roughly the required distribution as of the buoyancy term analyzed from the DNS data close to the walls.

Analysis of the model 1 as given in eqn (4.14) shows a considerable improvement in the prediction of the turbulent diffusion of turbulent kinetic energy compared to the gradient-diffusion approximation in internally heated fluid layers with $Ra = 10^7, 10^8$. This model gives a small improvement in comparison to the gradient-diffusion approximation for predicting the turbulent diffusion in Rayleigh-Bénard convection of liquid metal at $Ra = 10^5$, $Pr = 0.025$. In case of Rayleigh-Bénard convection of air this model for the turbulent diffusion does not show any negative consequences.

The analysis of the model 2 as given in eqn (4.20) reveals its better predictive capability compared to the model 1 for the turbulent diffusion of turbulent kinetic energy in internally heated fluid layers with $Ra = 10^7, 10^8$, especially close to the upper wall. In Rayleigh-Bénard convection of air there is almost not much difference between the model 2 and model 1 close to the walls for the turbulent diffusion. In certain height

points the model 2 shows slightly better prediction of the turbulent diffusion compared to model 1 in this flow type. The inclusion of these models in the CFD codes or with the advanced models allows expecting more accurate results in such thermally stratified flow types. It is also possible to adapt these RANS models to LES. This holds for the common volume integration to deduce the equations for the resolved scales. These equations look formally identical to the RANS equations, although they have different meaning and physics involved. Thus, mainly the length and time scales which are involved in these equations need to be suitably adapted from RANS to LES.

The applications of models 1 and 2 for the turbulent diffusion make use of an additional transport equation for the auto-correlation $\overline{u_3'^2}$. These models for the turbulent diffusion extend the standard $\overline{E'}-\overline{\varepsilon'}$ model to a $\overline{E'}-\overline{\varepsilon'}-\overline{u_3'^2}$ model which is a 3-equation model. The transport equation for the auto-correlation is a particular form of the transport equation for the Reynolds stresses as given in e.g. Launder et al. (1975). This additional transport equation is necessary to incorporate the strong anisotropic effects due to the buoyancy and the presence of the walls along the vertical direction. This also follows the notion of Durbin (1991) to include the near-wall effects of in-homogeneity and anisotropy in the form of an additional transport equation. The investigations in meteorology and in astrophysics recommend the use of an algebraic model (ASM) for the turbulent heat flux as in Launder (1988) for describing the heat transfer in buoyant flow types. This ASM model makes use of an additional transport equation for the temperature variance $\left(T'^2\right)$. Therefore, incorporating this ASM model for the turbulent heat flux into the present work further extends the $\overline{E'}-\overline{\varepsilon'}-\overline{u_3'^2}$ model to a $\overline{E'}-\overline{\varepsilon'}-\overline{u_3'^2}-\overline{T'^2}$ model which is a 4-equation ASM model.

Additionally an approach to model not the velocity-pressure correlation but its derivative has been presented. In this method, the differential equations for the velocity-pressure correlation are derived. In these equations an anisotropic-form of the gradient diffusion model for the triple-correlation is used. For validation, a simplified RANS model form of these differential equations as in eqn (C.7) along the vertical direction has been obtained. The RANS model for the derivative of velocity-pressure correlation is acceptable in internally heated fluid layers and Rayleigh-Bénard convection.

This model for the derivative of velocity-pressure correlation also makes use of the additional transport equation for the auto-correlation $\overline{u_3'^2}$ in order to introduce the effect of anisotropy as explained above.

The validations of the models 1 and 2 for the turbulent diffusion of the turbulent kinetic energy show that these models are having acceptable predictive capability in internally heated fluid layers and Rayleigh-Bénard convection along the vertical direction. The model 2 may be more accurate in comparison to the model 1 especially in internally heated fluid layers. On the other hand, the model 2 includes additional terms. This means, more computational effort compared to the model 1. Thus, the application of these models depends on the type of problems and their accuracy requirement.

An approach to model the derivative of the velocity-pressure correlation is also presented. In case of flow types like, e.g. Rayleigh-Bénard convection, in which the triple-correlation is having smaller contribution to the turbulent diffusion of turbulent kinetic energy it may be sufficient to apply a simple model for the triple-correlation and use the RANS model for the derivative of velocity-pressure correlation. Consequently, a priori information about the flow type and the closure terms in the turbulent diffusion is needed for applying this model.

Future activities, following this thesis, could be on the following subjects:

The time development of the DNS of internally heated fluid layers with $Ra = 10^9$ shows that this simulation should be proceeded to achieve the accurate fully developed steady state. The analysis of the turbulent kinetic energy in internally heated fluid layers with different Ra indicates that a fully turbulent regime in which the distribution of statistical turbulence data is qualitatively independent of Ra is not yet achieved. Thus, simulations of this flow type at even higher Ra are needed for the validation of the various turbulence models in this flow type.

Implementation of the RANS models 1 and 2 for the turbulent diffusion of the turbulent kinetic energy in the commercial or in-house code is required to test their practical performance in other flow type, e.g. flows in which both shear and buoyancy plays an important role and flows which are not horizontally homogeneous. Such tests can

explore the limitations of these models. Inclusion of these models for the turbulent diffusion in engineering CFD codes may further enhance the predictive capability of the standard as well as advanced RANS models in investigating buoyant flow types.

The above discussion indicates that a $\overline{E'} - \overline{\varepsilon'} - \overline{u_3'^2} - \overline{T'^2}$ model which is a 4-equation ASM model can be used to compute engineering buoyancy influenced flows in horizontal fluid layers. For even better prediction in the thermally stratified flow types an additional transport equation for the dissipation of $\overline{T'^2}$ $\left(\overline{\varepsilon_T'}\right)$ is needed at Pr widely different form 1, see e.g. Carteciano (1996) and Otić et al. (2005) which further extends the $\overline{E'} - \overline{\varepsilon'} - \overline{u_3'^2} - \overline{T'^2}$ to a $\overline{E'} - \overline{\varepsilon'} - \overline{u_3'^2} - \overline{T'^2} - \overline{\varepsilon_T'}$ model which is a 5-equation ASM model. This means additional computational effort to solve the system of equations. Therefore, the best compromise will be a $\overline{E'} - \overline{\varepsilon'} - \overline{u_3'^2} - \overline{T'^2}$ model in case Pr around 1. If Pr significantly differs from 1 then a $\overline{E'} - \overline{\varepsilon'} - \overline{u_3'^2} - \overline{T'^2} - \overline{\varepsilon_T'}$ model is required. This system can be implemented in the Turbulence Model for Buoyant Flows (TMBF) model as in Carteciano (1996) with the help of an additional transport equation for $\overline{u_3'^2}$. This allows expecting even better predictive capability of this advanced model in buoyant flow types.

7 Bibliography

Bauer, W., Haag, O. and Hennecke, D. K., (2000) “Accuracy and Robustness of Nonlinear Eddy Viscosity Models,“ Int. J. Heat and Fluid Flow, 21, pp. 312-219.

Canuto, V. M. and Dalsgaard-C. J., (1998) “Turbulence in Astrophysics,” Annu. Rev. Fluid Mech., 30, pp. 167-198.

Carteciano, L. N., (1996), “Entwickling eines Turbulenzmodells für Auftriebsströmungen,“ PhD thesis, KfK 5775, Forschungszentrum Karlsruhe.

Carteciano, L. N. and Grötzbach, G., (2003) “Validation of Turbulence models in the Computer Code FLUTAN for a Free Hot Sodium Jet in Different Buoyancy Flow Regimes,” Tech. Rep., FZKA 6600, Forschungszentrum Karlsruhe.

Chandra, L. and Grötzbach, G., (2005) “Analysis of an Extended Gradient Diffusion RANS Model for the Turbulent Diffusion of the Turbulent Kinetic Energy,“ Jahrestagung Kerntechnik 2005, Nürnberg, 10.-12.5.2005 , Kerntechnische Gesellschaft e. V., INFORUM Bonn 2005, CD-ROM, S.88-91.

Chavanne, M., Chilià, F., Castaing, B. and Hébral, B. (2001) “Turbulent Rayleigh-Bénard Convection in Gaseous and Liquid He,” Phys. Fluids, 13(5), pp. 1300-1320.

Clever, R. M. and Busse, F. H., (1974) “Transition to Time-dependent Convection,” J. Fluid Mech., 65, pp. 625-645.

Clever, R. M. and Busse, F.H., (1981) “Low-Prandtl Number Convection in a Layer Heated from Below,” J. Fluid Mech., 102, pp.61-74.

Daly, B. J. and Harlow, F. H., (1970) “Transport Equations in Turbulence,” Phys. Fluids, 18, pp. 2634-2649.

Davidson, L., (1990) “Second-order Corrections of the $k-\varepsilon$ Model to account for Non-isotropic effects due to Buoyancy,” Int. J. Heat Mass Transfer, 33, pp. 2599-2608.

Deardroff, J. W. and Willis, G.E., (1967) “Investigation of Turbulent Thermal Convection Between Horizontal Plates,” J. Fluid Mech., 28, 675-704.

Deardorff, J.W., (1974) “Three-dimensional Numerical Study of the Height and Mean Structure of a Heated Planetary Boundary Layer,” Boundary-Layer Meteorology, 7, pp. 81-106.

Dinh, T.N. and Nourgaliev, R. R., (1997) “Turbulence Modelling for Large Volumetrically Heated Liquid Pools,” Nuclear Engn. and Design, pp. 131-150.

Dol, H. S., Hanjalić, K. and Kenjereš, S., (1997) “A Comparative Assessment of the Second-moment Differential and Algebraic Models in Turbulent Natural Convection,” Int. J. Heat and Fluid Flow, 18, pp. 4-14.

Dol, H. S. (1998) “Turbulence Models for Natural Convection in Side-heated Enclosures,” Ph.D. thesis, Technische Universiteit Delft.

Dol, H. S., Hanjalić, K. and Verstgeegh, T. A. M., (1999) “A DNS-based Thermal Second-moment Closure for Buoyant Convection at Vertical Walls,” J. Fluid Mech., 391, pp. 211-247.

Domaradzki, J.A. and Metcalfe, W., (1988) “Direct Numerical Simulations of the Effect of Shear on Turbulent Rayleigh-Bénard Convection,” J. Fluid Mech., 193, pp.499-531.

Donaldson, C. duP., (1969) “A Computer Study of an Analytical Model of Boundary Layer Transition,” AIAA Journal, 7, pp. 272-278.

Durbin, P.A., (1991) “Near Wall Turbulence Modeling Without Damping Functions,” Theoret. Comput. Fluid Dyn., 3, pp. 3-13.

Durbin P. A. (1993). A Reynolds Stress Model for Near-wall Turbulence. J. Fluid Mech. 249, 465-498.

Dwyer, M. J., Patton, G. E. and Shaw R. H, (1997) “Turbulent Kinetic Energy Budgets from a Large Eddy Simulation of Airflow Above and Within a Forest Canopy,” Boundary-Layer Meteorology, 84, pp. 23-43.

Eidson, T. M., (1985) “Numerical Simulation of the Turbulent Rayleigh-Bénard problem using Subgrid Modelling,” J. Fluid Mech., 158, pp. 245-268.

Gray, D. D. and Giorgini, A., (1976) “The validity of the Boussinesq approximation for Liquids and Gases,” Int. J. Heat and Mass Transfer, 19, pp. 545-551.

Grötzbach, G., (1977) “Direkte Numerische Simulation turbulenter Geschwindigkeits-, Druck-, und Temperaturfelder bei Kanalströmungen,“ PhD thesis, KfK 2426, Forschungszentrum Karlsruhe.

Grötzbach, G., (1981) “Spatial Resolution Requirements for Numerical Simulation of Internally Heated Fluid Layers,” Proc. Numerical Methods in Laminar and Turbulent Flow., Italy, July 13 – 16, Ed. Taylor, C. and Schrefler, B. A., Pineridge Press Ltd., pp. 593-604.

Grötzbach, G. (1982a) “Direct Numerical Simulation of the Turbulent Momentum and Heat Transfer in an Internally Heated Fluid Layer,” Proc. 7th Int. Heat Transfer Conference, München, Ed. Grigull, U., Hahne, E., Stephan., K and Straub, J., Hemisphere Publishing Corporation, Washington, pp.141-146.

Grötzbach, G., (1982b) “Direct numerical simulation of laminar and turbulent Bénard convection,” J. Fluid Mech., 119, pp.27-53.

Grötzbach, G., (1983) “Spatial Resolution Requirements for Direct Numerical Simulation of the Rayleigh-Bénard Convection,” J. Comput. Phys., 49 (2), pp. 241-264.

Grötzbach, G., (1987) “Direct Numerical and Large Eddy Simulation of Turbulent Channel Flows,” Encyclopedia of Fluid Mechanics, Complex Flow Phenomena and Modeling, 6, Ed. Chreminisinoff, N. P., Gulf Publishing Company, Houston, pp. 1337-1391.

Grötzbach, G., (1989) “Turbulent Heat Transfer in an Internally Heated Fluid Layer,” Proc. 3rd Int. Symposium on Refined Flow Modelling and Turbulence Measurements, Ed. Iwasa, Y., Tamai, N. and Wada, A., Universal Academy Press Inc., pp. 267-275.

Grötzbach, G., (1990) “Simulation of Turbulent Flow and Heat Transfer for Selected Problems of Nuclear Thermal Hydraulics,” The 1st international conference on Supercomputing in Nuclear Applications (SNA’90), March 12-16, Japan, Ed. Japan Atomic Energy Research Institute, Nuclear Energy Data Center, pp. 29-35.

Grötzbach, G., Batta, A., Lefhalm, C. –H. and Otić, I. (2004) “Challenges in Thermal and Hydraulic Analysis of ADS Target Systems,” The 6th International conference on Nuclear Thermal Hydraulics Operations and Safety (Nuthos-6), Nara, Japan, October 4-8.

Hanjalić, K. and Launder, B. E., (1972) “ A Reynolds Stress Model of Turbulence and its Application to Thin Shear Flows”, J. Fluid Mech., 52 (4), pp. 609-638.

Hanjalić, K., Kenjereš, S. and Durst, F., (1996) “Natural Convection in Partitioned Two-dimensional Enclosures at Higher Rayleigh Numbers,” Int. J. Heat and Mass Transfer, 39, pp. 1407-1427.

Hanjalić, K., (1999) “Second-Moment Turbulence Closures for CFD: Needs and Prospects,” Int. J. Comput. Fluid Dyn., 12, pp. 67-97.

Hanjalić, K., (2002) “One Point Closure Models for Buoyancy-driven Turbulent Flows,” Annu. Rev. Fluid Mech., 34, pp. 321-347.

Hartlep, T., Tilgner, A. and Busse, F. H., (2003) “Large Scale Structures in Rayleigh-Bénard Convection at High Rayleigh Numbers,” Phys. Rev. Lett., 91 (6), pp. 064501-4.

Hiltner, I., (1993) Unveröffenlichter Bericht, Forschungszentrum Karlsruhe.

Hinze, J.O., (1959) “Turbulence: An introduction to its mechanism and theory,” McGraw-Hill Book Company, New York.

Hossain, M.S. and Rodi, W., (1974) “Equations for Turbulent Buoyant flows and Their Modelling,” SFB 80/F/46, Universität Karlsruhe.

Jahn, M., (1975) “Holographische Untersuchung der Freien Konvektion in einer Kernschmelze,” PhD thesis, Tech. Universität Hannover, F. R. G.

Kerr, R. M., (1996) “Rayleigh Number Scaling in Numerical Convection,” J. Fluid Mech., 310, pp. 139-179.

Kimmel, S. J. and Domaradzki, J. A., (2000) “Large Eddy Simulations of Rayleigh-Bénard Convection using Subgrid Scale Estimation Model,” Phys. Fluids, 12, pp. 169-184.

Krishnamurti, R., (1970a) “On the Transition to Turbulent Convection. Part 1. The Transition from Two- to Three-dimensional Flow,” J. Fluid Mech., 42, pp. 295-307.

Krishnamurti, R., (1970b) “On the Transition to Turbulent Convection. Part 2. The Transition to Time-dependent Flow,” J. Fluid Mech., 42, pp. 309-320.

Kulacki, F. A. and Goldstein, R. J., (1972) “Thermal Convection in a Horizontal Fluid Layer with Uniform Volumetric Energy Sources,” J. Fluid. Mech., 55 (2), pp. 271-287.

Kulacki, F. A. and Richards, D. E., (1985) “Natural Convection in Plane Layers and Cavities with Volumetric Energy Sources,” Natural Convection Fundamentals and Applications, Ed. Kakaç, S., Aung, W. and Viskanta, R., Hemisphere publishing corporation, pp.179-255.

Lai, Y. G. and So, R. M. C., (1990) “Near-wall modeling of turbulent heat fluxes,” Int. J. Heat Mass Transfer, 33 (7), pp. 1429-1440.

Launder, B. E. and Spalding, D. B., (1972) “Lectures in Mathematical Models of Turbulence,” Academic Press, London.

Launder, B. E., Reece, G. J. and Rodi, W., (1975) “Progress in the Development of a Reynolds-Stress Turbulence Closure,” J. Fluid Mech., 68 (3), pp.537-566.

Launder, B. E., (1988) “On the Computation of Convective Heat Transfer in Complex Turbulent Flows,” ASMEC J. Heat Transfer, 110, pp. 1112-1128.

Launder, B.E., (1989) “Second-Moment Closure: Present… and Future,” Int. J. Heat and Fluid Flow., 10, pp. 282-300.

Lee, J. S. and Pletcher, R. H., (2001) “Large Eddy Simulation of a Turbulent Channel Flow with Buoyancy Effects”, AIAA Journal, 22R, pp. 1-11.

Lumley, J. L., (1978) “Computational Modeling of Turbulent Flows,” Adv. Appl. Mech., 18, pp. 123-176.

Lumley, J.L., Zeman, O. and Siess, J., (1978) “The Influence of Buoyancy on Turbulent Transport,” J. Fluid Mech., 84 (3), pp. 581-597.

Liu, F. and Wen, X.J., (2002) “The Effect of Turbulence Modelling on the CFD Simulation of Buoyant Diffusion Flames,” Fire Safety Journal, 37, pp. 125-150.

Millionshtchikov, M. D., (1941) “On the Theory of Homogeneous Isotropic Turbulence, “ C.R. Acad. Sci. S.S.S.R., 32, pp. 615-619.

Moeng, C. –H. and Wyngaard, J.C., (1989) “Evaluation of Turbulent Transport and Dissipation Closures in Second-Order Modelling,” J. Atmospheric Sc., 46, pp. 2311-2330.

Monin, A. S. and Yaglom, A. M., (1971) “Statistical Fluid Mechanics: Mechanics of Turbulence,” The MIT Press, Cambridge, Massachusetts.

Murakami, S., Kato, S., Chikamoto, T., Laurence, D. and Blay, D., (1996) “New low-Reynolds-number k-ε Model Including Damping Effect due to Buoyancy in a Stratified Flow Field”, Int. J. Heat Mass Transfer, 39, No. 16, pp. 3483-3496.

Nagano, Y and Kim, C., (1988) ”A Two Equation Model for Heat Transport in Wall Turbulent Shear Flows,” ASME J. Heat Transfer, 110, pp. 583-589.

Nieuwstadt, F. T. M., (1990) “Direct and Large-eddy simulation of free convection,” Proc. 9th International Heat Transfer Conference, Jerusalem, ASME, 1, pp. 37-47.

Oberlack M. and Peters N., (1993) “Closure of the dissipation Tensor Equation and the Pressure Velocity Correlation based on the Two-point Correlation Equation,” Proc. of the 9th Symposium on Turbulent Shear Flows, Kyoto, Japan.

Oertel, H. (Ed.) (2004) “Prandtl’s Essentials of Fluid Mechanics,“ Ed. Oertel, H., With Contributions from Böhle, M., Etling, D., Müller, U., Sreenivasan, K. R., Riedel, U and Warnatz, J., Second Edition, Springer Verlag New York, Inc.

Otić, I. and Grötzbach, G., (2004) “Direct Numerical Simulation and RANS Modeling of Turbulent Natural Convection for low Prandtl Number Fluids,” Proc. of 5th Int. Bi-Annual ASME/JSME Symposium on Computational Technology for Fluid/ Thermal/ Chemical/ Stressed Systems with Industrial Applications, July 25-29 San Diego/La Jolla, California, USA, Ed. Kudriavtsev, V., Kleijn, C. R., Kawano, S., ASME, 491-2, pp. 159-165.

Otić, I., Grötzbach, G. and Wörner, M., (2005) “Analysis and Modelling of the Temperature Variance Equation in Turbulent Natural convection for low-Prandtl-number Fluids,” J. Fluid Mech., 525, pp. 237-261.

Perot, B. and Moin, P., (1995) “Shear-free Turbulent Boundary Layers. Part 1. Physical Insights into near-wall Turbulence,” J. Fluid Mech., 295, pp. 199-227.

Prandtl, L., (1945) “Über ein Neues Formelsystem für die Ausgebildeten Turbulenz,“ Nachrichten der Gesellschaft für Akademische Wissenschaften Göttingen, Mathematisch-Physikalische Klasse.

Rodi, W., (1972) “The Prediction of Free Turbulent Boundary Layer by use of a Two-equation Model of Turbulence,” PhD thesis, Imperial College, London.

Rotta, J., (1951) “Statistische Theoreie Nichthomogener Turbulenz,” 1. Mitteilung, Zeitschrift für Physik, 129, pp. 547-572.

Sander, J., (1998) “Dynamical Equations and Turbulent Closure in Geophysics,” Continuum Mech. Thermodyn., Springer-Verlag, 10, pp. 1-28.

Schemm, C., E. and Lipps, F., B., (1976) “Some Results from a Simplified Three – Dimensional Numerical Model of Atmospheric Turbulence,” J. Atmospheric Sciences, 33, pp. 1021-1041.

Schlichting, H., (1958) “Grenzshichtheorie,” Verlag G. Braun, Karlsruhe.

Schmidt, M., Wörner M. and Grötzbach, G., (1997) “Direkte Numerische Simulation der Konvektion in einer Fluidschicht mit Internen Wärmequellen,“, Tech. Rep., FZKA 5916, Forschungszentrum Karlsruhe.

Schumann, U.,(1973) “Ein Verfahren zur Direketen Simulation Turbulent Strömungen in Platten- und Ringspaltkanälen und über seine Anwendung zur Untersuchung von Turbulenzmodellen,“ PhD thesis, KfK1854, Forschungszentrum Karlsruhe.

Schumann, U., (1975) “Subgrid Scale Model for Finite Difference Simulations of Turbulent Flows in Plane Channels and Annuli,” J. Comp. Phys., 18, pp. 376-404.

Schumann, U., (1987) “The Counter-gradient Heat Flux in Turbulent Stratified Flows”, Nuclear Engn. and Design, 100, pp. 255-262.

Seiter, Ch., (1995) “Numerische Simulation Turbulenter Auftriebsströmungen in Horizontalen Kanälen,” PhD thesis, FZKA 5505, Forschungszentrum Karlsruhe.

Seki, Y., Kawamoto, N. and Kawamura, H., (2003) “Proposal of Turbulent Heat Flux Model with Consideration of Linearity and Its Application to Turbulent Channel Flow with Various Thermal Boundary Conditions,” Turbulence, Heat and Mass Transfer 4, Ed. Hanjalić, K., Nagano., Y and Tummers, M., Bagell House Inc.

Shih, T. H., Zhu, J. and Lumley, J. L., (1995) “A New Reynolds Stress Algebraic Equation Model,” Comput. Methods. Appl. Mech. Engg., 125, 287-302.

Spalart, P. R., Jou, W. –H., Strelets, M. and Allmaras, S. R., (1997) “Comments on the feasibility of LES for wings, and on a hybrid RANS/LES approach,”, First AFOSR International Conference on DNS/LES, Advances in DNS/LES, 4-8 August, Ruston, LA, Ed. Liu, C., Liu, Z., Greyden Press, Columbus, OH.

Speziale, C. G., (1985) “Galilean Invariance of Subgrid-scale Stress Models in Large-Eddy Simulation of Turbulence,” J. Fluid Mech., 156, pp. 55-62.

Speziale, C. G., (1991) “Analytical Methods for the Development of Reynolds-stress Closures in Turbulence,” Annu. Rev. Fluid Mech., 23, pp. 107-157.

Sugiyama, K., Ma. Y. and Ishiguro, R., (1991) “Laminar Natural Convection Heat Transfer from a Horizontal Circular Cylinder,” ASME J. Heat Transfer, 113, pp. 91-96.

Tasaka, Y. and Takeda, Y., (2005) “Effects of Heat Source Distribution on Natural Convection Induced by Internal Heating,” Int. J. Heat and Mass Transfer, 48, pp. 1164-1174.

Tennekes, H. and Lumley, J.L., (1972) “A first course in turbulence,” The MIT Press, Cambridge, Massachusetts.

Townsend, A. A., (1976) “The structure of turbulent shear flow,” Cambridge University Press, Cambridge, London.

Tveitereid, M., (1978) “Thermal Convection in a Horizontal Fluid Layer with Internal Heat Sources,” Int. J. Heat and Mass Transfer, 21, pp. 1055-1069.

Weinstock, J., (1989) “A theory of turbulent transport,” J. Fluid Mech., 202, pp.319-338.

Wörner, M., (1994) “Direkte Simulation Turbulenter Rayleigh-Bénard-Konvektion in Flüssigem Natrium,“ PhD thesis, KfK 5228, Forschungszentrum Karlsruhe.

Wörner, M. Schmidt, M., and Grötzbach, G., (1997) “Direct Numerical Simulation of Turbulence in an Internally Heated Convective Fluid Layer and Implications for Statistical Modelling,“ J. Hydraulic Research, 35, pp. 773-797.

Wörner, M. and Grötzbach, G., (1998) “Pressure transport in direct numerical simulations of turbulent natural convection in horizontal fluid layers,” Int. J. of Heat and Fluid Flow, 19, pp.150-158.

Yan, Z. and Holmstedt, G., (1999) “A Two-equation Turbulence Model and Its Application to a Buoyant Diffusion Flame, Int. J. Heat and Mass Transfer, 42, pp. 1305-1315.

Zeman, O. and Lumley, J. L. (1976), “Modeling Buoyancy Driven Mixed Layers,” J. Atmos. Sci., 33, pp. 1974-1988.

Appendix A The turbulent Reynolds number in IHL and RBC

The coefficients in the RANS models for $\overline{u_j' p'}$ as in eqn (4.7) and for $\overline{u_3'^2 T'}$ as in eqn (4.9b) may not be constant. There are indications e.g. as in Daly and Harlow (1970), Dol et al. (1997) and Wörner et al. (1997) that these coefficients may depend on the local turbulent Reynolds number. Therefore, this quantity is analyzed in this Appendix.

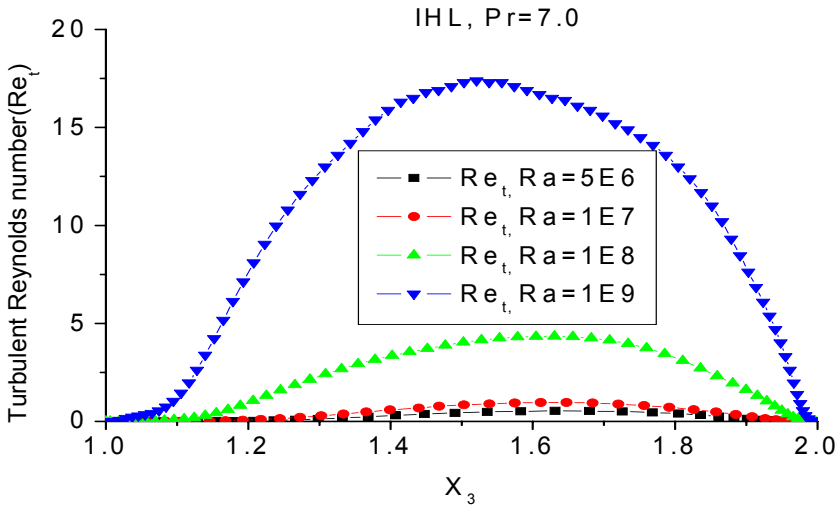

Fig. A-1 Vertical profiles of the turbulent Reynolds number analyzed from the DNS data of IHL.

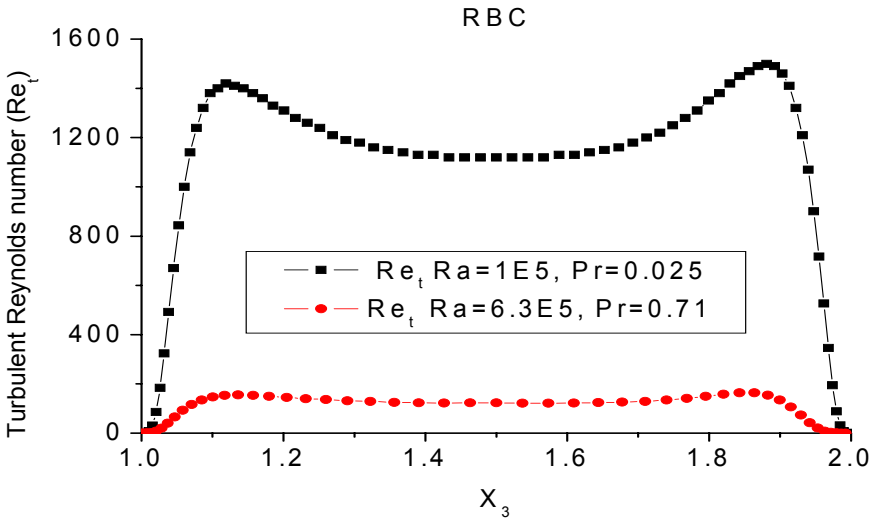

Fig. A-2 Vertical profiles of the turbulent Reynolds number analyzed from the DNS data of RBC.

The vertical profiles of turbulent Reynolds number $Re_t = \dfrac{\overline{E'^2}}{\nu\overline{\varepsilon'}}$ analyzed from the DNS data of IHL and RBC are shown in figures A-1 and A-2. In IHL the values of this term

are much smaller in comparison to RBC. This is in principle accordance with the finding by Wörner et al. (1997) that some of the coefficients which appear in the different standard RANS models (e.g. modified RANS model for $\overline{u_j' p'}$ as in eqn (4.7)) have higher values in IHL. Thus, this indicates a possibility to correlate the coefficient e.g. C_2', with Re_t.

Appendix B Coefficients in the RANS model for $\overline{u_j' E'}$, $\overline{u_j' p'}$, $\overline{u_3'^2 T'}$ and $D_{E,t}$

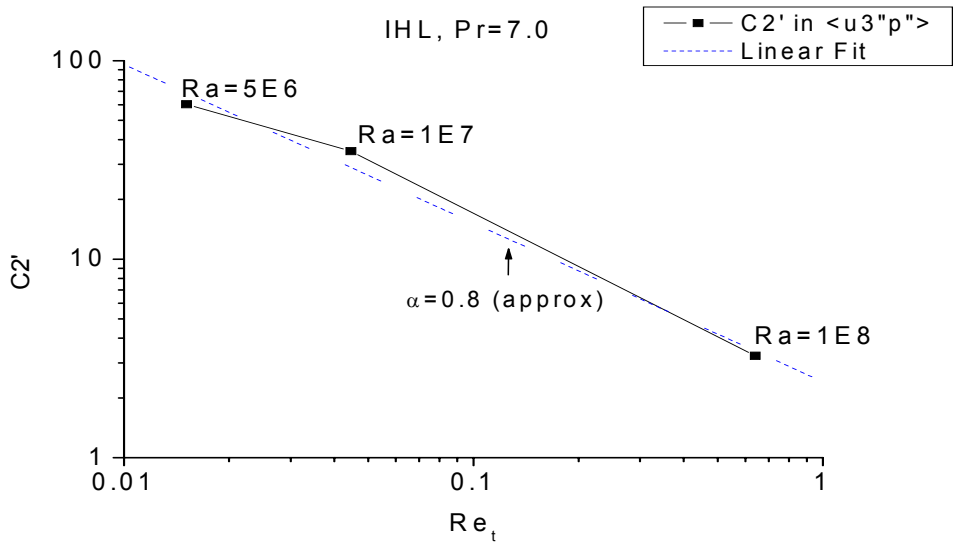

Fig. B-1 The coefficient C_2' as in eqn (4.7) analyzed from the DNS data of IHL at $x_3 \approx 1.18$.

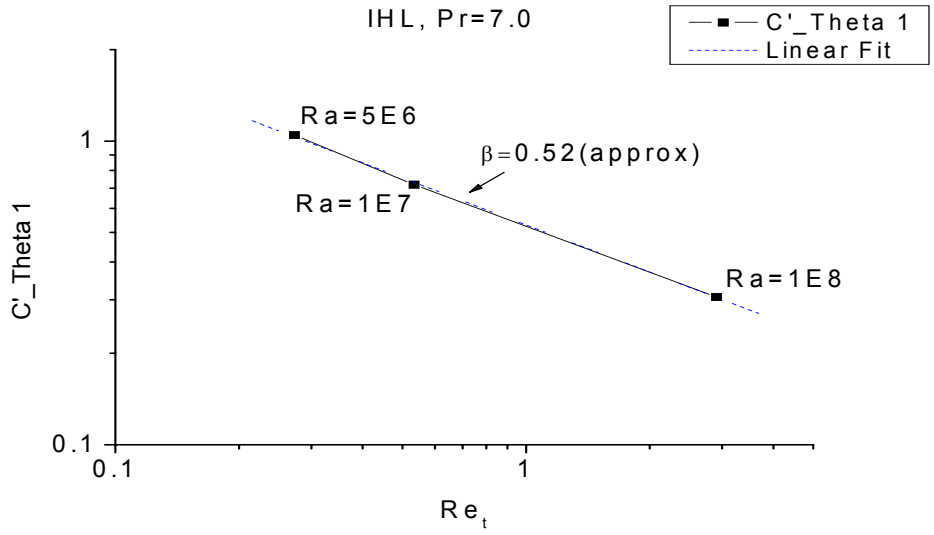

Fig. B-2 The coefficient $C_{\theta 1}'$ as in eqn (4.11) analyzed from the DNS data of IHL at $x_3 \approx 1.366$.

The logarithmic plot of C_2' versus the turbulent Reynolds number Re_t indicates an inverse relationship of the form $C_2' \sim \frac{1}{Re_t^{\alpha}}$ as in figure B-1 in IHL. The logarithmic plot of $C_{\theta 1}'$ versus the turbulent Reynolds number Re_t also indicates an inverse re-

lationship of the form $C_2' \sim \frac{1}{Re_t^{\beta}}$ in figure B-2 in IHL. The exponents α and β are estimated at a certain x_3. However, these values will be applied throughout the height of the channel in IHL i.e. for all values of x_3. Same values of these exponents will be used in RBC as well.

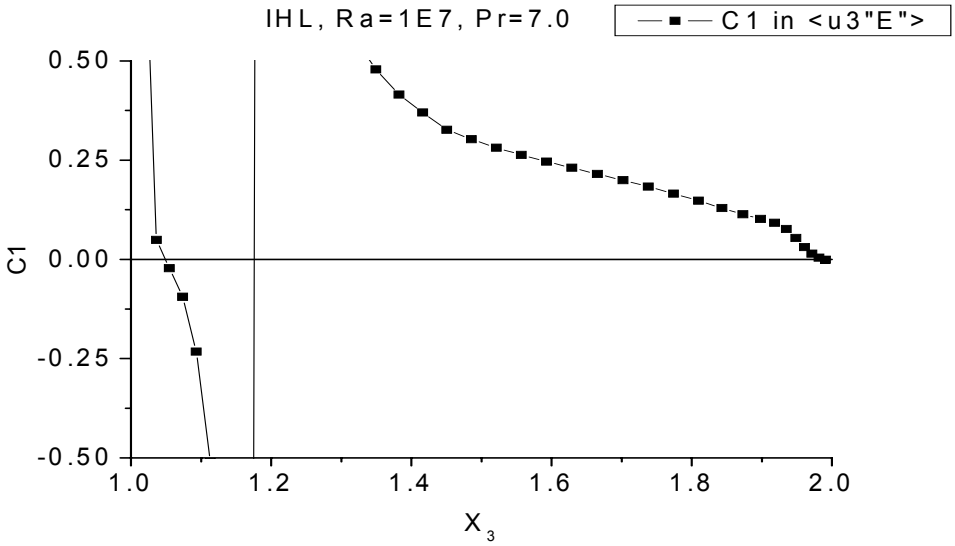

Fig. B-3 Vertical profile of the coefficient C_1 as in eqn (4.5) analyzed from the DNS data of IHL.

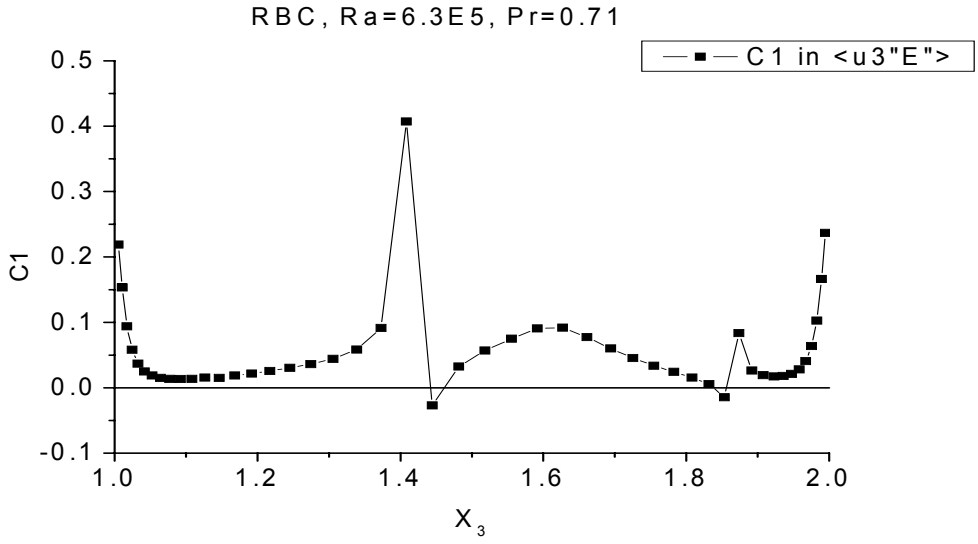

Fig. B-4 Vertical profile of the coefficient C_1 as in eqn (4.5) analyzed from the DNS data of RBC or air.

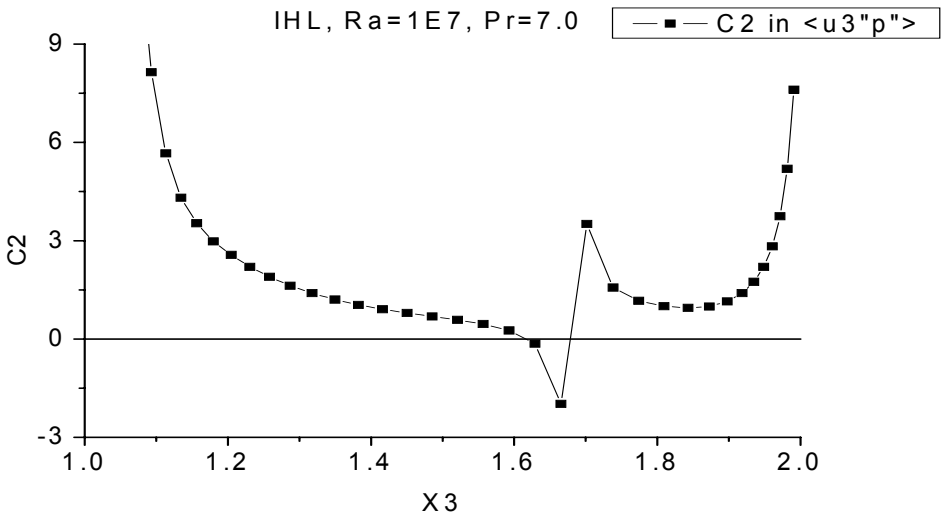

Fig. B-5 Vertical profile of the coefficient C_2 with $\alpha = 0.8$ as in eqn (4.7) analyzed from the DNS data of IHL.

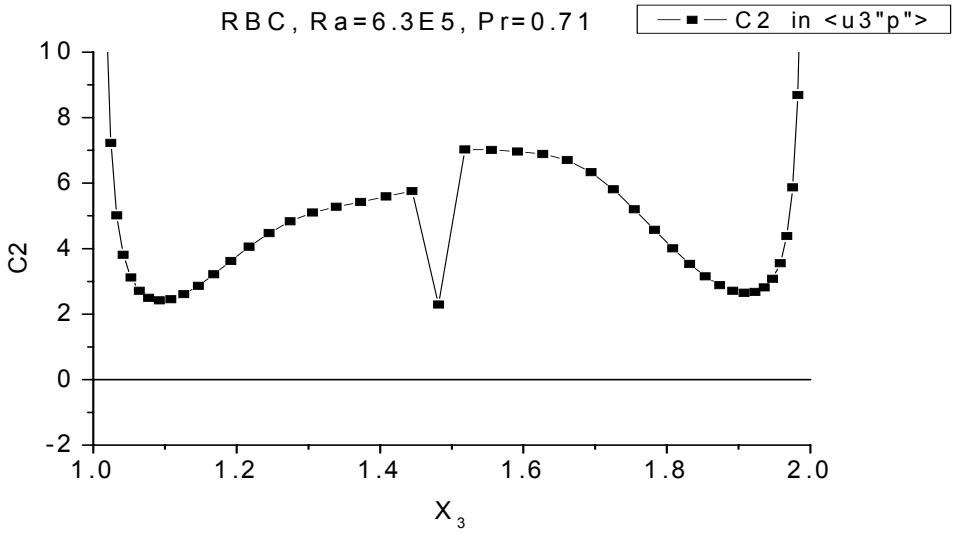

Fig. B-6 Vertical profile of the coefficient C_2 with $\alpha = 0.8$ as in eqn (4.7) analyzed from the DNS data of RBC of air.

The coefficients which are involved in the RANS models for $\overline{u_j' E'}$ as in eqn (4.5) and for $\overline{u_j' p'}$ as in eqn (4.7) with $\alpha = 0.8$ (see figure B-1) are analyzed from the DNS results in IHL and RBC. Their vertical profiles are shown in the figures B-3, B-4, B-5 and B-6. The positive values of the coefficients indicate the region of similar qualitative behavior. The negative values indicate the region in which the RANS models are not adequate in this flow type. However, the figure 3-24 shows that $\overline{u_j' E'}$ is having a significant contribution to $D_{E,t}$ in IHL away from the walls. As a result, its model plays an important role only in the central region in this flow type. Higher values of the coef-

ficients, e.g. close to the walls, in IHL and RBC indicate that the modeled values of $\overline{u_j' E'}$ and $\overline{u_j' p'}$ are smaller than their DNS analyzed values. A recommended common range of values for $0.04 \le C_1 \le 0.17$ and for $1.5 \le C_2 \le 7$ in both flow types.

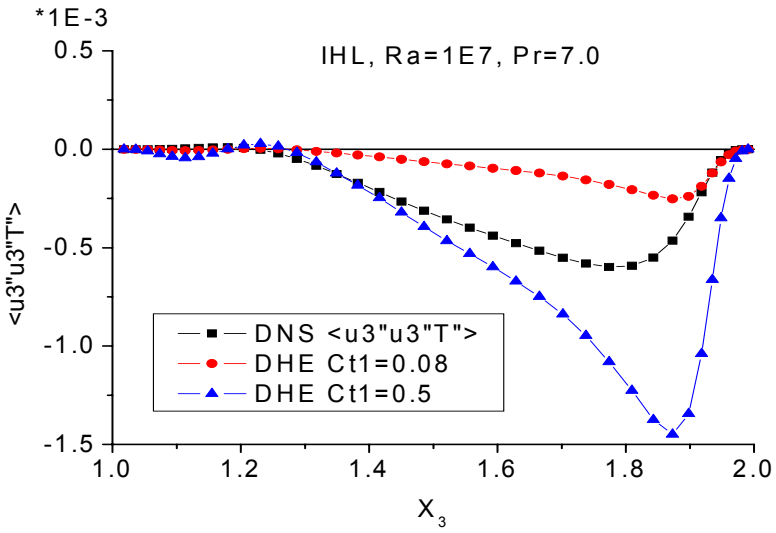

Fig. B-7 Vertical profiles of $\overline{u_3'^2 T'}$ and its DHE model as in eqn (4.11) analyzed from the DNS data of IHL at different $C_{\theta 1}$ ($\equiv$ Ct1).

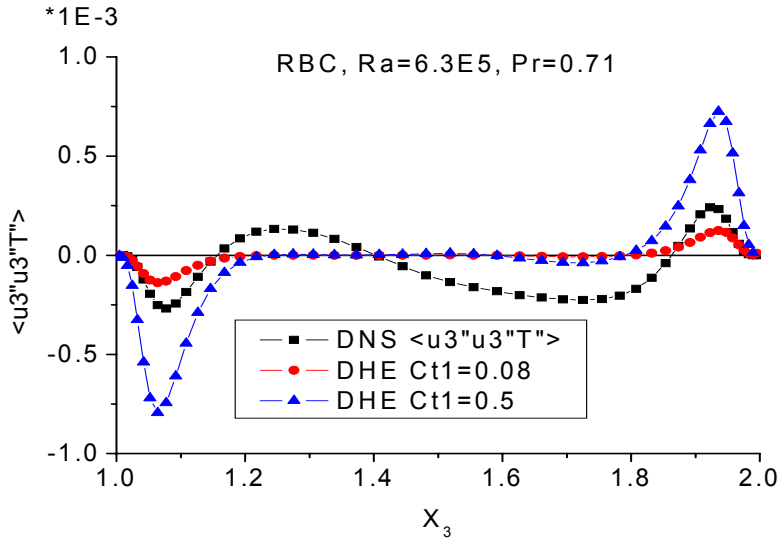

Fig. B-8 Vertical profiles of $\overline{u_3'^2 T'}$ and its DHE model as in eqn (4.11) analyzed from the DNS data of RBC of air at different $C_{\theta 1}$ ($\equiv$ Ct1).

Comparisons between $\overline{u_3'^2 T'}$ and its DHE modeled values as in eqn (4.11) at different $C_{\theta 1}$ are shown in figures B-7 and B-8 in IHL and RBC. The under prediction and over prediction of $\overline{u_3'^2 T'}$ in most of the regions for different values of $C_{\theta 1}$ indicates its

possible range of values in between 0.08 and 0.5 in both flow types. In the validation $C_{\theta 1} = 0.25$ is used as an optimal value for both flow types.

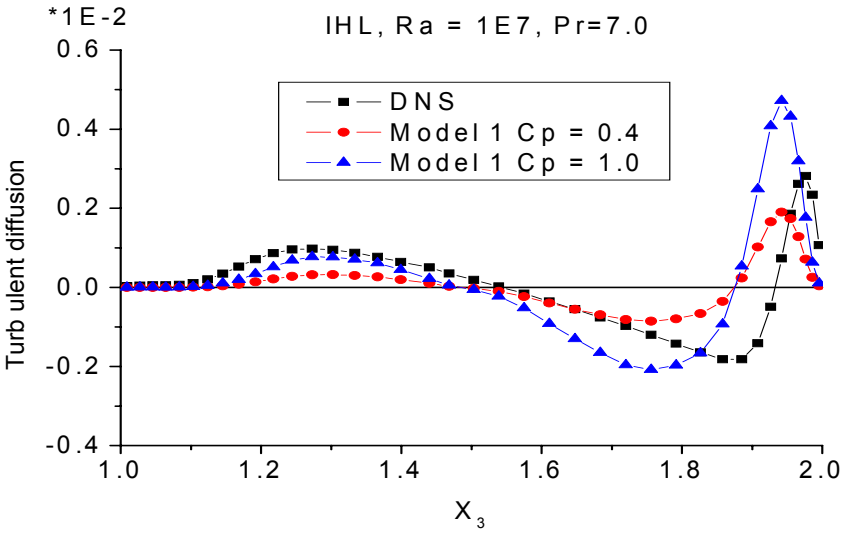

Fig. B-9 Vertical profiles of $D_{E,t}$ and its model 1 as in eqn (4.14) analyzed from the DNS data of IHL at different C_p.

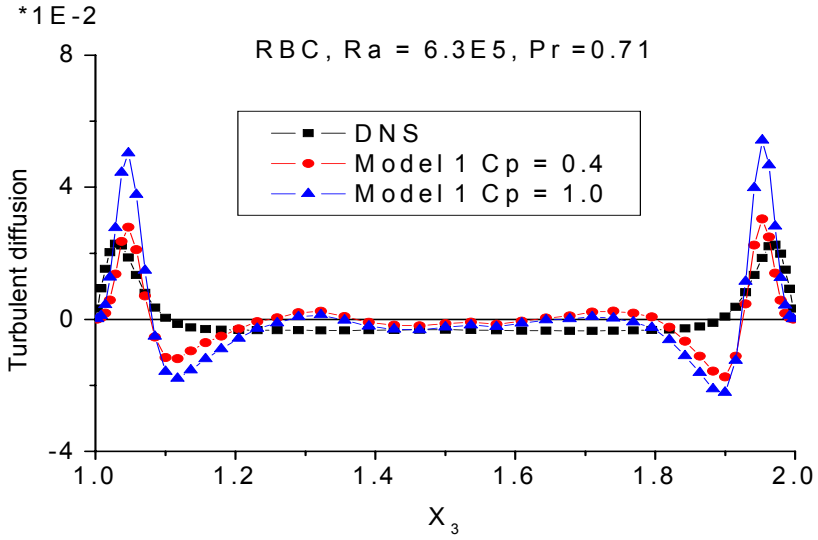

Fig. B-10 Vertical profiles of $D_{E,t}$ and its model 1 as in eqn (4.14) analyzed from the DNS data of RBC of air at different C_p.

Comparisons between $D_{E,t}$ and its modeled values as given by eqn (4.14) at different C_p are shown in figures B-9 and B-10 in IHL and RBC. Under and over prediction of $D_{E,t}$ in IHL indicates a possible range of the values of C_p in between 0.4 and 1.0. In RBC the modeled values show significant difference only close to the walls at

different C_p. For validation C_p is set to 0.7 in the model 1 in both flow types as an optimal value.

Appendix C Mathematical modeling of the derivative of $\overline{u_j' p'}$

In flow types like e.g. RBC, in which contribution of $\overline{u_j' E'}$ to $D_{E,t}$ is small, a better model for the derivative of $\overline{u_j' p'}$ may be needed. In this Appendix, a RANS model for the derivative of $\overline{u_j' p'}$ is deduced. The work by Oberlack and Peters (1993) is considered as a starting point to derive a differential equation for $\overline{u_j' p'}$ using the transport equation of $\overline{E'}$ (eqn (2.6)). This results in a RANS model for $\frac{\partial \overline{u_j' p'}}{\partial x_j}$. In this study the anisotropy between the different components of velocity fluctuations (see figures 3-16 and 3-17) will be taken into account.

C.1 Model development

Taking the gradient of the transport equation for $\overline{E'}$ as given in eqn (2.6) results in,

$$\nabla\left[\frac{\partial \overline{E'}}{\partial t}+\frac{\partial}{\partial x_j}\left(\overline{u_j}\,\overline{E'}\right)\right]=\nabla\left[P_E-\overline{\varepsilon'}+\frac{\partial}{\partial x_j}\left\{\frac{1}{\sqrt{Gr}}\frac{\partial \overline{E'}}{\partial x_j}\right\}-\frac{\partial}{\partial x_j}\left\{\overline{u_j' E'}+\overline{u_j' p'}\right\}\right]. \qquad \text{(C.1)}$$

Considering the convection in the horizontal fluid layer is shear free (as in the present case) and using the $\overline{E'}$ equation in the steady state, eqn (C.1) reduces to,

$$\nabla\left(P_E-\overline{\varepsilon'}\right)+\nabla\left(\frac{\partial}{\partial x_j}\left\{\frac{1}{\sqrt{Gr}}\frac{\partial \overline{E'}}{\partial x_j}\right\}-\frac{\partial}{\partial x_j}\left\{\overline{u_j' E'}+\overline{u_j' p'}\right\}\right)=0\,. \qquad \text{(C.2)}$$

Let us consider,

$$\frac{\partial}{\partial x_{[k]}}\left(\frac{\partial \overline{u_{[j]} p'}}{\partial x_{[j]}}\right)=0=\frac{\partial^2 \overline{u_{[j]} p'}}{\partial {x_{[k]}}^2},\ \textit{for}\ k\neq j=1,2,3. \qquad \text{(C.3)}$$

In other words,

$$\frac{\partial \overline{u'_{[j]} p'}}{\partial x_{[j]}} = f\left(x_{[j]}\right), \; for \; j = 1,2,3. \tag{C.4}$$

Here the indices within [ ] indicate each component separately and no Einstein-summation. The eqn (C.3) is valid under the constraint given by eqn (C.4). This equation indicates the dependence of the derivative of j^{th} component of the velocity-pressure fluctuation correlation with respect to $x_{[j]}$ along the j^{th} direction only. It is clear that the above approximation is a limitation in this derivation. Using eqn (C.3) in eqn (C.2) results in,

$$\frac{\partial^2 \overline{u'_{[k]} p'}}{\partial x_{[k]}^2} \approx \frac{\partial (P - \varepsilon)}{\partial x_k} + \frac{1}{\sqrt{Gr}} \frac{\partial}{\partial x_k} \left(\frac{\partial^2 \overline{E'}}{\partial x^2{}_j} \right) - \frac{\partial}{\partial x_k} \left(\frac{\partial \overline{u'_j E'}}{\partial x_j} \right), \; for \; j,k = 1,2,3 \; . \tag{C.5}$$

The eqn (C.5) represents three differential equations for the three velocity-pressure fluctuation correlations. In accordance with Launder (1989) the velocity-fluctuation tripe correlation on the RHS is approximated by,

$$\overline{u'_j E'} \approx -\frac{\nu_{jt}}{\sigma_k} \frac{\partial \overline{E'}}{\partial x_j}, \text{ with } \nu_{jt} = C_\mu \overline{u'^2_j} \tau, \text{ for } j = 1,2,3.$$

This means, here ν_{jt} is an anisotropic eddy viscosity and τ is a time scale (Durbin (1993)). The previous author has defined the time scale τ as follows,

$$\tau = max\left(\overline{E'} / \overline{\varepsilon'}, C_\tau \left(\nu / \overline{\varepsilon'} \right)^{1/2} \right).$$

This definition of τ also includes the effect of viscosity. In the present case for simplicity the following standard definition of τ has been used,

$$\tau = \overline{E'} / \overline{\varepsilon'} .$$

Using the above definition for τ it follows,

$$\nu_{jt} = C_\mu \overline{u_j'^2}\left(\overline{E'}/\overline{\varepsilon'}\right).$$

This Durbin definition of ν_{jt} was intended to avoid the use of damping functions in the isotropic eddy viscosity. Using the above simplifications in eqn (C.5) gives,

$$\frac{\partial^2 \overline{u'_{[k]}p'}}{\partial x_{[k]}^2} = C'_{u3p}\frac{\partial}{\partial x_k}\left[\left(P_E - \overline{\varepsilon'}\right) + \left(\frac{1}{\sqrt{Gr}}\frac{\partial^2 \overline{E'}}{\partial x_j^2} + \frac{\partial}{\partial x_j}\left(\frac{\nu_{jt}}{\sigma_k}\frac{\partial \overline{E'}}{\partial x_j}\right)\right)\right], k = 1,2,3. \quad \text{(C.6)}$$

In order to validate eqn (C.6), it can be reduced to a simple form making use of $\langle\ \rangle$ to average the variables, i.e. the averaged variables depend only on x_3. Finally from integrating eqn (C.6) with respect to x_3 follows,

$$\frac{\partial\langle u_3'' p''\rangle}{\partial x_3} = C_{u3p}\left[\langle P_E''\rangle - \langle\varepsilon''\rangle + \left(\frac{1}{\sqrt{Gr}} + \frac{C_\mu}{\sigma_k}\right)\frac{\partial}{\partial x_3}\left(\langle u_3''^2\rangle\left(\frac{\langle E''\rangle}{\langle\varepsilon''\rangle}\right)\frac{\partial\langle E''\rangle}{\partial x_3}\right)\right]. \quad \text{(C.7)}$$

Here, $\langle E''\rangle$ indicates the turbulent kinetic energy in which the variables are averaged using $\langle\ \rangle$, e.g. $\langle E''\rangle = \frac{1}{2}\langle u_i''^2\rangle$, and $\langle P_E''\rangle$ is the production of $\langle E''\rangle$ and $\langle\varepsilon''\rangle$ is its dissipation. Application of this RANS model for $\langle u_3'' p''\rangle$ as in eqn (C.7) requires an additional transport equation for $\langle u_3''^2\rangle$ (see sub-section 4.4.3). C_μ is the well known coefficient from the $\langle E''\rangle$-$\langle\varepsilon''\rangle$ model, $C_\mu = 0.09$ and C_{u3p} is the relevant new coefficient.

C.2 Validation of the RANS model for $\frac{\partial \overline{u_3' p'}}{\partial x_3}$

In order to validate the RANS model for $\frac{\partial \overline{u_3' p'}}{\partial x_3}$ as given in eqn (C.7) C_{u3p}=0.7 seems to be an adequate value. In case of the modified RANS model for $\overline{u_3' p'}$ as in eqn (4.7) the coefficient C_2 is set to 1.5 for IHL and 3.0 for RBC and the parameter $\alpha = 0.8$.

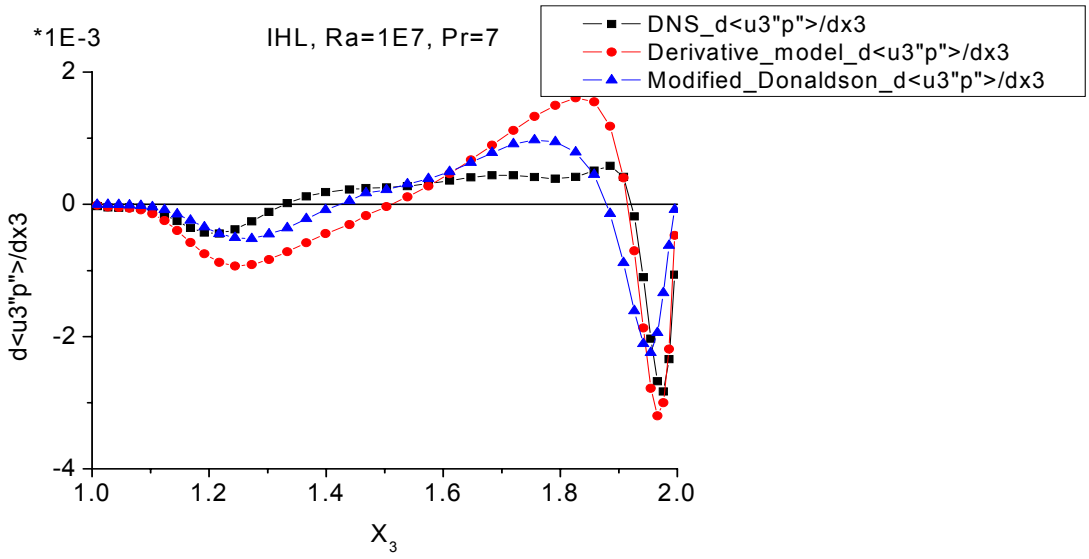

Fig. C-1 Vertical profiles of $\frac{\partial \overline{u_3' p'}}{\partial x_3}$ and its models analyzed from the DNS data of IHL with $Ra = 10^7$.

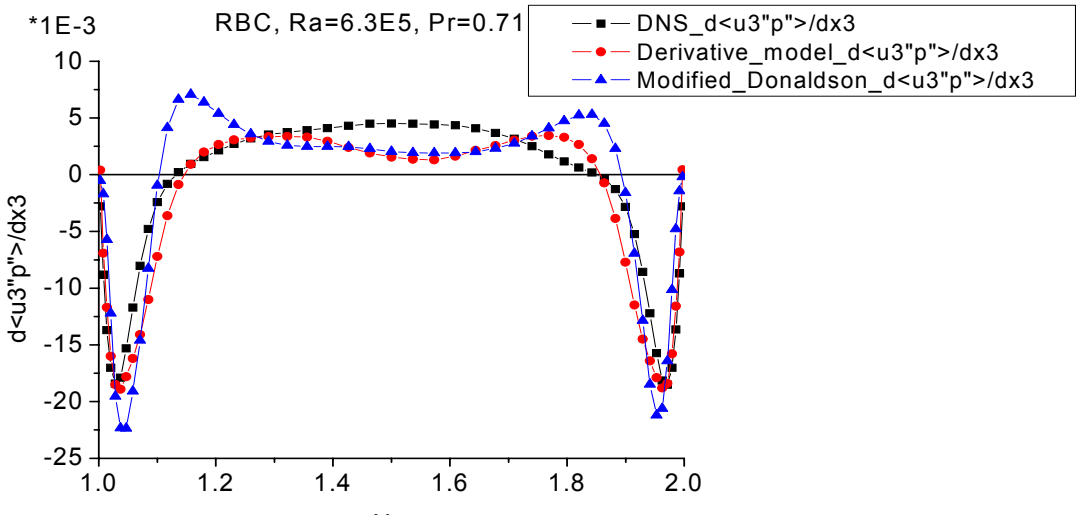

Fig. C-2 Vertical profiles of $\frac{\partial \overline{u_3' p'}}{\partial x_3}$ and its models analyzed from the DNS data of RBC of air.

The comparisons between $\frac{\partial \overline{u_3' p'}}{\partial x_3}$ and its RANS models (see eqn (4.7) called the modified Donaldson model and eqn (C.7) called the derivative model) analyzed from the DNS data of IHL and RBC are shown in figures C-1 and C-2. In IHL both RANS models for $\frac{\partial \overline{u_3' p'}}{\partial x_3}$ show acceptable agreement with $\frac{\partial \overline{u_3' p'}}{\partial x_3}$. These also indicate that

the RANS model for $\frac{\partial \overline{u_3' p'}}{\partial x_3}$ as given in eqn (C.7) has a somewhat better agreement with $\frac{\partial \overline{u_3' p'}}{\partial x_3}$ analyzed from the DNS data of RBC in most of the region along $j = 3$. However, both models predict the position of the minima of $\frac{\partial \overline{u_3' p'}}{\partial x_3}$ close to the boundaries approximately at the same value of x_3 in this flow type. These figures are also showing some deviations between $\frac{\partial \overline{u_3' p'}}{\partial x_3}$ and its modeled values in both flow types, especially in the central region $(1.2 \le x_3 \le 1.8)$.

Resume

12.05.1975	Born in India (Kumardhubi, Dhanbad)
Status	Unmarried
1981-1989	Visited Middle School Nirsha, Dhanbad
1989-1991	Visited S. S. K. B. C. High School Nirsha, Dhanbad
1991-1993	Studied in the R. S. More College Govindpur Dhanbad
1995-1998	B. Sc. (Hons.) from the Banaras Hindu University, Varanasi
1998-2000	M. Sc. from the University of Roorkee (IIT Roorkee), Roorkee.
2000-2002	M.Sc. from the University of Kaiserslautern, Kaiserslautern.
since 2002-	Working in the Institute for Nuclear and Energy Technologies, Forschungszentrum Karlsruhe GmbH, Karlsruhe.
	Head of Institute: Prof. Dr. –Ing. T. Schulenberg
	Supervisor: Dr. –Ing. G. Grötzbach.